Chem Soc Rev

REVIEW ARTICLE

View Article Online
View Journal | View Issue

Cite this: *Chem. Soc. Rev.*, 2022, **51**, 293

Supramolecular assemblies of organo-functionalised hybrid polyoxometalates: from functional building blocks to hierarchical nanomaterials

Jamie M. Cameron,[a] Geoffroy Guillemot,[b] Theodor Galambos,[b] Sharad S. Amin,[a] Elizabeth Hampson,[a] Kevin Mall Haidaraly,[b] Graham N. Newton *[a] and Guillaume Izzet *[b]

This review provides a comprehensive overview of recent advances in the supramolecular organisation and hierarchical self-assembly of organo-functionalised hybrid polyoxometalates (hereafter referred to as hybrid POMs), and their emerging role as multi-functional building blocks in the construction of new nanomaterials. Polyoxometalates have long been studied as a fascinating outgrowth of traditional metal-oxide chemistry, where the unusual position they occupy between individual metal oxoanions and solid-state bulk oxides imbues them with a range of attractive properties (*e.g.* solubility, high structural modularity and tuneable properties/reactivity). Specifically, the capacity for POMs to be covalently coupled to an effectively limitless range of organic moieties has opened exciting new avenues in their rational design, while the combination of distinct organic and inorganic components facilitates the formation of complex molecular architectures and the emergence of new, unique functionalities. Here, we present a detailed discussion of the design opportunities afforded by hybrid POMs, where fine control over their size, topology and their covalent and non-covalent interactions with a range of other species and/or substrates makes them ideal building blocks in the assembly of a broad range of supramolecular hybrid nanomaterials. We review both direct self-assembly approaches (encompassing both solution and solid-state approaches) and the non-covalent interactions of hybrid POMs with a range of suitable substrates (including cavitands, carbon nanotubes and biological systems), while giving key consideration to the underlying driving forces in each case. Ultimately, this review aims to demonstrate the enormous potential that the rational assembly of hybrid POM clusters shows for the development of next-generation nanomaterials with applications in areas as diverse as catalysis, energy-storage and molecular biology, while providing our perspective on where the next major developments in the field may emerge.

Received 31st August 2021

DOI: 10.1039/d1cs00832c

rsc.li/chem-soc-rev

1. Introduction

The elaboration of well-defined nanostructured architectures through the self-assembly of individual molecular building blocks is a challenging and contemporary research issue, and increasingly vital to the ongoing development of new nanotechnologies.[1] Nanostructured materials obtained *via* the hierarchical assembly of molecular units show promising applications in various domains, including catalysis,[2] medicine,[3] molecular electronics,[4] information processing,[5,6] gas storage[7,8] and energy conversion.[9,10] Classical bottom-up strategies use preformed entities as elementary building blocks, which are combined through self–assembly processes to form the target material.[11] Obtaining these complex, artificial assemblies relies on the use of molecular components that are capable of displaying directional, orthogonal and/or switchable interactions (*e.g.* metal coordination, electrostatic pairing, hydrophobic effects). Indeed, the cooperation of multiple non-covalent interactions is typically the key to forming ordered extended assemblies with emergent properties.[12–14] Although often difficult to predict, the emergence of novel properties frequently accompanies the formation of complex superstructures from the combination of even the most simple of components.[15]

[a] *Nottingham Applied Materials and Interfaces (NAMI) Group, The GSK Carbon Neutral Laboratories for Sustainable Chemistry, University of Nottingham, UK. E-mail: graham.newton@nottingham.ac.uk*
[b] *Sorbonne Université, CNRS, Institut Parisien de Chimie Moléculaire, IPCM, 4 Place Jussieu, F-75005 Paris, France. E-mail: guillaume.izzet@sorbonne-universite.fr*

Polyoxometalates (POMs) are nanosized molecular metal-oxides with diverse, albeit very well-defined, structures. They are often seen as key intermediates between small, soluble metal oxo complexes and insoluble solid-state bulk metal oxides.[16,17] POMs have attracted considerable interest in recent years thanks to their attractiveness as transferable building blocks for the elaboration of multi-functional materials,[18,19] which is in large part thanks to their unique structural and chemical properties. POMs are large and charge-delocalised polyanionic species, which develop strong electrostatic interactions with cationic species. They are also prone to associate with hydrophobic and neutral polar phases and frequently behave as chaotropic agents.[20,21] The highly charged and chaotropic nature of POMs often results in their self-assembly into larger supramolecular architectures and the emergence of new structures and even functionalities. Beside the spontaneous formation of single-walled hollow vesicles known as "blackberry" structures,[22] the formation of POM-based supramolecular assemblies often relies on their association to organic components through electrostatic interactions. Some remarkable examples such as artificial quantasomes (*i.e.* photoactive 2D nanostructured amphiphilic assemblies),[23] nanoporous 2D frameworks,[24,25] hexagonally ordered nanocomposite films,[26] well-ordered supramolecular hydrogels,[21] polypseudorotaxanes,[27] or liquid crystalline materials,[28] were developed using this approach. In most of these cases, organisation at both the molecular level, and the long-range ordering of these systems, mostly relies on the combination of the close electrostatic interactions between the POM and the cationic species with an additional driving force (*e.g.* the chaotropic effect, void filling behaviour or nanophase segregation). As such, these approaches are often highly unpredictable due to the lack of any directionality

Jamie M. Cameron

Jamie M. Cameron is a Research Associate in the Nottingham Applied Materials and Interfaces Group at the University of Nottingham (UK). He completed his PhD with Prof. Lee Cronin at the University of Glasgow (UK) on the self-assembly of metal-oxide clusters, before becoming a Postdoctoral Team Leader in the same group. In 2015, he was awarded a JSPS Postdoctoral Fellowship to work with Prof. Hiroki Oshio at the University of Tsukuba (Japan) on organic–inorganic hybrid materials. His current research explores the use of molecular design strategies to prepare new hierarchical nanomaterials for applications in next-generation energy technologies.

Geoffroy Guillemot

Geoffroy Guillemot is a graduate of the Université Pierre et Marie Curie (UPMC). He obtained his PhD in Chemistry from the Ecole Polytechnique Fédérale de Lausanne in 2002 under the supervision of Prof. Carlo Floriani. After postdoctoral stays with Prof. Dr A. Pfaltz (University of Basel), Dr J.-M. Basset (Université Claude Bernard à Lyon), Prof. O. Reinaud (Université René Descartes) and Dr P. LeFloch (Ecole Polytechnique), he returned to the UPMC in 2008 where he was appointed Assistant Professor and later Associate Professor of Inorganic Chemistry. His research focuses on the design of isolated site models using polyoxometalates for applications in metal-catalyzed atom or group transfer reactions.

Theodor Galambos

Theodor Galambos studies chemistry at the Georg-August-University Göttingen where he also obtained his BSc in 2018 under the supervision of Prof. P. Vana. During his master's studies he joined the group of Prof. M. M. Hansmann in late 2019 for a short-term research internship before leaving for a six-month stay at Sorbonne Université, Paris, including a three-month internship under the supervision of Dr Guillaume Izzet. After his return to Germany, he completed an internship at Covestro AG, Leverkusen and is currently working on his master's thesis at Volkswagen AG, Wolfsburg.

Sharad Amin

Sharad S. Amin is a Research Associate at the University of Nottingham (UK) in the Nottingham Applied Materials and Interfaces group. He completed his PhD in 2021 on the supramolecular assembly of redox-active polyoxometalate soft-materials under the supervision of Dr Graham Newton. Following his PhD, Sharad was awarded an EPSRC doctoral prize to conduct research on the development of these redox-active hybrid organic–inorganic soft materials to towards solid-state nanostructured metal-oxide architectures for energy devices.

imparted by the isotropic structure of many POMs. Typically, the self-assembly processes are predominantly governed by the ratio of the volumes occupied by the organic and inorganic components. Synthetic control of the organisation of these materials therefore relies almost entirely on the structure-directing effect of the associated organic components (either cationic or neutral), which surround the POM and behave as a steering 'glue' to direct the assembly of the system.

Covalently functionalised hybrid polyoxometalates (hybrid POMs) provide an attractive alternative route for the integration of POMs into complex molecular architectures.[29–33] Although the design and synthesis of hybrid POMs is typically much more synthetically demanding than the preparation of systems based on discreet organic and inorganic components, these species allow a far greater degree of control and directionality between the tethered organic and inorganic sub-units. POM functionalisation not only allows combination of the POM's properties with those of the appended subunit,[34] and in some cases can even modify the POMs own electronic structure,[35] but also greatly facilitates integration of the POM into more complex supramolecular assemblies. Indeed, the communities' expertise in the synthesis, functionalisation and characterisation of hybrid POMs has now reached a sufficient level of maturity to envision their integration into increasingly elaborate multi-functional supramolecular architectures.

Here, we will describe the current state of the art in the design and synthesis of hybrid POMs, with a particular focus on how this facilitates their assembly into larger supramolecular nanostructures. In particular, we will structure our discussion around the two key routes which have emerged as a means to incorporate hybrid POMs into larger nanostructures: (i) the direct self-assembly of hybrid POMs as unique building blocks,

Elizabeth Hampson

Elizabeth Hampson is a Research Associate in the Nottingham Applied Materials and Interfaces Group at the University of Nottingham (UK). She received an MSci in Medicinal and Biological Chemistry in 2017 at the university before she carried out her PhD under the supervision of Dr Graham Newton, on the synthesis of asymmetric organic–inorganic hybrid polyoxometalates. Following completion of her PhD earlier in 2021, she is now researching electrolytes and additives for next-generation batteries.

Kevin Mall Haidaraly

Kevin Mall Haidaraly was born and grew up in Madagascar. He travelled to France to pursue a degree in chemistry where he spent the majority of his scholarship at the UniversitÖ de Nantes but moved to Canada during to complete a final year project with Prof. Garry Hanan at the University of Montreal. He is currently studying towards a PhD under the guidance of Dr Guillaume Izzet and Dr Fabrice Mathevet, where he works on the development of a new family of mesomorphic polyoxometale-based hybrids for photonics applications.

Graham N. Newton

Graham N. Newton obtained his PhD from the University of Glasgow (UK) in 2009. After carrying out a JSPS postdoctoral research fellowship he was appointed Assistant Professor at the University of Tsukuba, Japan, in 2011. In 2015 he moved to the University of Nottingham, UK, where he is now Associate Professor of Inorganic and Materials Chemistry and a leader of the Nottingham Applied Materials and Interfaces group. His research interests include the synthesis and characterisation of redox-active materials, from molecular species through to complex nanomaterials. He has a particular interest in the development of organic–inorganic hybrid molecular metal oxides for applications in energy storage and photocatalysis.

Guillaume Izzet

Guillaume Izzet is a graduate of the Ecole Nationale Supérieure de Chimie de Paris. He obtained his PhD at the University Paris-Sud under the guidance of Prof. O. Reinaud in 2004. He was then appointed as a postdoctoral research fellow in the group of Prof. A. Harriman in Newcastle University. In 2006 he moved to Prague to join the research group of Prof. J. Michl at the Academy of Sciences of the Czech Republic. He finally became CNRS associate researcher in 2008 at the Institut Parisien de Chimie Moléculaire in the e-POM group. His research interests are focused on inorganic supramolecular chemistry, polyoxometalate functionalization, artificial photosynthesis, molecular electronics & photonics.

either in solution (*via* metal-directed self-assembly, or by exploiting the tuneable amphiphilic properties of some hybrid POMs), or in the solid-state (as liquid crystals, or other nanostructured soft materials); (ii) the combination of hybrid POMs with a secondary substrate (macrocyclic hosts, carbon nanotubes, or biological macromolecules/assemblies), where specific interactions between the organic sub-unit of the hybrid POM and the substrate predominate. This review will aim to comprehensively demonstrate the enormous potential that the rational design and functionalisation of hybrid POMs shows as a means to access the next-generation of multi-functional, hierarchical supramolecular nanostructures. Note that the preparation of crystalline POM-based coordination networks is an emerging field, which has been discussed elsewhere recently,[36,37] but mostly remains out of the scope of this review (the examples given here will only concern systems in which the hybrid POM is pre-formed prior to preparation of the crystalline network). Similarly, we will not provide detailed descriptions of the synthetic approaches to each hybrid POM platform, nor any associated post-functionalisation techniques, since these have been discussed in detail in several excellent recent reviews.[31,38,39]

2. Hybrid polyoxometalate platforms

This section briefly describes the hybrid POM platforms which have been explored thus far as molecular components or precursors for the self-assembly of larger supramolecular architectures (Fig. 1), in order to establish a common terminology which will be used throughout the remainder of this review. For the purposes of this review, each 'platform' described below simply reflects the most commonly occurring structural archetypes in the literature at present, and (though these are, of course, highly significant in the supramolecular assembly of each hybrid POM platform) we will consider neither the specifics of the covalently grafted ligands or the associated cations when briefly introducing each type of hybrid-POM platform below. It should also be noted that the array of hybrid POM platforms described in the following is by no means a complete account of all possible hybrid POM scaffolds, and again, these have been largely reviewed elsewhere.[31,38,39]

2.1 Triol-functionalised hybrid POMs

2.1.1 Anderson–Evans POMs. Anderson–Evans type POMs of the general formula $[XM_6O_{24}]^{n-}$ (X = transition metal or main group heteroatom; M = Mo or W) can be functionalised with tris-alkoxide ligands occurs through the partial replacement of the oxo-ligands at the central $\{MO_6\}$ heterometal position. This functionalisation mode is much more commonly observed in polyoxomolybdate species than in polyoxotungstate analogues due to the former's increased lability. By controlling the degree of protonation during the reaction, both single- and twofold-functionalisation is possible (though single-sided functionalisation is rare), generating the corresponding POM platforms $\{XM_6O_{21}((OCH_2)_3C–R)\}$ and $\{XM_6O_{18}((OCH_2)_3C–R)_2\}$ respectively, where R corresponds to the organic group(s)being appended to the POM. Asymmetric functionalisation of this POM has also been demonstrated,[38] allowing two different organic moieties to be appended to either side of the POM core. Topologically, the planar structure of the POM results in the tris moieties extending outwards from each side of the POM in a linear fashion, with a 180° angle between the two arms.

2.1.2 Lindqvist hexavanadates. Lindqvist-based hybrid POM platforms also commonly rely on tris-alkoxo ligands as the anchoring group for the organic moieties. Here, the replacement of bridging oxo-ligands in $[V_6O_{19}]^{8-}$ clusters by tris-alkoxo moieties also offers additional stabilisation to the POM. Depending on the reaction protocol, hybrid POM platforms containing one, two, three or four organic units may be synthesised. Bis-trisalkoxide stabilised hexavanadates display two distinct geometric isomers. The *anti*-isomer allows for an angle of 180° between the two linker units whereas the *syn*-isomer displays a 90° angle between the two linker units. A closely related

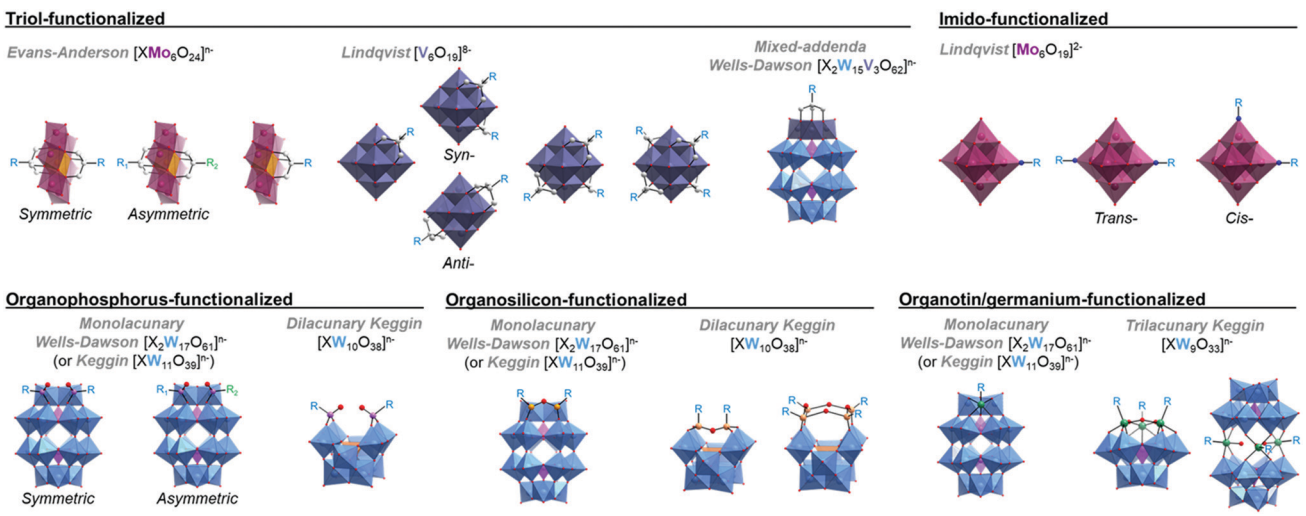

Fig. 1 Library of the most commonly studied hybrid POM platforms and functionalisation strategies. Colour code: $\{MoO_6\}$ = purple polyhedra, $\{MnO_6\}$ = orange polyhedra, $\{VO_6\}$ = grey/blue polyhedra, $\{WO_6\}$ = blue polyhedra, $\{PO_4\}$ = purple tetrahedra, $\{SiO_4\}$ = orange tetrahedra, O = red, N = blue, P = pink, Si = orange, Sn = green.

strategy (which will not be discussed at length herein) exploits organofunctionalisation using alkoxide-,[40] or even siloxide-moieties.[41] Though this has not typically been used as a supramolecular design strategy, it has been shown to allow for interesting control of the electronic properties of the POM cluster (permitting, for example, stabilisation of low-valent V^{III} oxidation states).[41,42]

2.1.3 Mixed-addenda Wells–Dawsons. Tris-alkoxides are also encountered as anchoring units in Wells–Dawson hybrid POM platforms. This sort of functionalisation is only encountered in the mixed-addenda Wells–Dawson POM $[P_2W_{15}V_3O_{62}]^{9-}$, where the incoming triol binds to the face of the capping $\{V_3\}$ unit in a manner analogous to that observed in the hexavanadate Lindqvist clusters mentioned previously. This results in strictly monotopic hybrid POM platforms.[39]

2.2 Imido-functionalised hexamolybdates

It is possible to incorporate nitrogen-based ligands through the formal substitution of terminal oxo-groups on the hexamolybdate Lindqvist-structure, $[Mo_6O_{19}]^{2-}$. Either one or two terminal oxo sites may be exchanged, resulting in both monotopic hybrid Lindqvist platforms as well as ditopic species which preferentially adopt a *cis* conformation with a 90° angle between the two linker units (though a *trans* configuration with a 180° orientation of the organic moieties has previously been reported).

2.3 Organophosphorus-functionalised POMs

Functionalisation with organophosphorus groups is also a viable route for preparation of hybrid POM platforms, typically exploiting the monovacant $[P_2W_{17}O_{61}]^{6-}$ Wells–Dawson cluster. Unlike some other hybrid POM platforms, caution must be taken to avoid hydrolysis of the anchoring P–O–W bonds,[43–45] with Wells–Dawson clusters typically proving more stable than their Keggin-type analogues. Though functionalisation of multivacant clusters has been demonstrated, functionalisation of monovacant species is by far the more common approach. This yields ditopic hybrid POM platforms with two phosphonyl moieties incorporated on either edge of the single lacunary site. Interestingly, the new bis-phosphonate site can even coordinate additional metal cations.[46] As in the case of Anderson–Evans based platforms, it has also recently been shown to be possible to prepare and purify asymmetrically functionalised species. An interesting feature of organophosphorus based POM platforms is the very high angle of *ca.* 160° between the organic moieties, providing a close to linear functionalisation topology.

2.4 Organosilicon-functionalised POMs

2.4.1 Monovacant Keggin and Wells–Dawson POMs. As in the related organophosphorus derivatives, Organosilicon based organic species are equally suited for the synthesis of hybrid POM platforms and are also typically formed using monovacant Keggin and Dawson polyoxotungstate clusters as the basis. Much like P^V, as the ionic radius of Si^{IV} is significantly smaller than that of W^{VI}, condensation of two organosilicon moieties per lacuna is typically observed. Unlike phosphorus-based groups however, incoming organosilicon species form bridged siloxane type linkers upon coordination to the POM unit, typically resulting in more hydrolytically stable hybrid POM platforms as a result. Furthermore, as a consequence of the formation of the Si–O–Si bridge between the two anchoring Si^{IV} sites, hybrid POM platforms such as $[PW_{11}O_{39}\{O(Si–R)_2\}]^{3-}$ and $[P_2W_{17}O_{61}\{O(Si–R)_2\}]^{6-}$ also display a considerably narrower angle of *ca.* 90° between the two organic units.[47–50]

2.4.2 Divacant Keggin POMs. Ditopic and even tetratopic hybrid POM platforms are also accessible *via* the functionalisation of divacant Keggin POMs, such as $[\gamma\text{-}SiW_{10}O_{36}]^{10-}$, with organosilyl derivatives. As shown by Thouvenot and co-workers, these functionalisations require precise control of the stoichiometry of the reagents leading selectively to synthesis of either bis-functionalised $[\gamma\text{-}SiW_{10}O_{36}\{O(Si–R)_2\}]^{4-}$ or tetra functionalised $[\gamma\text{-}SiW_{10}O_{36}(OSiR)_4]^{4-}$ hybrid POM platforms.[51]

2.5 Organotin-functionalised POMs

Incorporation of organotin ligands into several POM frameworks has been observed for a variety of lacunary POM species.[52–55] A particular benefit of the organotin functionalisation of POMs is the similar ionic radius of Sn^{IV} compared to W^{VI} (and Mo^{VI}), which facilitates the 1:1 inclusion of organotin fragments at lacunary sites, corresponding to the formal replacement of a W^{VI} atom by the corresponding Sn^{IV} ion. Though, as in the organophosphorus and organosilicon examples above, the functionalisation of monovacant Keggin and Wells–Dawson clusters yielding monotopic platforms is by far the most common approach, the aforementioned capacity of Sn^{IV} to formally replace vacant W^{VI} positions on the POM allows for the relatively simple formation of trifunctionalised species as well.

3. Direct self-assembly strategies

3.1 Metal coordination

Coupled to the aforementioned tuneable topologies of hybrid POM platforms, metal-driven self-assembly is an extremely powerful tool for the rational synthesis of discrete 0D, through to extended 3D assemblies, as it exploits strong and highly directional metal–ligand bonds.[56–58] 3D crystalline networks (including MOFs) have a wide range of properties and applications.[59,60] In comparison to crystalline networks, discrete supramolecular coordination complexes display well-defined structures that are prone to form elaborate hierarchical systems based on weak interactions between the molecular units. Indeed, the construction of self-assembled systems with multiple levels of organisation is often achieved following a stepwise synthetic strategy relying on the design of a preassembled structural motif that can further self-assemble into more complex nanostructures through additional non-covalent interactions.[61,62] These hierarchical self-assemblies of supramolecular complexes are at the basis of nanostructured soft materials with multifunctional properties for material science.[11] Besides the formation of crystalline POM-based coordination networks, the elaboration of supramolecular

coordination complexes containing POMs is thus particularly attractive to develop hierarchically organised species that could be at the basis of future soft multi-functional material with emergent properties.

A considerable number of POM-supported transition metal complexes have been obtained by reaction of POMs with either mixtures of transition metal salts and organic ligands or with pre-formed metal–organic compounds. Such reactions most often lead to unpredictable results with the notable exception of some POM-based metal–organic frameworks (POMOFs),[63,64] or ionic crystals.[65] In contrast to those mentioned above, there have been relatively few reports of the synthetic strategy of metal coordination to chelating ligands on a pre-formed covalent POM hybrid. This approach can enable effective control in the preparation of supramolecular architectures, ranging from discrete nano-oligomers to coordination polymer frameworks and macroions, by fine-tuning in the POM hybrid design, selection of the metal linker and the reaction conditions. The plan of the following section will be oriented according to the topology of the hybrid ligand and that of the metal linker, which are crucial parameters to determine the nature of the resulting supramolecular assembly.

3.1.1 Ditopic ligands with linear (160–180°) geometries. Hybrid POMs that possess two chelating sites with a coordination vector close to 180° have been mostly associated to linear metal acceptors, leading to the formation of linear coordination polymers. Most common reports use ditopic Anderson–Evans or Lindqvist platforms that can display suitable 180° coordination vectors. Additionally, although less widely reported, bisphosphonate functionalised Dawson hybrids can also be expected to direct assembly of near linear coordination chains due to the high angle (~160°) between the grafted organophosphonate moieties at a single lacunary site. This linearity, maintained in hybrid structures functionalised by chelating ligands, has directed the assembly of various 1D coordination polymers, 2D layered architectures and 3D frameworks with a huge variety of transition metal cations. One of the earliest reported examples was the coordination of Pd^{II} with an amido-pyridyl Anderson hybrid $[MnMo_6O_{18}\{(OCH_2)_3CNHCO\text{-}4\text{-}Py\}_2]^{3-}$ by Hasenknopf and co-workers.[66] Rather than a crystalline material, they obtained a birefringent gel upon addition of methanol and aging of the solution.

In a study comparing the coordination of four metal cations – Mn^{II}, Co^{II}, Ni^{II} and Zn^{II} with a bis-capped hexavanadate, Hill and co-workers reported almost isostructural 3D networks assembled for all, comprising polymer chains linked by H-bonding pyridyl and coordinated solvent moieties.[67] The group later prepared a carboxylate terminated oxocluster analogue, which, when coordinated to Tb^{III} ions in the presence of an organic linker, 4,4′-bis(pyridine-*N*-oxide), assembled into a porous 3D network that displayed catalytic activity in aerobic oxidation.[68]

Coordination networks demonstrating magnetic properties were built from the complexation of 2,6-bis(pyrazol-1-yl)pyridine (bpp) functionalised Mn-Anderson oxoclusters, $[MnMo_6O_{18}\{(OCH_2)_3CNHCO\text{-}(bpp)\}_2]^{3-}$, with Fe^{II},[69] by altering

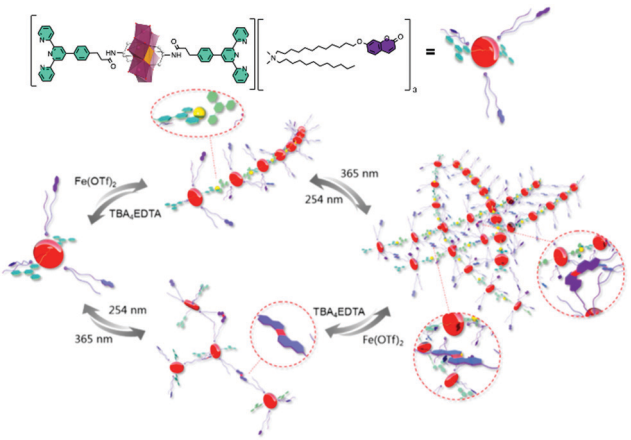

Fig. 2 Schematic illustration of the elaboration of supramolecular polymer *via* orthogonal self-assembly strategy combining metal coordination and photo-cross-linking. This figure has been adapted from ref. 70 with permission from the American Chemical Society, copyright 2019.

the stoichiometry of the metallic cation. A coordination polymer material formed with equimolar Fe^{II}, which demonstrated significant spin-crossover photoconversion (*ca.* 8%), although its structure could not be sufficiently characterised. A crystalline cationic 2D network was isolated, however, when Fe^{II} was added in excess. In the latter compound, two additional Fe^{II} centres were shown to be coordinated to each POM *via* the oxo-ligands, and with complexed solvent in place of a second bpp. Yet, no significant spin conversion was observed in this compound as a result of the weaker coordination sphere around the Fe^{II} centres in comparison to the bis(bpp) complex. The authors also suggest that some sensitivity to intermolecular arrangements, regarding the nature of counterions and labile solvent molecules in the materials, limited spin transition.

More recently, a more complex covalent terpyridine hybrid system demonstrated orthogonal chelation and photo-cross-linking into a multi-responsive supramolecular polymer.[70] The coordination of 1 to 1.2 eq. Fe^{II} to the hybrid POM and subsequent formation of gels or fibres was shown to be reversible using a competitive ligand, EDTA. An additional reversible pathway to polymerisation by the photo-dimerisation of a coumarin-terminated quaternary ammonium surfactant in place of the Mn-Anderson oxocluster cations could be used separately or together with coordination to tune supramolecular polymerisation (Fig. 2).

Covalently bonded Pt^{II} and Hg^{II} acetylide units connected to bisphosphonate functionalised Dawson derivatives forming oligomeric hybrids were reported by Liu, Li, Wong and co-workers.[71,72] The oligomeric compounds, processed as thin films by the Langmuir-Blodgett technique, displayed photoelectric properties. Interestingly, oligomer chains of a comparable length comprising five repeating organometallic units were observed according to MALDI-TOF experiments for both the Pt^{II} and Hg^{II} materials.

Hybrid POMs with *ca.* 180° ligand coordination vectors have also been associated to metal acceptors with higher connectivity. The formation of porous POM-based organic frameworks by

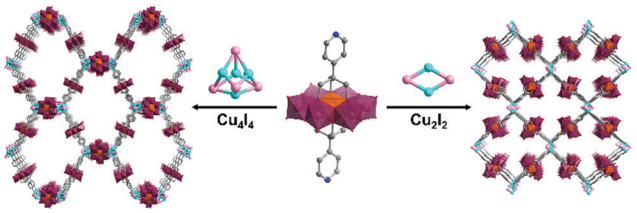

Fig. 3 Structures of the POM-based crystalline organic frameworks associating bis pyridyl Anderson hybrids connected to a Cu_xI_x halide cluster. This figure has been adapted from ref. 73 with permission from John Wiley and Sons, copyright 2016.

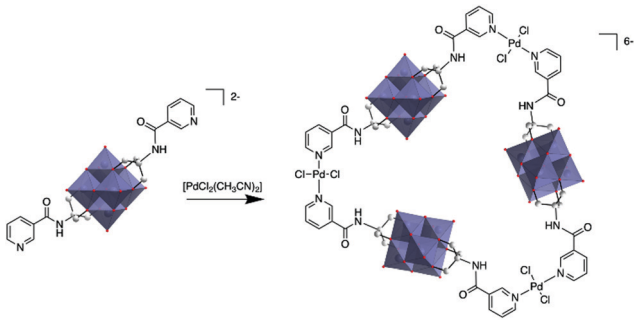

Fig. 4 Synthesis of a POM-based trimer from a bis(pyridine-trisalkoxo)-hexavanadate anion and *trans*-$[PdCl_2(CH_3CN)_2]$. This figure has been adapted from ref. 80 with permission from the Royal Society of Chemistry, copyright 2012.

reaction of the ditopic bis-pyridine Mn-Anderson POM hybrid with CuI was reported by Yang and co-workers.[73] This reaction yielded two kinds of crystalline oxocluster organic framework differing by the nature of coordinating cuprous iodide cluster (Cu_xI_y) formed *in situ*. Cu_4I_4 and Cu_2I_2 halide clusters, which were obtained by varying the synthetic conditions, were shown to link to four remote pyridine ligands in tetrahedral and square planar geometries respectively, allowing the construction of an interpenetrated anionic diamondoid structure and a 2D anionic layer (Fig. 3).

Using similar bis-pyridine terminated ditopic Anderson hybrids, Forgan and co-workers explored several design considerations for the elaboration of coordination framework materials. In addition to the reaction conditions, the combination of metal cations, co-ligands, and the nature of the remote pyridyl ligand capping the Mn-Anderson oxocluster, were varied to serendipitously isolate six kinds of structural frameworks.[74]

The pyridyl N-position has also been explored as a directing factor in a recent study reported by Guo, Wang and co-workers. The authors showed that while two 2D coordination polymers were obtained by reaction of $[Cu(PPh_3)_2(CH_3CN)_2]ClO_4$ with $[MnMo_6O_{18}((OCH_2)_3CN{=}CH\text{–}3\text{-}Py)_2]^{3-}$ using different molar ratios between the POM hybrid and Cu complex, only one structure, a 1D double chain, was obtainable using the (4)-pyridyl terminated analogue hybrid.[75] In all structures, Cu^I centres were similarly coordinated to one pyridine function and a terminal oxygen atom of an adjacent oxocluster. Metal-directed assembly has also been demonstrated using octamolybdates that were previously functionalised with amino acids (proline and lysine). Carboxyl or amino binding sites on proline or lysine moieties were coordinated with Cu^{II}, Zn^{II} and Co^{II} cations to form a range of extended framework structures, some with antitumor selectivities.[76]

3.1.2 Ditopic ligands with perpendicular/acute (60–90°) geometries. When the coordination vector is considerably lower than 180°, discrete species (*e.g.*, metallomacrocycles, coordination cages) are likely to be obtained since formation of such species is thermodynamically favourable.[77,78] Thus, the reaction of ditopic hybrids displaying a 60–90 degree coordination vector with a linear metal linker generally forms discrete species rather than coordination polymers. Hybrid POMs displaying such ditopic topology can be obtained with organoimido hexamolybdates, bis-capped hybrid hexavanadate and bis-organosilyl derivatives of monovacant Keggin or Dawson POMs which display coordination vectors of 60° and 90° upon functionalisation with an appropriate remote ligand.

The first example of the metal-driven self-assembly of a ditopic hybrid displaying 90° coordination vector is reported by Peng and co-workers.[79] They observed the precipitation of a Fe^{II} bis-terpyridine hybrid after the coordination of Fe^{II} to a hexamolybdate hybrid. The low solubility of the supramolecular species was due to the neutralisation of the POM charge by the metal linker, which precluded its further characterisation. The authors also proposed the plausible formation of cyclic oligomers but could not go deeper in the investigation of the supramolecular species.

The first characterisation of a metallomacrocycle by metal coordination of a hybrid POM was reported by Hasenknopf and co-workers.[80] In this study they used a bis-capped hybrid hexavanadate that was post-functionalised with two remote pyridine ligands at the metal position, forming a 60° coordination vector. Upon reaction with 1 equiv. *trans*-$[PdCl_2(CH_3CN)_2]$, they managed to isolate a molecular triangle comprised of three POMs and three metal linkers and characterised it by combination of DOSY NMR and mass spectrometry (Fig. 4).

Izzet and co-workers then reported several similar metal-directed cyclic oligomers from organosilyl derivatives of POMs (for which the angle between the two arms is *ca.* 90°) using the same ligand (pyridine) and metal linker (*trans*-$[PdCl_2(CH_3CN)_2]$).[81,82] They characterised the resulting supramolecular species by combination of DOSY NMR, mass spectrometry and SAXS. SAXS is a powerful technique to characterise structures of large synthetic molecules, molecular assemblies, nanoparticles[78] and aggregates with sizes ranging from 1 to 100 nm.[77,83] This technique is particularly well-suited to characterise nanosized metal–oxo clusters assemblies.[84–86] In order to understand the thermodynamics of the formation of the discrete metallomacrocycle, they compared the self-assembly behaviour of two analogue ditopic building units differing by the nature (and hence the charge) of the POM (*i.e.* a Keggin and a Dawson). While Dawson-type hybrids selectively led to the formation of molecular triangles, the same reaction with Keggin-type analogues provided a mixture of molecular triangles and squares. These studies outlined the decisive effect of the charge of the POM disfavouring the formation

of large assemblies probably owing to an important entropic contribution. This was confirmed by an isothermal titration calorimetry (ITC) experiment that confirmed the stronger association in the case of the Keggin hybrids. They also showed that the formation of the cyclic assembly was a noncooperative process, since the entropic term was not compensated by the chelate effect. They also observed that while the POM-based molecular building block and related coordination oligomers displayed different shapes, a power law between the diffusion coefficient D and the molecular mass M was applicable to this series of hybrids,[81] indicating that the diffusion coefficient of these compounds was mainly determined by their occupied volume rather than by their shape. Izzet and co-workers also used the Dawson organosilyl platform functionalised with remote terpyridine ligands to study the metal driven self-assembly in the presence of cationic metal linkers. In the presence of 1 equiv. of divalent cations (Fe^{2+} or Co^{2+}),[87,88] they observed the formation of discrete metallomacrocycles in a highly dissociating solvent (*i.e.* DMSO). While the formation of molecular triangles was initially postulated,[87] the authors concluded that a mixture of molecular triangles and squares was more likely.[88] By contrast to the self-assembly in the presence of neutral "$PdCl_2$" metal linker, which only afforded discrete species, the presence of charged subunits in the metallomacrocycle (POM and metal linker) can drive their aggregation, which results from a competition between the solvation energy of the discrete species and intermolecular electrostatic interactions. Consequently, in a less dissociating solvent (MeCN) or a protic solvent (H_2O), the primary supramolecular structures that combine negatively charged POMs and cationic metal linkers, further self-assembled through intermolecular electrostatic interactions in a reversible process. The solvent composition and the charge of the metal linker were found to be key parameters that steer the supramolecular organisation. Different types of hierarchical self-assemblies, zero-dimensional (0D) dense nanoparticles, and 1D worm-like nanoobjects, could be selectively formed owing to different aggregation modes of the metallomacrocycles (Fig. 5). Similar worm-like nanoaggregates were also formed in the presence of H_2O and displayed promising molecular carrier properties with a polyaromatic guest.

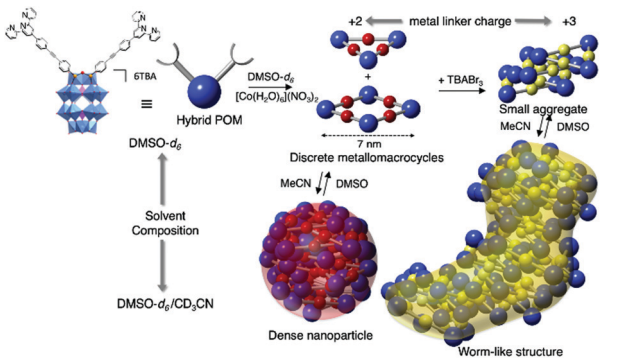

Fig. 5 Schematic representation of the formation of nanosized aggregates by hierarchical metal-driven self-assembly of a bis-terpyridine terminated hybrid POM according to the solvent composition and the metal linker charge. This figure has been adapted from ref. 88 under Creative Commons Licence 4.0 (CC-BY-NC-ND).

As ditopic organosilyl derivatives of POMs afforded mixtures of triangle- and square-shaped secondary building units upon reaction with a linear metal linker, some mismatches and defects in the stacking of the metallomacrocycles occurred, which can in part explain the formation of the worm-like structures. Following their initial work, Izzet and co-workers investigated the self-assembly of a bis-pyridine terminated Keggin hybrid with a cationic 90° Pd(II) acceptor, since a unique type of square-shaped metallomacrocycle (containing two hybrid POMs and two Pd nodes) could be formed using this strategy.[89] Again, in DMSO only discrete species were observed which formed hierarchical species upon solvent change. Strikingly different hierarchical assemblies were then observed, with the dimeric cycle organising into either branched worms-like structures or multi-layer vesicles dependent on the nature of the solvent.

Singly-organofunctionalised hybrid POMs have also be used as building blocks, forming dumbbell-like species in the presence of a linear metal linker. Following their initial work with ditopic hybrids, Izzet and co-workers reported the aggregation of dumbbell-shaped polyoxometalate hybrids, using organotin derivatives of monovacant Keggin- or Dawson-type POMs terminated with a remote terpyridine function.[90] They observed the formation of dumbbell-like species in DMSO and showed using ITC that the metal coordination to the POM-based building unit was reinforced by coulombic interactions between the POMs and the metal linker and counter balanced by an entropic cost associated to the POM (the entropic contribution being higher for the Dawson than for the Keggin). They also evaluated the effect of the nature of the POM (Keggin *vs* Dawson) and the charge of the metal linker (2+ and 3 +) on the aggregation of the dumbbell species. In MeCN, they characterised by SAXS the formation of nanostructured aggregates of different sizes according to the nature of the POM and the charge of the cobalt linker and concluded that aggregation was favoured (bigger size and shorter POM–POM distances) when the charge of the metal linker approached that of the POM. They also observed the formation of organogels retaining some nanostructuration of the aggregates in the presence of EtOH owing to a low solvation energy in this solvent. They showed that the redox state and the nano-organisation of the gels could be photoswitched, providing potentiality to these compounds as redox-responsive smart materials. Finally, molecular dynamics simulations combined to DFT calculations corroborated that the dumbbell-like species can aggregate according to the solvent composition. Interestingly, the computational results outlined the non-innocent role of the TBA counter ions in the aggregation process (Fig. 6).

Several single-side functionalised oxoclusters have demonstrated directed assembly into complex supramolecular assemblies using higher connectivity metal acceptors. Yang and co-workers used a monopyridyl-terminated Anderson-type oxocluster $[CrMo_6O_{18}(-OH)_3\{(OCH_2)_3C-4\text{-}Py\}]^{4-}$ building unit

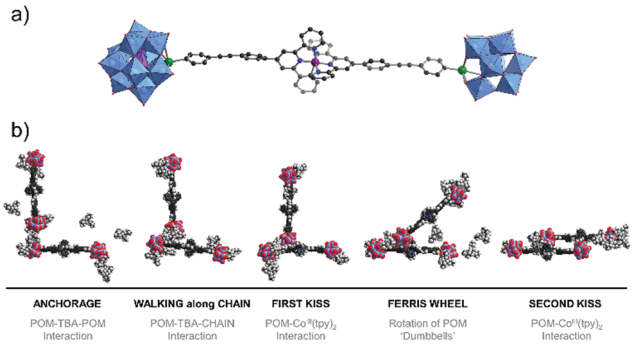

Fig. 6 Molecular dynamic study of Keggin-type organotin dumbbell-like species in H_2O outlining the role of the TBA counter-cations in the aggregation process (Sn = green spheres, Co = purple sphere). This figure has been adapted from ref. 90 with permission from the Royal Society of Chemistry, copyright 2020.

to develop different crystalline frameworks by metal coordination.[91] Upon reaction with CuI they obtained a cube-like nanocomposite structure, which differed from their coordination frameworks made with a ditopic Anderson hybrid.[73] An uncommon octanuclear $[Cu_8I_6]^{2+}$ halide cluster was formed around which eight hybrid POMs were coordinated by the terminal pyridine ligand. Furthermore, the nanocomposite compound itself self-assembled *via* H-bonding into a crystalline 3D porous supramolecular framework, in which large tetragonal channels were constructed from effectively edge-sharing octahedron-like cages comprised of 16 macroclusters (Fig. 7).

A mono-carboxylate functionalised hexamolybdate, $[(Mo_6O_{18})NC_6H_4\text{–}4\text{-}COOH]^{2-}$, assembled into a tetrameric species with a paddle-wheel formation upon coordination with Cu^{II}, in which two metal ions resided in the centre. Liu, Wang, Wei and co-workers demonstrated their hierarchical assembly as a

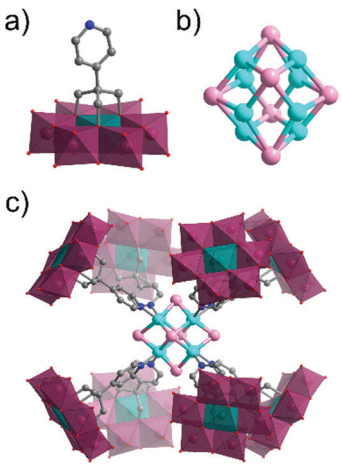

Fig. 7 Structure of the monotopic Anderson–Evans-type metal halide cluster, highlighting: (a) the $\{CrMo_6\}$ hybrid POM building block ($\{CrO_6\}$ = teal green octahedra); (b) the Cu_8I_6 metal halide core and; (c) the assembled octameric nanostructure. This figure has been adapted from ref. 91 with permission from the American Chemical Society, copyright 2016.

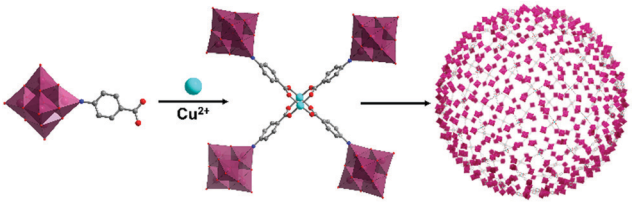

Fig. 8 Model of the electrostatically assembled "blackberry" structure formed by the self-assembly of tetrameric hexamolybdate hybrids. This figure has been adapted from ref. 92 with permission from the American Chemical Society, copyright 2013.

secondary building unit into large "blackberry" structures (Fig. 8).[92] The formation and size of the latter could, to some extent, be tuned by adjusting the polarity of the solvent composition. Blackberry size was in fact found to depend linearly on solvent dielectric constant ($1/\varepsilon$), within a certain polarity range. Outside this polarity range, too low or too high surface charge of the tetrameric species prevented the aggregation due to unfavourable electrostatic interactions.

3.2 Hybrid POM amphiphiles

In solution, self-assembly of large and charge-delocalised polyanionic POMs can be triggered by their association with hydrophobic tails, *i.e.* long alkyl chains. Early strategies relied on the exchange of charge balancing counterions by cationic ammonium surfactants. This electrostatic approach historically led to the emergence of a family of core–shell like assemblies, called surfactant-encapsulated-POMs (SEPs). Driven by solvophobic interactions, these SEPs can self-assemble at the air/water interface to form Langmuir–Blodgett films as optical or catalytic materials,[93,94] while in solution they may form nanostructures such as vesicles and onion like spheres by controlling the solvent polarity.[95] The field of SEPs has been widely explored by Kurth and Wu and recently reviewed.[96] A main drawback associated to this electrostatic approach is the formation of compounds that display poor solubility in aqueous solutions. Keggin-type polyoxometalates when combined to amphiphilic cations have been reported to preferentially form POM-based nanoparticles able to stabilise Pickering type emulsions in water–oil mixtures.[97] Bauduin and co-workers also reported that POM-surfactant may spontaneously form in water through self-assembly of Keggin type anions and non-ionic surfactant leading to micelles containing POMs at the interface.[98] Such unexpected self-assembly process has been associated to the tendency of POMs as super chaotropic anions to adsorb on hydrophilic neutral surfaces. As fascinating these results are, the lack of solubility in water restricts the scope of their potential applications.

The alternative approach consists in chemically grafting hydrophobic tails through covalent linkage to POM scaffolds, through either direct or post-functionalisation paths. This leads to a class of POM-based surfactants that is commonly called covalent amphiphilic POM–organic hybrids. While being more sophisticated and requiring multistep synthesis as explained in former sections, this procedure allows the development of

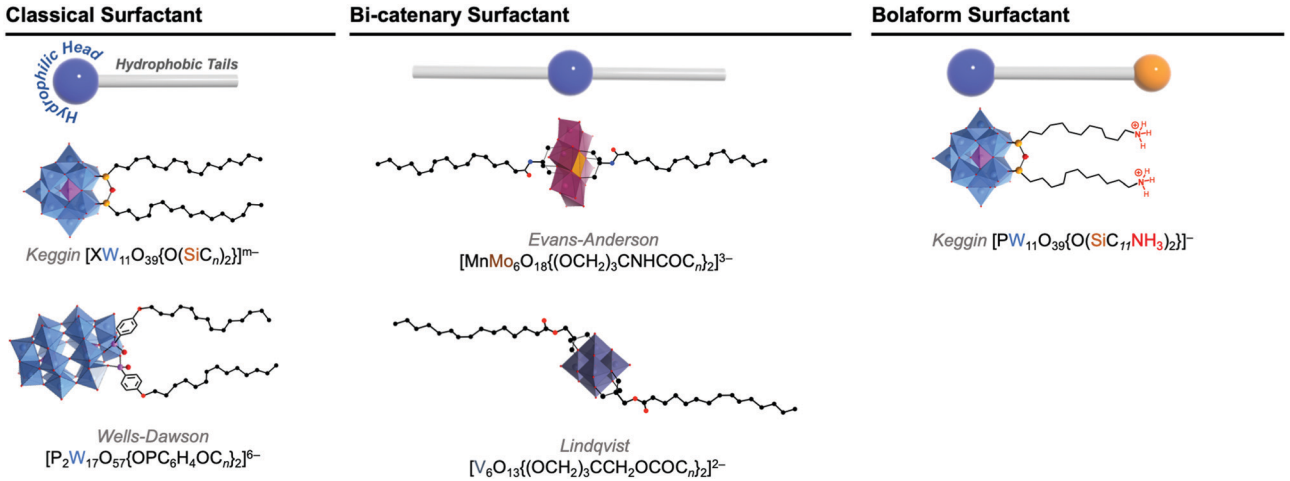

Fig. 9 Molecular structures of some representative amphiphilic POMs and their comparison to: classical 'head–tail'-type surfactants, bi-catenary-type surfactants, and bolaform type surfactants.

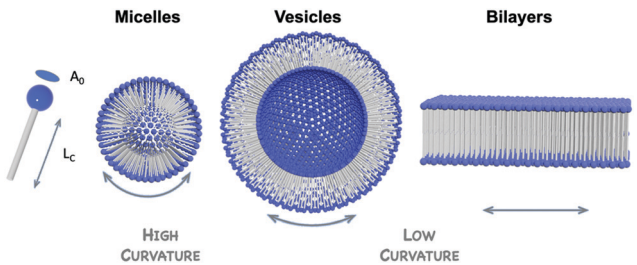

Fig. 10 Schematic highlighting the common structures of amphiphilic hybrid-POM supramolecular assemblies, which depend on both the shape of the POM-surfactant and the packing parameter (defined as $P = V/(A_0L_C)$, where V represents the volume occupied by the hydrophobic tails, A_0 the area of the polar head and L_C the length of the hydrophobic tails).

tailor-made amphiphilic POMs by controlling the number and the relative orientation of the hydrophobic chains, as sketched in Fig. 9. This variety of functionalisation produces a very unique family of POM-based surfactants containing polar heads that are adjustable in size, charge and shape and allows controlled self-assembly formation as a function of the packing parameter, a characteristic number related to the shape of one single surfactant molecule (Fig. 10).[99,100] Another key point brought by the covalent approach is to enable the substitution of alkaline cations (or even protons) for the conventional bulky ammonium, thus improving the hydrophilicity of the POM polar head and increasing water solubility (*i.e.* increasing the critical aggregation concentration, CAC). While covalent POM-based surfactants have already been the subject of several reviews,[22,99,101] the next sections aim to emphasize the peculiarities of the POMs as a large inorganic polyanionic head in the self-assembly processes and to highlight recent results in which self-assembly of POM surfactants provided new opportunities to produce nanofunctional materials with potential to transfer POM properties to the supramolecular domain. As with any smart materials, the challenge is to organise these inorganic objects into supramolecular structures with long-range order; allowing preparation of micellar structures or fibers with potential as nanocatalysts, or switchable materials.

3.2.1 Synthetic strategies. Although many hybrid POMs can be considered as amphiphiles, their assembly behaviours are heavily dictated by their associated cations. For synthetic convenience, hybrid POMs are usually prepared as tetra-alkyl ammonium salts (*e.g.*, tetrabutylammonium, TBA). The cations are prone to strongly associate with the POM polar head, significantly reducing its hydrophilicity. In such cases, the self-assembly of covalent amphiphilic hybrid POMs is a very slow process[102] that can be triggered by increasing solvent polarity, which weakens the association between the ammonium cations and the POM.[103,104] Following this procedure, the formation of a large numbers of complex supramolecular assemblies such as vesicles[102,105] reverse vesicles[106] or nanofibrils of several micrometres at the solvent/air interface[104] were reported when using POM amphiphiles based on Anderson–Evans-type POM or Wells–Dawson or bolaform inorganic–organic–inorganic hybrids. In these systems the polarity of the solvent mixtures (acetone/water for example), hydrocarbon chain length and shape of organic linkers are multi-factors that have major influences and drive the self-assembly of the aggregates, in terms of size and shape.[106–108]

Alkaline counter ions are also playing a crucial role, not only in screening the charge of the POMs, but also in displaying specific interactions.[109] The attractive electrostatic forces between POMs and these counterions are actually involved in the formation and stability of self-assembled structures, be they organised monolayers on planar surfaces or nanoparticles, or "blackberry" structures.[110–112] Substitution of protons or alkali counterions for quaternary ammoniums in covalent amphiphilic hybrid POMs has therefore rapidly emerged as a privileged method for amplifying the dipolar character of the POM surfactants, favouring the self-assembly kinetics and promoting micellisation and emulsifying properties.

A relevant example has been reported by Wang and co-workers. The authors depicted the preparation of a triol-functionalised

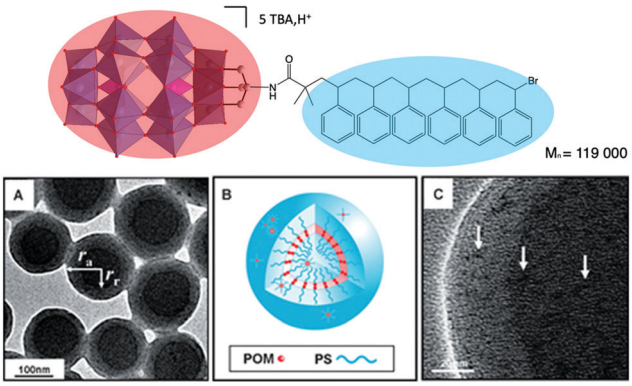

Fig. 11 (Top) Molecular structure of a POM–polystyrene hybrid; (bottom) representations of its vesicular aggregates, showing: (a,c) high-resolution TEM images and, (b) a schematic representation of the vesicle. This figure has been adapted from ref. 114 with permission from John Wiley and Sons, copyright 2012.

mixed-addenda Wells–Dawson $[P_2W_{15}V_3O_{59}\{(OCH_2)_3C–R\}]^{9-}$ bearing an ATRP initiator group, from which polymerisation of styrene was initiated.[113,114] The reaction led to a well-defined POM–polystyrene hybrid (Fig. 11). Upon proton exchange for TBA, the DMF solution became opaque revealing the amphiphilic character of the H^+–POM–polystyrene compound, which displayed supramolecular assembly into vesicular aggregates. TEM and SEM analysis allowed to determine that the aggregate structure is similar to a reversed vesicle, the POM polar head being located in the middle of the membrane, which size varies from 150 to 350 nm depending on the experimental conditions.

The formation and size of vesicles is triggered by the nature of the counterions. This has been highlighted by two independent reports by the groups of Wei and Hill. In 2011, Wei and co-workers reported the preparation of $[V_6O_{13}\{(OCH_2)_3CCH_2OOC(CH_2)_{16}CH_3\}_2]^{2-}$ by covalently grafting two C_{18} chains through esterification reaction between stearic acid and a triol-functionalised hexavanadate cluster (Fig. 9).[103] As a TBA salt this amphiphilic POM self-assembles into vesicles only when water is added to acetone solutions (R_H = 180–220 nm) whereas the proton and sodium derivatives, prepared by ion-exchange chromatography, readily self-assemble in pure aqueous solutions into vesicles of much smaller sizes (R_H = 57 nm and 55 nm respectively).

The assemblies display remarkable fluorescence properties and the origin of the emission is thought to involve an emissive state derived from a ligand to metal charge transfer (LMCT). The authors speculated that the exchange of cations triggers a structural change in the self-assembly, with an increased interaction between the POM heads resulting in an increase of the fluorescence intensity. Although POMs are known to be luminescence quenchers due to their ability to readily store electrons, the study of these assemblies using fluorescence microscopy revealed that the intensity did not decay over time demonstrating a high stability compared to organic fluorophores that undergo photo-bleaching when exposed to UV light. The effect of the cation on the packing structure and fluorescence profile of hybrid POM vesicles was also nicely

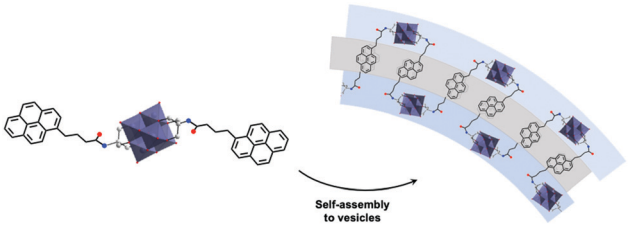

Fig. 12 The molecular structure of a hexavanadate hybrid cluster bearing two pendant arms functionalised by pyrene groups showing the proposed arrangement of the vesicular structures it forms in solution. This figure has been adapted from ref. 115 with permission from the American Chemical Society, copyright 2011.

exemplified by Hill and co-workers when studying similar Lindqvist type hexavanadate clusters functionalised by pyrene fluorescent groups (Fig. 12).[115] The presence of two pyrene moieties led to smaller assemblies (R_H =50 nm) in H_2O/DMSO (80 : 20 v/v) mixture as a result of additional bending energy required, which led to increased curvature in the packing. The fluorescent profile of the pyrene groups was employed as a useful tool to investigate the molecular packing within the superstructure. Changes in the pyrene fluorescence were notably observed when TBA cations were exchanged for protons, which induced the formation of smaller aggregates (R_H = 30 nm), as a result of a decrease of alkyl chains in the hydrophobic layer of the vesicles. Hill *et al.* observed the formation of an excimer fluorescence peak (480 nm) that is ascribed to the close packing of two pyrene molecules. This unique result was further tested by varying the pH of the solution where a decrease in R_H was observed with increasing pH, the process being reversible. The works of the groups of Wei and Hill demonstrate interesting luminescence properties associated with the self-assembly of amphiphiles hybrid POMs in solution. The combination of the photo-activity and controlled self-assembly displays great potential to fabricate state-of-the-art photo-active colloidal materials.

In 2012, Polarz and co-workers reported an original bolaform surfactant bearing a Keggin-type POM and an antipodal positively charge ammonium group connected by a hydrophobic spacer.[116] The asymmetric size of the polar heads creates highly curved interfaces leading to the formation of monolayer membrane vesicles in water with unusually small diameter (15 nm). The authors also reported that the membrane of the vesicle is highly impermeable favoring the encapsulation of hydrophilic or ionic compounds in the confined aqueous nanophase.

The bi-catenary POM hybrids based on Anderson–Evans and Lindqvist oxoclusters and the bolaform-type hybrid POMs displayed structures that are not well suited for the formation of micelles. Special interests have therefore also been devoted to POM surfactants whose shapes are more related to classical surfactant sodium dodecyl sulfate (SDS). These compounds exhibit an anionic polar head, alkali-metals counter ions and long alkyl chains directed on one single side. An elegant study has been nicely detailed in the case of double-tailed surfactant derived from monovacant Keggin anions $[XW_{11}O_{39}]^{q-}$.

A pioneering work by Chambers *et al.* in 2003 detailed the ability of the bis(silyl) derivative $[SiW_{11}O_{39}\{O(SiC_{12}H_{25})_2\}]^{4-}$, as tetrabutylammonium salts, to reversibly form thin monolayers at the air/water interface by using Langmuir–Blodgett technique.[117] This work highlighted the fact that such covalent amphiphilic POMs are robust and gave an impetus to further studies in the field. Polarz and co-workers prepared alkaline (Na^+, K^+) and acid derivatives of the analogous $(TBA)_3[PW_{11}O_{39}\{O(SiR)_2\}]$ by postpreparative ion-exchange chromatography in order to study their aggregation in water. Using X-ray reflectivity studies, Polarz and co-workers confirmed that the interfacial self-assembly of these bi(silyl) derivatives in the LB films was driven by the packing of the polar heads in a hexagonal lattice, whereas the hydrophobic tails did not relevantly contribute to the overall process, an unusual behavior for surfactants.[118] More importantly, these authors reported the formation of lyotropic liquid crystalline phases, whose structures depend on the alkyl chain lengths and counterions associated with POM surfactants: while an hexagonal phase of packed cylinders is obtained with sodium as counterions, the acid salt leads to a lamellar structure (see Part 3.3.1. for more details). By studying aqueous solution at lower surfactant concentration, Polarz *et al.* also observed the formation of micelles, whose sizes scale with the length of the alkyl chain (based on DLS and SAXS measurements). The authors finally demonstrated that this class of POM surfactant could act as emulsifying agents, *i.e.* decreasing surface and interfacial tensions.[119,120] These results again highlighted the crucial role played by the nature of the counterions in the kinetics of aggregate formation in solution.

The structure of the aggregates formed in solution also strongly depends on the geometry of the surfactant in its complete environment, which can be described by using the packing parameter *P*.[101] To this respect amphiphilic POMs are very uniquely polarisable agents with a charge/volume ratio at the polar head that can be modified without changing the overall shape of the surfactant. Polarz and co-workers extended their series of POM surfactants $[XW_{11}O_{39}\{O(SiC_{16}H_{33})_2\}]^{n-}$ to X = Si(IV) and B(III) and as a consequence n = 4 and 5 respectively. Unusual self-assembled structures such as a new type of micelle with dumbbell shape was reported in the case of higher charged POMs. Such structuration was tentatively attributed by the authors to the presence of stronger repulsive electrostatic while the contribution of attractive, hydrophobic (van der Waals) interactions remains constant (same size and shape of the hydrophobic tails).[121]

In 2014, Proust *et al.* also reported the preparation of double-tailed POM surfactants $TMA_3K[\gamma\text{-}SiW_{10}O_{36}(C_nH_{2n+1}PO)_2]$ (TMA = tetramethylammonium) based on the divacant $[\gamma\text{-}SiW_{10}O_{36}]^{8-}$ anion (Fig. 13).[122] Proton and alkaline cations can substitute TMA in these systems using a cation-exchange resin leading to water soluble derivative $A_4[\gamma\text{-}SiW_{10}O_{36}(C_nH_{2n+1}PO)_2]$ (A = K, Na, H). SWAXS measurements on water solutions of $A_4[\gamma\text{-}SiW_{10}O_{36}(C_{12}H_{25}PO)_2]$ allowed estimation of the critical aggregation concentration and, in combination with DOSY NMR, indicated the formation of micelles with an aggregation

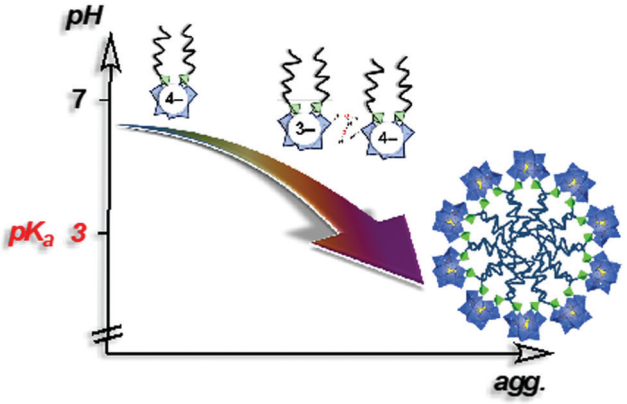

Fig. 13 Schematic showing aggregation as a function of the pH in a 10 mM aqueous solution of $K_3H[\gamma\text{-}SiW_{10}O_{36}(POC_{12}H_{25})_2]$ (>CMC).[122]

number $n_{agg} \approx 33$ and a hydrodynamic radius R_H = 1.8 nm.[123] A peculiarity stems from the presence of a proton as counter ion in the potassic derivatives $K_3H[\gamma\text{-}SiW_{10}O_{36}(OPC_nH_{2n+1})_2]$ making these amphiphilic POMs weak acids (pK_a of 3.0). As a result, the apparent negative charge was found to be pH dependent, strongly affecting the self-assembly process. A 10 mM solution of $K_3H[\gamma\text{-}SiW_{10}O_{36}(OPC_{12}H_{25})_2]$ (>CAC) resulted in a pH of 2.6 and formation of micelles was observed by NMR. Increase of the pH forced a disassembling process to monomers due to the increase of the apparent negative charge and consequently an increase of the CAC (Fig. 13). Note that special attention should always be addressed to the stability of the covalent amphiphilic POMs in aqueous solution. Whereas highly basic pH conditions are known to promote the disassembly of the polyoxometalate framework, highly acidic conditions may also catalyze the chemical degradation of the W–O–P linkage, a mixed anhydride of tungstic acid and phosphoric acid, hence sensitive to hydrolysis. Overall, the formation of micelles when using these bis(silylated) or bis(phosphonylated) POM derivatives, which are related to SDS structures, reveals the low packing parameter (less than 1/3) exhibited by these POMs surfactants that is consistent with a large polar head and a rather low volume of hydrophobic tails, thus exhibiting a cone-like shape.[100] The emulsifying ability of this series of POM surfactants opened the scope of applications to catalytic reactions in complex media.

3.2.2 Engineering POMs at interfaces for catalysis. Catalysis represents an important application of POMs, mostly referring to acid catalysis due to the superacidity of heteropolyacids and to oxidation catalysis, based on intrinsic redox properties of POMs or the incorporation of active transition metal cations.[124,125] It therefore appeared very attractive to combine the catalytic properties of POMs with those of a surfactant. Such an approach can bring several advantages together, namely (i) formation and stabilisation of controlled nanoscale structures, including emulsions and microdispersed media, (ii) increase of POM concentration at interfaces and thus (iii) improvement of catalytic activity. A common methodology has been the association of quaternary ammoniums with metalates,[126,127] peroxometalates[128–130] and

polyoxometalates[131–133] to carry out oxidation reaction in liquid–liquid biphasic media through phase transfer catalysis. Early in 1994, Neumann and co-workers suggested that the use of quaternary ammoniums behaving as surfactants (such as hexadecyltrimethylammonium or dioctadecyl dimethylammonium cations) actually promotes rather stable water in oil emulsion (3–4 h until separation) in which well-known Venturello peroxometalate $\{PO_4[W(O)(O_2)_2]_4\}^{3-}$ anion[128] concentrates at the internal side of the interface producing an enhanced catalytic activity in oxidation reaction.[129] The same research group also reported that Keggin-type POM, such as $H_3PMo_{12}O_{40}$ and $H_5PV_2Mo_{12}O_{40}$, self-organise into nanoparticle using cesium SDS micelles as template. When heterogenised on hydrophilic silica these clustered assembly of polyoxometalates showed superior catalytic activity to non-aggregated polyoxometalates in the aerobic oxidation of sulfides.[134] Nardello-Rataj and co-workers reported later on that Keggin type polyoxometalates when combined with surfactant cations preferentially form POM-based nanoparticles able to stabilise emulsions (called Pickering type emulsions) as catalytic oxidizing reaction media able to perform oxidation of a large family of terpenic substrates using eco-friendly solvents and with high recyclability.[135]

Design of amphiphilic hybrid POMs reported in Fig. 9 was also driven by their use as a catalytic surfactant able to (i) stabilise (micro)emulsion or micelles, and (ii) enhance catalytic activity at the interfaces or in compartmentalised environments. The emulsifying properties of Polarz's POM surfactants $H_3[PW_{11}O_{39}\{O(SiC_{16}H_{33})_2\}]$ have been used in acid-based catalysis for the polymerisation of styrene. Indeed, stable styrene/water emulsions can be prepared and stirring under gentle heating (50 °C) produced white solids containing POM surfactants and polystyrene. DLS and TEM measurements revealed the formation of spherical objects with diameters in the size range 300–350 nm with POM surfactants located on the surface of the polymer particle (Fig. 14a).[119]

The ability of these POM surfactants to fulfill multiple tasks was further demonstrated by Polarz and co-workers.[132] Similarly, $H_3[PW_{11}O_{39}\{O(SiC_{16}H_{33})_2\}]$ was used as a catalytic surfactant for, first, the formation of stable emulsions of octamethylcyclotetrasiloxane in water and, secondly, the acid-catalyzed generation of polydimethylsiloxane (PDMS) upon the addition of $PhSi(OEt)_3$ as cross linker. DLS and TEM measurements of the resulting dispersion confirmed the formation of spherical large nanoparticles (around 155 nm) with narrow size distribution. The dispersion also exhibited high stability for weeks and no leaching of tungstate species or degradation of the surfactant was detected, which was tentatively attributed to the fact that the alkyl chains of the surfactant are tightly buried into the polysiloxane matrix. Of particular interest, Polarz and co-workers also reported that solvent removal allowed to irreversibly assemble a nanoporous network from these particles (Fig. 14b). Since the POM polar heads of the surfactant are still located at the surface of the network, the overall materials are characterised by proton-conductivity inside its channels, which make them promising candidates for applications as membranes in fuel cells.

Double-tailed covalent POM surfactants have also been investigated in biphasic oxidation reactions following the same strategy to both stabilise polydisperse media and catalyze an oxidation reaction using aqueous hydrogen peroxide. From the series of compounds reported by Proust and co-workers, $K_3H[\gamma\text{-}SiW_{10}O_{36}(C_{12}H_{25}PO)_2]$ was shown to provide a Winsor I system (WI) in water–ether mixtures, *i.e.* oil-in-water microemulsion (μem), in equilibrium with an excess of the organic phase.[122] Quantification by NMR spectroscopy clearly confirmed that the amphiphilic POM-based hybrid was mainly localised in the μem phase and 2D heteronuclear chemical shift correlation between ^{31}P and ^{183}W nuclei observed by HMQC experiments proved the structural integrity of the hybrid POM. Distribution of the POM surfactant in the phases can also be ascertained by using small and wide-angle X-ray scattering (SWAXS). The SWAXS results indicate that both diethylether and water coexist as two distinct phases in the solution, as expected in μems, and that the ether droplets of the WI μem have a diameter of *ca.* 5.0 nm (Fig. 15). Stabilisation of a WI type

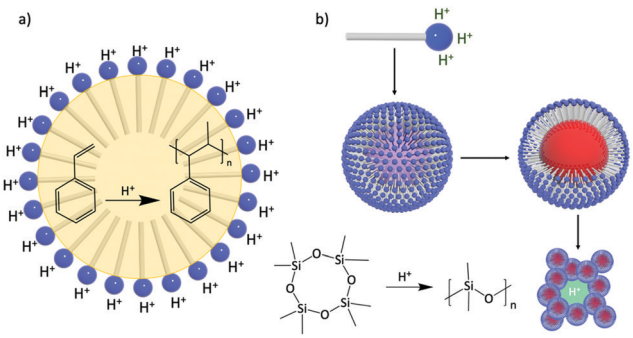

Fig. 14 The catalytic surfactant $H_3[PW_{11}O_{39}\{O(SiC_{16}H_{33})_2\}]$ acts as an emulsifying agent and a catalyst for (a) the acid-catalyzed polymerisation of styrene, and (b) the polymerisation of siloxane to polysiloxane and formation of nanocomposites as promising candidates for proton-conducting materials. This figure has been adapted from ref. 119 with permission from the American Chemical Society, Copyright 2010, and ref. 120 with permission from the Centre National de la Recherche Scientifique (CNRS) and the Royal Society of Chemistry, copyright 2016.

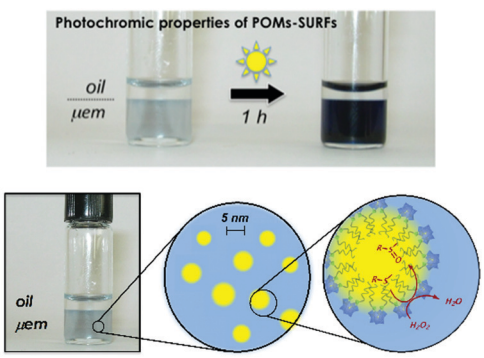

Fig. 15 (a) The partitioning of POM surfactants between the two phases of a WI microemulsion is easily achieved by irradiation with UV or even sunlight; (b) microemulsion is made of 5 nm diameter oil-containing micelles. Adapted from ref. 122 with permission from the Royal Society of Chemistry, copyright 2014.

μem confirms that $K_3H[\gamma\text{-}SiW_{10}O_{36}(C_{12}H_{25}PO)_2]$ belongs to the class of hydrophilic surfactant, *i.e.* with large polar head and a rather small hydrophobic chain. The use of microemulsions for catalysis is particularly interesting since it provides a thermodynamically stable nanostructured phase and an extended oil–water interface (much higher than classical biphasic system)[51] that favors the exchange of reagents and products between the nano-domains. As an example, the WI-type system in Fig. 15 was able to conduct the oxidation of organic sulfide to a sulfone/sulfoxide mixture at room temperature using hydrogen peroxide without demixing phenomenon.

The water soluble sodium and acid derivatives of the bi catenary hexavanadate $[V_6O_{13}\{(OCH_2)_3CCH_2OC(O)C_{17}H_{35}\}_2]^{2-}$ were also used by Liu, Wei and co-workers to stabilise hexane/water emulsions and catalyze the oxidation of thiophene with hydrogen peroxide, as a model reaction for oxidation desulfurisation of diesel.[136] Enhanced catalytic activity was described as a consequence of high concentration of the catalytic surfactant at the water–oil interface. Liu and Wei also reported that the single-tailed hexavanadate–organic hybrid surfactant was able to self-assemble into micelle structures in water solutions, and to further coagulate into a 1D anisotropic structure with high surface area. These hierarchical self-assemblies were reported to be a highly efficient heterogeneous catalyst for the oxidation of organic sulfides.[137] Segregation of reactants in specific nanodomains have been more recently reported by the same authors, who demonstrated that bilayer vesicles formed from double-tailed hexavanadate–organic hybrid surfactant with long alkyl chains were efficient catalysts for the oxidation of TMB (3,3′,5,5′-tetramethylbenzidine) with H_2O_2, a model reaction mimicking a peroxidase activity. The authors claimed that the increase in the oxidation rate of TMB compared to reaction carried out with unassembled systems was promoted by the bilayer self-assembly that create hydrophobic domains that segregate the TMB and favors its accessibility to the hydrophilic catalytic POM head.[138]

3.2.3 Solvent-controlled and photoswitchable systems. The functionalisation of POMs *via* organic linkage creates opportunities to introduce organic fragments exhibiting switchable character. Thus, external stimulus can trigger a modification in the original interaction between the POM hybrid and a change in the aggregation processes. An early report by Wu and co-workers introduced a photo-induced smart-assembly using the hybrid $POM\{MnMo_6O_{18}[(OCH_2)_3CNHCOCH_2C_6H_4NNC_6H_5]_2\}^{3-}$, which was synthesised by grafting a photo-isomerisable azo-benzene moiety to a manganese centred molybdate Anderson POM.[139] As an extension of the surfactant-encapsulated-POMs field, the employment of dimethyldioctadecylammonium amphiphilic cations (DODA) allowed the hybrid molecules to assemble into layered fiber-like assemblies, where azo-benzene moieties were found predominantly in their *trans*-configuration. By irradiating these fibres with UV-light (365 nm), isomerisation to *cis*-configuration resulted in a structural change, from fibre aggregates to spherical aggregates (D = 150 nm). Furthermore, this fascinating photo-induced structural transition displayed high reversibility and a thermally induced *cis–trans* isomerisation was accessed in the dark.

The versatility of this concept was further exploited by the same group to produce photo-switchable materials based on the self-assembly of an organotin-functionalised POM.[140] In this inorganic–organic hybrid system, a propargyl azobenzene moiety was connected using a copper-catalysed Huisgen reaction to a lacunary Keggin-type POM functionalised by an organo-tin chain containing an amido group and terminated by an azido function. The POM-Azo hybrid was prepared as a TBA salt and substitution with protons by an ionic exchange reaction over a silica led to a water-soluble hybrid POM exhibiting amphiphilic character. Spontaneously self-assembly into hollow vesicles with a bilayer structure was demonstrated by dynamic light scattering and transmission electron microscopy (D = 60 nm). Photo-switching of the azobenzene function to the *cis*-configuration upon UV-light irradiation induced a modulation of the POM-Azo assemblies, the regular spherical assembly being transformed into an irregular morphology. *Cis–trans* isomerisation under light irradiation (450 nm) brought the assembly back to regular spherical vesicles, thus proving the dynamic reversible transformation. An expansion of this work, in which the authors extended their photoisomerisation strategy to include the formation of host–guest complexes with cyclodextrin hosts is described in more detail in Section 4.1 below.

In 2016, Mialane, Liu *et al.* reported the synthesis of asymmetrical Evans–Anderson hybrid POM, $(TBA)_3[MnMo_6O_{18}\{(OCH_2)_3CNHC_{21}H_{19}N_2O_4\}\{(OCH_2)_3CNHCOC_{15}H_{31}\}]$, by covalently grafting a photoswitchable spiropyran (SP) fragment and a long hydrophobic alkyl chain.[141] Under UV irradiation (λ = 365 nm) colourless and hydrophobic SP underwent a C–O bond cleavage resulting in the formation of a zwitterionic merocyanine (MC) isomer, which is hydrophilic and strongly absorbs in the visible regions. This conversion triggered the self-assembly processes in mixed solvents (Fig. 16). In water/acetonitrile mixture (2 to 2.5 v/v%) hollow vesicles were formed, which sizes depended on the water content (R_H from 13 to 110 nm, respectively). The aggregation processes are reported

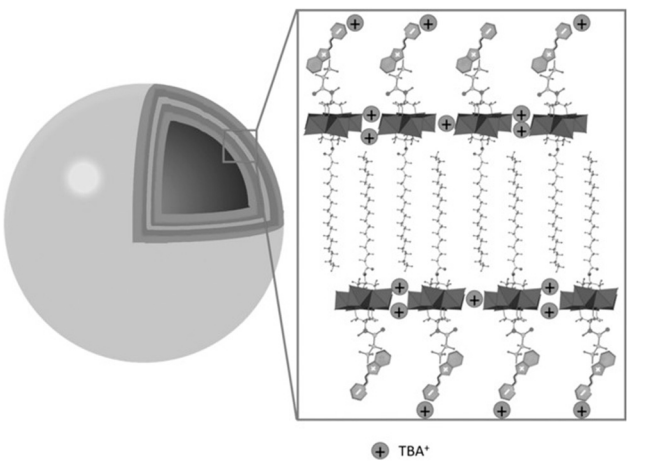

Fig. 16 Self-assembly of the photoswitchable asymmetric POM hybrid, SP–POM–C16 (SP = spiropyran, C16 = decahexane) in polar solvents to form hollow vesicles. This figure has been adapted from ref. 141 with permission from John Wiley and Sons, copyright 2016.

to reach equilibrium after *ca.* 30 h. In less polar solvent mixtures, 84 v/v% toluene/acetonitrile, an equilibrium was reached after three days, leading to spherical assemblies thought to be reverse vesicles due to solvent polarity, exhibiting a R_H = 112 nm. These assembly processes are reported to be reversible and sizes of the assemblies were found to be inversely proportional to the dielectric constant of the mixed solvent. The system reported by the groups of Mialane and Liu represented an original example of a light and solvent-controlled self-assembly of a photoresponsive hybrid POM.

3.2.4 Redox-responsive assemblies. The particularly rich and reversible redox chemistry of POMs allows them to act as electron and proton reservoirs. The molecular electronic states of these molecules and hybrid materials are well studied, but very little is known with regards to the redox activity of these molecules when confined within a supramolecular assembly. Newton *et al.* reported the first investigation comparing the electrochemical states of Wells–Dawson hybrid molecule $H_6[P_2W_{17}O_{61}(PO_2C_{17}H_{27}S)_2]\cdot 3C_4H_9NO$ and its supramolecular conjugate (Fig. 17).[142] This hybrid molecule consists of hydrophilic POM and two hydrophobic carbon chains, which are terminated by hydrophilic thiols. This hybrid exhibited excellent solubility in DMF and is solubilised in aqueous solutions upon rapid heating. The electrochemical profile of the hybrid was studied in DMF ($TBAPF_6$ supporting electrolyte) and displayed a 400 mV positive shift in the first redox process compared to the parent anion $\{P_2W_{18}\}$, as a result of the phosphonate linker electron-withdrawing effect lowering the LUMO energy level. Comparatively, the electrochemical profile of the assembly was probed in 0.1 M H_2SO_4, which displayed two redox processes centred at $E_{1/2}$ = 0.26 V and $E_{1/2}$ = 0.11 V *vs.* NHE, each ascribed to 2 electron processes. To develop upon the observations, DMF was added to the solution to break up the vesicles. This resulted in the CV displaying 3 redox processes resolved redox processes at $E_{1/2}$ = 0.39 V and $E_{1/2}$ = 0.23 V *vs.* NHE, replacing the one broad redox process. This coalescing of the first two redox process of a molecular electrochemical profile to 1 process in a supramolecular assembly is speculated to be a result of intermolecular cooperation. The idea of redox active assemblies serves as a great opportunity to develop state-of-the-art soft materials of applications in energy storage, drug delivery and catalysis.

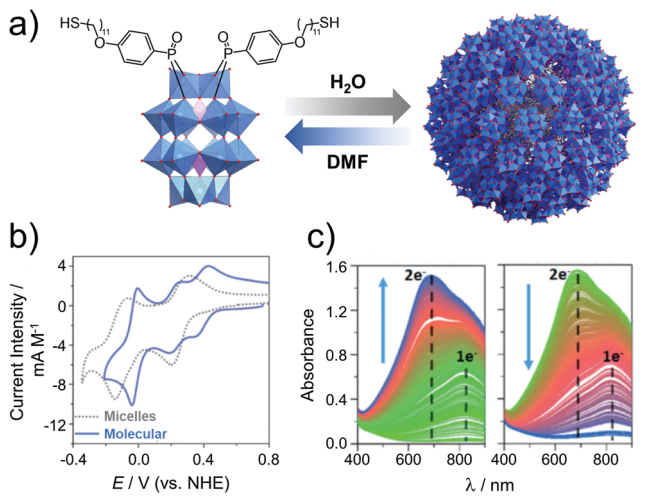

Fig. 17 (a) Structure of the amphiphilic hybrid POM, $H_6[P_2W_{17}O_{61}(PO_2C_{17}H_{27}S)_2]$, showing its reversible assembly into micelles (D_{avg} = 9 nm); (b) cyclic voltammograms of the hybrid POM micelles in 0.1 M H_2SO_4 (aq.) and the molecular cluster species (after addition of DMF), and; (c) spectroelectrochemical analysis of the micellar system showing reduction (left, E = 0.05 V) and reoxidation (right, E = 0.61 V). This figure has been adapted from ref. 142 with permission from the Royal Society of Chemistry, copyright 2017.

The concept of redox active assemblies was further developed by Newton *et al.* to understand the relationship between the structure of the surfactant on the structure and redox chemistry of its supramolecular assembly. Here, the authors studied the effects of chain-length on the structure and the electronic properties of the supramolecular assembly.[143] A library of POM-surfactants were synthesised based on Wells–Dawson grafted to alkyl chains of varying lengths, $K_6[P_2W_{17}O_{61}(POC_6H_4O(C_nH_{2n+1}))_2]$ (n = 10, 12, 14, 16, 18 and 20). Based on increasing chain lengths, the assemblies seemed to decrease in size, owing to a larger hydrophobic driving force to pack tighter together. Furthermore, the electrochemical properties of these hybrids were investigated in 0.1 M H_2SO_4. Observation aligned accurately with the typical two redox processes assigned to the assembly state established in the previous study for longer chain lengths C_{16-20}, however shorter chain lengths C_{10-14} displayed 3 redox processes, with the first redox process shifting closer to the second as the chain length increased. Based on the assembly morphology, C_{10} displayed polydisperse aggregates, which is attributed to the lack of hydrophobic interactions which may also increase its solubility in the molecular state, this reason is speculated to be why a molecular electrochemical profile is observed. Overall, it was established that longer chain-lengths lead to smaller assemblies, with a clear contrast in the CV *vs.* the molecule. This fundamental study clarified the correlation between the level of hydrophobicity and the electrochemical profile of the superstructure.

More recently, Newton *et al.* reported a simple synthetic procedure to tailor a multifunctional hybrid system using an asymmetrically functionalised Dawson type POM hybrid.[144] The authors described the preparation of the mono-lacunary Wells–Dawson bearing two distinct aryl-phosphonic acids, a terpyridine-based ligand (tpy) and a long alkyl chain group (C_{18}). As a potassium salt, the POM hybrid displayed amphiphilic properties and the presence of the C_{18} alkyl chain enabled self-assembly into micellar structures (D_H = 6 nm). Similar electrochemical trends to that reported above were observed in this new system, as a typical fingerprint of these assemblies. By using 0.5 eq. of an Fe^{II} linker a dimeric POM–Fe^{II}–POM compound could be isolated, which, lacking the distinct "head–tail" polarity of the uncoordinated precursor, formed variably shaped non-hollow aggregates in a H_2O–MeCN (9 : 1 v/v) mixture in comparison to the micelles assembled by the precursor. In contrast, in a successive study on the Pt^{II} coordinated

oxocluster,[145] micellar assemblies were enabled by the retained amphiphilic polarity that can be considered metal-decorated, as, unlike in the aforementioned bis-organosilyl Dawson oxoclusters, a high angle (approx. 160°)[44] exists between the two distinct arylphosphonate ligands. Notably, individual micelles appeared to coalesce into small worm-like structures likened to those of Izzet and co-workers,[88,89] suggestive of some degree of further supramolecular aggregation.

The concept of redox-active assemblies has been applied to energy storage, specifically redox flow batteries (RBFs) as POM assemblies possess the ability to carry large amounts of charge and are less susceptible to membrane leaching due to their size.[146] Polarz and co-workers reported a fully conjugated surfactant by grafting a redox active ligand, anthraquinone (AQ), to a lacunary Keggin type POM $K_7[PW_{11}O_{39}]$ *via* a conjugated chain and siloxane linkers, to afford AQπPOM.[147,148] The motive behind this novel design was to fabricate a redox active amphiphile, where the hydrophobic moiety could also be employed as a charge carrier, therefore increasing the charge loading capacity of these assemblies. DFT calculations suggested that the HOMO is located on the centre of the conjugated ligand and extends to the AQ, while the LUMO is located on the POM.[148] At very low concentrations (0.01 g L^{-1}) in aqueous solutions, AQπPOM assembled into micelles (D_H = 8.7 nm). The CV data of the AQπPOM micelle displays reduction of the POM with the electron transferring to the core AQ and then reversibly oxidised back. Furthermore, the size of the micelles was analysed by DLS post bulk electrolysis of the micelles where a 3 nm increase was observed. This proved that the structural integrity of the battery like micelles was maintained and therefore, electrochemically stable. This supramolecular electron storage characteristic is a great opportunity to create innovative nano-scale micellar batteries or develop the field of RBFs.

3.2.5 Decorated nanoparticles with POM amphiphiles. In Section 3.2.2. we described amphiphilic POMs that were used as catalytic surfactants for the controlled-formation of polystyrene and polysiloxane particles. Additional examples relying on the formation of POM-latex core–shell structures have been reported more recently. However, in the latter cases, the covalent POM surfactants did not behave as catalysts themselves but only as emulsifying agents. In 2015, Yin, Liu and co-workers described the preparation of $K_3[PW_9O_{34}\{((C_7H_{11}O_2)SiO)_3(SiC_7H_{11}O_2)\}]$, a classical shaped POM surfactant based on the trivacant Keggin A-type $[PW_9O_{34}]^{9-}$ to which four methacryloxypropylsilane groups were covalently grafted.[149] The hybrid POM behaves as a surfactant molecule and self-assembles in aqueous solution into micelle structures with 5 nm hydrodynamic radii. Radical emulsion polymerisation of styrene was initiated in water and led to the formation of latex nanoparticles (hydrodynamic radii of *ca.* 100 nm), the TEM analysis of which revealed a typical core–shell structure with a polystyrene core and a POM close-packed shell. The POMs are expected to be chemically linked to the PS particles thanks to the participation of the carbon–carbon double bond located at the end of the alkyl chains into the polymerisation process.

A similar strategy has also been employed by Rieger and co-workers in 2015 using a Wells–Dawson POM hybrid substituted with a hydrophobic dodecylamide chain $[\alpha_1\text{-}P_2W_{17}O_{61}\{Sn(CH_2)_2\text{-}CONHC_{12}H_{25}\}]^{7-}$ and ammonium (NH_4^+) as counterions.[150] Aqueous emulsion polymerisation of styrene was also reported to lead to the formation of stable latexes in which the amphiphilic POMs act as stabiliser adsorbed at the surface of the PS particles. This strategy actually reproduced the seminal work by Judeinstein[151] that was successively developed by Maatta[152] and Thouvenot[153,154] for the preparation of organically modified POMs bearing polymerisable functionalities (vinyl, allyl, methacryl, styryl), some of which behaving as surfactants when the counterions are alkaline cations. These POM hybrids may act either as a co-monomer or as reticulating agent or cross-linkers in the polymerisation of organic monomers promoting the formation of either hybrid polymers with POM pendant units or hydrogels.[155] It is worth mentioning that the inclusion of POMs in polymeric networks has been the mean of many studies within the aim to develop catalytic, magnetic and photo- or electrochromic materials from inert matrices.[156–158] The works by Yin, Liu and Rieger nevertheless represent a new methodology for the preparation of POM–polymer conjugates with core–shell structures. Major objectives were to synthetically control and stabilise nanoparticles and to generate covalent interactions between the NPs and the POM in order to avoid leaching of the latter in solution under extreme conditions and finally to overcome the poor processability of pristine POMs.[158] A more challenging objective was to associate integrated functions brought by the polyoxometalate entity itself. Rieger and co-workers described their POM–surface decorated polystyrene particles as photochromic materials due to the photoreduction of the POM core shell under UV irradiation. The POM mediated surface photoactivity was also observed by the photoreduction of silver ions which led to spatially controlled nucleation of small silver nanoparticles exclusively at the surface of POM–Polystyrene conjugate.[150]

The use of POMs as protecting ligands for electrostatically stabilised metal(0) nanoparticles and nanocomposites has been nicely reviewed by Weinstock *et al.*[159] Few examples of covalently bound POMs to gold (AuNPs)[160–162] and platinum[163] nanoparticles have also been reported using on-purpose designed hybrid POMs. Towards this end, hybrid POMs featuring thiol-terminated alkyl chains have been prepared as capping agents in order to create a strong interaction with the nanoparticles through a thiolate-type binding mode. Such strategy ensured the formation of ordered assemblies of POMs at the gold surface and as expected to prevent agglomeration of gold nanoparticles. Newton *et al.* prepared the orgonophosphoryl-modified Wells–Dawson POM, $K_6[P_2W_{17}O_{61}\{PO_2C_{17}H_{27}S\}_2]$ (Fig. 18), and reported that the nanocomposites that were obtained following this strategy exhibited much higher stability to temperature and pH values compared to their electrostatically stabilised analogues.[162] Nanomaterials that combine optical properties of gold nanoparticles with the electro- and photochemical features of the POM framework are of particular interest to obtain multifunctional nanomaterial with potential applications in catalytic

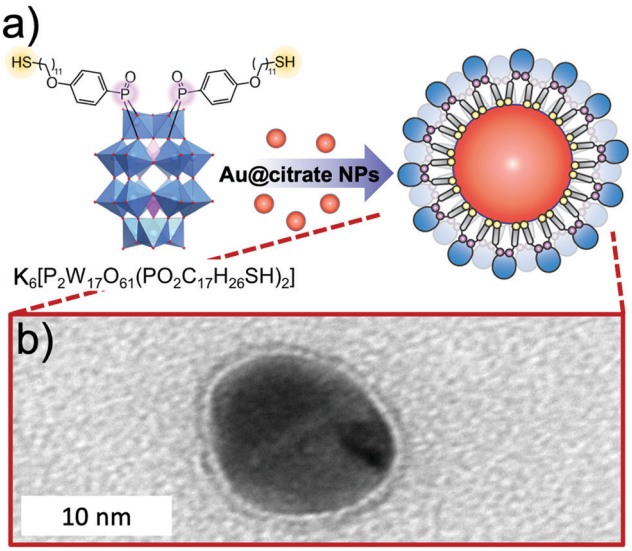

Fig. 18 (a) Structure of the thiolated hybrid POM, $K_6[P_2W_{17}O_{61}\{PO_2C_{17}H_{26}SH\}_2]$, showing its spontaneous exchange with citrate to produce covalently functionalised Au nanoparticles; (b) HR-TEM micrograph of a single Au@POM nanoparticle. This figure has been adapted from ref. 162 under the Creative Commons CC BY License.

and sensing technologies. Polarz *et al.* reported the preparation of the Keggin derivatives $[SiW_{11}O_{39}\{Si(CH_2)_n\text{–}SH\}_2O]^{4-}$ which were also attached to the surface of gold nanoparticles using thiolate-type binding mode.[161] With protons as the counter ions, the POM surfactant AuNp composites exhibited Brønsted acid catalytic activity in esterification reactions that could be significantly enhanced by radiation with light. The authors attributed these results to the synergetic interaction between the attached hybrid POM and the surface-plasmon resonance of AuNp as the effect was proven to depend on the distance between the POM head and the AuNp surface (by varying the alkyl chain length, n value). This example featured how synergetic interactions can arise through association of POM and nanoparticles and how rational preparation methodologies are central issues to prepare nanomaterials with controllable and tailored properties.

3.3 Nanostructured POM-based hybrid materials

As pristine POMs are often difficult to handle owing to their crystalline character, they often form inhomogeneous films with aggregated particles.[164] Their processing can be achieved by counterion exchange which allows their immobilisation on surfaces,[165–168] their embedding in polymers[26] or the formation of membranes[22] through self-assembly processes. Yet, as mentioned in the introduction the resulting soft materials rarely display internal nanostructuration owing to the isotropic character of pristine POMs, despite some notable exceptions.[21,23–28] The controlled assembly of hybrid POMs through combination of electrostatic interactions between POM units and another specific interaction between the organic moieties is thus an appealing strategy to process POMs into nanostructured soft materials. Among them, mesomorphic materials (including liquid crystals) are appealing since these organised and oriented nanostructures display a liquid state allowing an efficient control of the thin film's morphology for further device fabrication steps.

3.3.1 Mesomorphic materials. Liquid crystals exhibiting a liquid crystalline phase as a function of temperature are classified as thermotropic liquid crystals whereas materials forming a mesophase in combination with a solvent are classified as lyotropic liquid crystals. In a general manner, POM-based mesomorphic materials exhibit high viscosity in the fluid phase due to their high molecular weight and the strong electrostatic interactions between POMs and counter ions. A variety of POM-based liquid crystals has been reported in recent years, however the vast majority of these materials rely on the ion pairing of POMs with functionalised mesogenic or non-mesogenic cations (for detailed reviews see Wu and co-workers[28] and Floquet and co-workers),[169] whereas hybrid POM-based liquid crystals have been far less abundant in the literature. The first example of a covalent hybrid POM-based liquid crystal was reported by Polarz and co-workers in 2010.[119] In their work the authors functionalised Keggin-type POMs with two long-chain organo-alkoxysilanes. In their study Polarz and co-workers also investigated the influence of different alkyl chain lengths and counter ions on the formed liquid crystal structures (Fig. 19).

With regards to the $[PW_{11}O_{39}(SiC_{16})_2](Na)_3$ liquid crystal the authors found it to self-assemble into hexagonally packed cylinders in the space group P6/*mm*. While the C_{18} analogue exhibited a similar structure the authors observed a hexagonal close packing (P6/*mmc*) of spherical micelles for the hybrid-POM derivative of shorter chain length. Furthermore, upon changing the respective counter ions from sodium cations to protons and organic ammonium cations the authors observed the formation of lamellar structures. More recently Polarz and co-workers also reported the synthesis of a hybrid POM with a π-conjugated tail based on the same organosilane POM-based

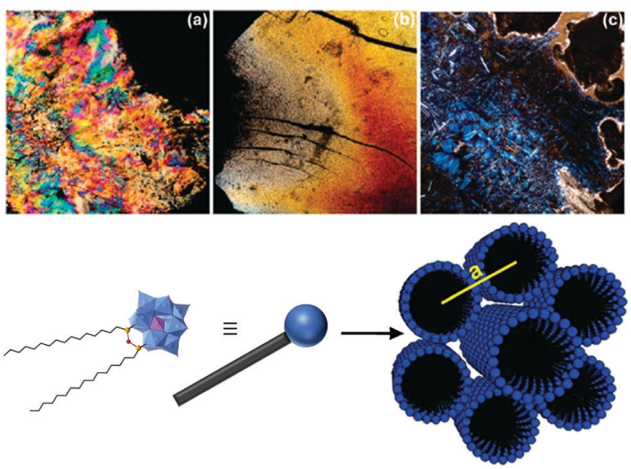

Fig. 19 Top: Polarisation microscopy images of (a) $Na_3[PW_{11}O_{39}(SiC_{12}H_{25})_2O]$, (b) $Na_3[PW_{11}O_{39}(SiC_{16}H_{33})_2O]$ and (c) $(TBA)_3[PW_{11}O_{39}(SiC_{16}H_{33})_2O]$. Bottom: Schematic representation of the $[PW_{11}O_{39}(SiC_{16}H_{33})_2O]^{3-}$ structure. This figure has been adapted from ref. 119 with permission from the American Chemical Society, Copyright 2010.

platform employed in their previous study using *para*-phenylene ethynylene remote units.[147] The authors determined a hexagonally ordered cylindrical structure for the liquid crystal phase in the space group P6/*mm* for the resulting lyotropic liquid crystals formed by the self-assembly of their compound. Moreover, the formed liquid crystals displayed semiconductor properties as shown by photosensor experiments. Finally, the authors also concluded that the decreased conformational freedom of the organic chains in the liquid crystal state enhanced the delocalisation of electrons compared to the micellar state of the hybrid POM compound in solution.

The synthesis of hybrid POM-based thermotropic liquid crystalline materials was recently pioneered by Song and co-workers.[170] In their study the authors coupled gallic acid derivatives with long alkyl chains to an amino-functionalised Keggin-POM derivative resulting in a fan-shaped structure. The liquid crystalline materials were determined to assemble into layered smectic A phases. In the model structure, the authors proposed that the organic chains are located between POM layers. More recently, the first example of a photoactive donor–acceptor POM-based material was reported by Izzet, Heinrich, Mathevet and co-workers. In their work the authors coupled two moieties of a novel bis(thiophene)thienothiophene (BTTT) derivative to the bis-iodo aryl terminated Keggin POM-based hybrid platforms.[171] The authors reported a multi-layered lamellar structure of the mesophase consisting in the alternation of POM/TBA counter ion double layers and double sub-layers of tilted BTTT mesogens, isolated from each other by a continuum of molten aliphatic chains (Fig. 20). Interestingly, the organisations of the POM and BTTT sub-units were found to be similar to that of BTTT and hybrid POM parent reference compounds. For instance, the branched terminal aliphatic chains impose high tilting of BTTT units in the hybrid as well as in the organic precursor and POM precursor and hybrid exhibit close quasi-hexagonal rectangular arrangements of POM and TBA. Finally, the authors were able to confirm the donor–acceptor properties of this material *via* photophysical studies making it a promising starting point for future investigations. The predictability of the individual sub-unit organisations in this system should facilitate the design of future generations of hybrids. Notably, using the same hybrid, the modification of the counter-ion should offer an effective way to tune the LC/conductive properties of POM-based mesogens.

3.3.2 Other nanostructured materials. Other examples of nanostructured materials formed by self–assembly of hybrid POMs have also been reported in the literature. By contrast to liquid crystalline materials, these compounds don't liquefy at high temperature, allowing an efficient processing step, but spontaneously crystallise into organised arrays of molecules thanks to orthogonal interactions between the organic and inorganic parts. An intriguing example of such spontaneous self-assembly has been reported by Cronin and co-workers (Fig. 21),[172] namely the formation of a helical structure, similar to the structure of Z-DNA. In their studies they employed a hybrid POM consisting of guanosine monophosphate (GMP) and a $\{Mo_5O_{15}\}$-based polyoxometalate in which the GMP units are incorporated into the structure of the corresponding Strandberg POM. Besides crystallographic evidence of the helical structure formed by the hybrid GMP–POM, the authors also showed that the self-assembled structure is stable in solution. Interestingly the observed helical structure does not rely on hydrogen-bond base pairing. Instead, hydrogen bonds from the amino-groups of the guanine moieties to neighbouring polyoxoanions, along with coordination of sodium cations by the hydroxy-groups of the GMP ribose rings and stacking interactions of the guanine rings are responsible for the structure's stability.

Very recently Zheng, Streb, Chen and co-workers.[173] reported the synthesis of novel hybrid POMs *via* functionalisation with organic boronic acids that can act as tritopic linkers. In their study the authors employed Wells–Dawson POMs of the general

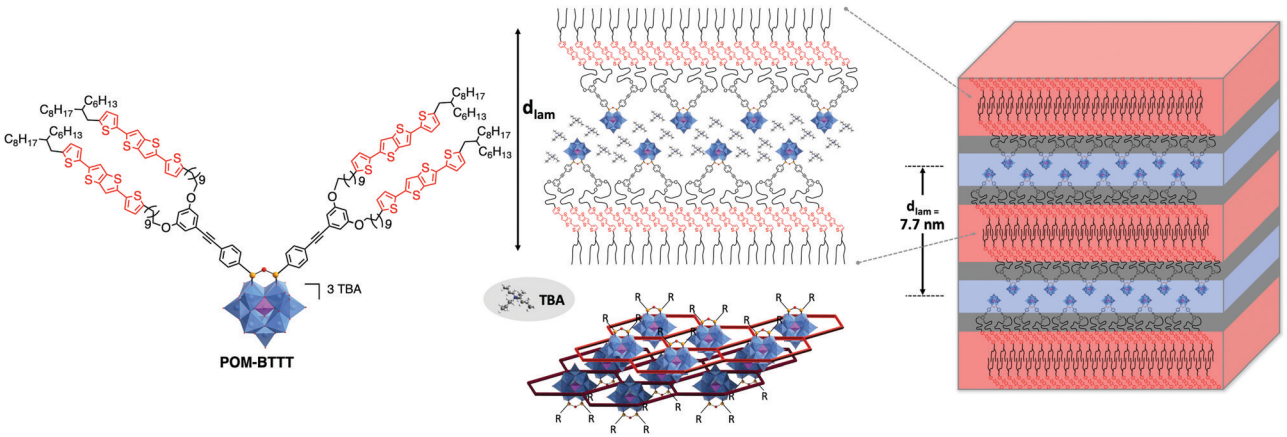

Fig. 20 Left: Molecular structure of the branched POM–BTTT hybrid oxocluster; middle: a schematic view of multi-layered self-assembly of the lamellar hybrid material, highlighting the specific arrangement of the POM/TBA double-layers (bottom, centre: showing POM clusters in blue and the surrounding TBA honeycomb structure in red – note the laterally offset bottom layer is shown in darker colours); Right: 3D schematic representation of lamellar nanomaterial, respecting the molecular segment sizes and shapes. This figure has been adapted from ref. 171 with permission from John Wiley and Sons, copyright 2021.

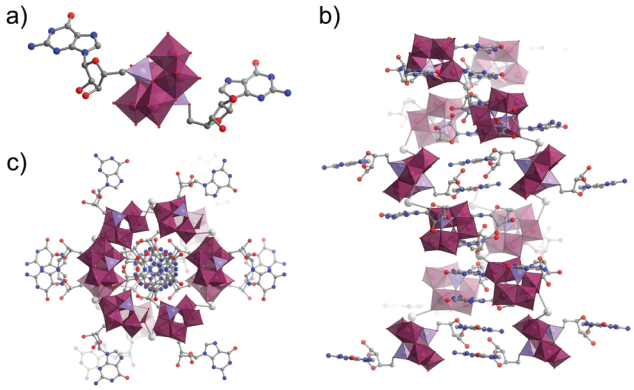

Fig. 21 (a) Molecular structure of the guanosine-functionalised Strandberg-type hybrid oxocluster; (b) Stacking of clusters into a Z-DNA like double helix through a combination of hydrogen bonding and Na± mediated interactions (not shown here for clarity) as viewed along the crystallographic *b*-axis and; (c) viewed along the crystallographic *c*-axis. This figure has been adapted from ref. 172 under Creative Commons Licence CC-BY.

formula $[M_3P_2W_{15}O_{62}]^{9-}$ incorporating Nb^V and Ta^V ions respectively. The resulting hybrid POMs were shown to self-assemble in the solid state into nanocapsules with a diameter of 2.8 nm to 4 nm depending on the organic moiety of the boronic acid. These nanocapsules were characterised by single-crystal X-ray diffraction. In case of 3-pyridineboronic acid the authors observed tetrahedral aggregates in which four POM core units are linked by four organoboron moieties. When employing 5-pyrimidinylboronic acid the authors observed the formation of dodecameric nanocapsules based on trimeric subunits connected by K^+ ions displaying an inner cavity of *ca.* 1.3 nm (Fig. 22). Certainly, this new functionalisation strategy could pave the way for a new class of hybrid POM architectures and applications.

Polymer–polyoxometalate hybrids are another class of compounds that may be considered of interest for the self-assembly of nanostructures. Most notably Wang and co-workers demonstrated the possibility to tune the self-assembly behaviour of nanostructures by varying the molecular weight of the hybrid's polymer component.[174] For their studies they linked

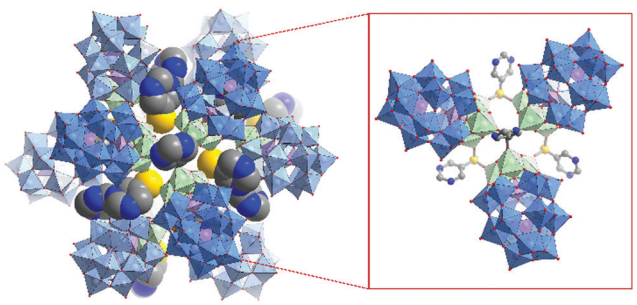

Fig. 22 Structure of the supramolecular nanocapsule formed by the self-assembly of four trimeric $\{P_2W_{15}Ta_3\}$ units linked by boronic acid groups; inset: detailed view of the boronic acid (5-pyrimidinylboronic acid) mediated linkage of the $(\{P_2W_{15}Ta_3\})_3$ trimers. This figure has been adapted from ref. 173 under Creative Commons Licence CC-BY.

linear poly(ε-caprolactone) (PCL) of two different molecular weights to a Wells–Dawson type POM. The polymer–POM hybrid of low molecular weight self-assembled into nanotubes consisting of a hybrid membrane in which an amorphous PCL-layer is sandwiched between two layers of the POM. In contrast, the polymer–POM hybrid of high molecular weight self-assembled into hexagonal nanosheets. Besides single-layer nanosheets the authors also observed multilayer nanosheets composed of a stack of single-layer nanosheets. With regards to the structure of the observed hexagonal nanosheets, the authors propose a crystalline PCL layer, which is sandwiched by two single POM layers. With respect to the molecular weight dependence of the observed nano-objects, the authors argued that the rigidity of the crystalline PCL layer formed by the polymer POM hybrids with the higher molecular weight prevents the formation of nanotubes, which would be the preferred structure as it further minimises the free energy of the structure in question. In addition to the characterisation of these individual nano-objects the authors were also able to synthesise tube-*graft*-sheet nano-objects *via* stepwise self-assembly.

Another class of hybrid POMs that has shown a remarkable variety of nanostructures in recent years are polyoxometalate–silsesquioxane (POM–POSS) hybrids.[175] These kind of heterocluster Janus molecules were pioneered by Wang and co-workers. In one of their early studies[176] they used a Wells–Dawson-type POM ($[P_2W_{15}V_3O_{62}]^{9-}$) tethered to an aminopropylisobutyl derivative of polyhedral oligomeric silsesquioxane *via* an organic linker and observed the self-assembly of hexagonal crystals with a filled honeycomb superstructure. In this case the POM moieties constitute the hexagonal honeycomb framework, while the POSS form close packed hexagonal cylinders within the honeycomb framework.

In a different study Liu, Yue, Cheng and co-workers[177] investigated the influence of molecular topology, surface functionality of the POSS blocks and solvent polarity on the nature of the self-assembled nanostructures. In their work they used organosilyl and organotin derivatives of Keggin-type POMs in combination with isobutyl (BPOSS) or cyclohexyl (CPOSS) functionalised POSSs (Fig. 23). By employing a solvent mixture of chloroform/methanol the POM–BPOSS hybrid self-assembled into multiple-layered lamellae in which POM- and BPOSS-layers are stacked in an alternating fashion. However, by using a water/acetonitrile mixture first the formation of colloidal spheres with an internal lamellar structure was observed followed after 10 additional days by the formation of extended nanobelts with internal lamellar crystals. The authors propose a mechanism of nucleation of the first observed colloidal spheres and subsequent growth into the thermodynamically more favourable nanobelt structure. However, the authors concluded that in both cases the molecular packing in the crystal lattice is dominated by the POM subunits. Regarding the CPOSS analogue of the POM hybrid in question the authors observed the formation of nanosheets that are composed of two internal crystalline POM layers sandwiched between two amorphous CPOSS layers when using a chloroform/methanol mixture as the solvent for

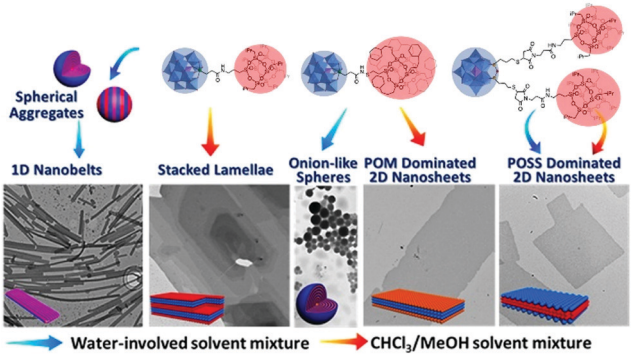

Fig. 23 Self-assembly of a series of molecular Janus particles constructed by chemically linking Keggin-type POMs with functionalised POSS cages. This figure has been adapted from ref. 177 with permission from the American Chemical Society, Copyright 2016.

self-assembly. When employing the water/acetonitrile mixture for self-assembly the authors observed, again, the formation of spherical aggregates with a very similar internal lamellar structure to their BPOSS counterpart, however they did not observe any further structural evolution into nanobelts. The authors attributed this different behaviour in both cases to the non-crystalline nature of the CPOSS moieties. With regard to the POM–2BPOSS hybrid the authors investigated in their studies, they found that these hybrid molecules also formed nanosheets, however in this case the internal layer consists of BPOSS single crystals sandwiched between two POM layers. This structure was observed in solvents of different polarity. This was attributed to the increased ratio of BPOSS-moieties to the POM; the self-assembly is hence no longer governed by the POM, instead the crystallisation of the BPOSS cages is the main driving force for the formation of the nanosheets.

Wang and co-workers expanded the concept of tethering multiple POSS blocks to a single POM unit.[175] The authors reported the self-assembly of mesoscale graphene-like honeycomb mono- and multilayers of a four-fold POSS-substituted Wells–Dawson type POM (4BPOSS–POM).[178] Like for graphene the mesoscale honeycomb monolayers of the 4BPOSS–POM hybrid were found to form multilayers *via* different stacking modes. The self-assembly mechanism was investigated *via* coarse-grained molecular simulations in which the authors identified three key steps of the self-assembly: First, the formation of trimers driven by the counterion-mediated electrostatic interactions between the POM blocks, second, the assembly of six such trimers into cells and third, the aggregation of cells into the observed honeycomb structure. In a subsequent study Wang and co-workers also investigated the self-assembly of similar POM–POSS hybrid molecules into cubosomes.[179] The authors observed the self-assembly of cubosomes with internal double diamond structure from an acetone/*n*-decane mixture (Fig. 24). They employed dynamic conditions in which the acetone was allowed to evaporate slowly over time, decreasing the solubility of the hybrid molecules and facilitating aggregation. Based on their observations of intermediates the authors proposed a mechanism for the self-assembly of cubosomes with an internal double diamond structure. According to their findings the formation of cubosomes takes place *via* a four-step process. The self-assembly of vesicles with a dual bilayer in which a POM double layer is sandwiched between two POSS monolayers occurs first. Subsequently the so formed vesicles accumulate into larger aggregates. Topological reorganisation takes place within larger aggregates, starting from the centre until the double diamond structure occupies the entire interior of the aggregates forming spherical cubosomes. Further growth occurs on the facets of the cubosome *via* crystal nucleation and growth.

4. Combination of hybrid POMs with substrates through non-covalent interactions

In addition to their ability to act as discrete molecular building blocks in the preparation of larger molecular and supramolecular nanosystems, hybrid POMs have also recently been explored as

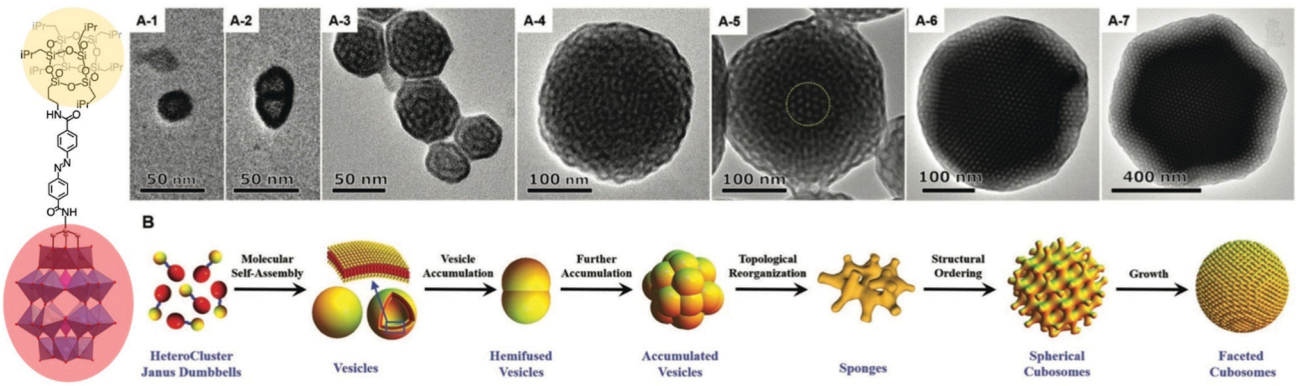

Fig. 24 Formation processes and mechanism of cubosomes. (A) TEM images demonstrating the size-dependent shapes and inner nanostructures of cubosomes growing under the dynamic conditions. (A-1–A-7) A vesicle, a hemi-fused vesicle, particles with a foam-like structure, an aggregate with a sponge-like nanostructure, an ordered nanostructure in the centre of the aggregate (highlighted by the yellow circle), a spherical cubosome, and faceted cubosomes. (B) Evolution from molecules to faceted cubosomes through different mechanisms. This figure has been adapted from ref. 179 with permission from the American Chemical Society, Copyright 2019.

functional components in combination with a range of other species capable of acting as either hosts or guests in relation to the POM. As in other well-established host–guest systems, this relies strongly on non-covalent interactions though, in this instance, these are usually more heavily directional and/or specific than in many of the other systems described above. Exploiting these host–guest interactions offers broad scope for the careful design of new supramolecular nanostructures and nanomaterials, which can display unique, dynamic responses (*e.g.* self-healing, switchable properties, chiral recognition or transfer). Hybrid POMs are particularly well-suited here, as their near-limitless scope for molecular design can be used to judiciously control both the self-assembly and physicochemical properties of the resulting complex. This is not necessarily trivial or, indeed, predictable however it does present enormous potential for novel supramolecular design strategies. The following section thus describes recent examples of the formation of more complex supramolecular systems, comprising a hybrid POM in combination with one or more additional components whereby the attractive properties of each component combine to present new functionalities.

4.1 Hybrid POM complexes with cavitands

The combination of both all-inorganic and hybrid POMs with macrocyclic hosts is a relatively recent area of interest, with the vast majority of studies reported only in the last decade. The most common cavitands – cyclodextrins, calixarenes, curcubiturils and pillar-arenes – have been widely studied for their remarkable inclusion properties,[180–183] which typically rely on their hydrophobic inner cavities. Owing to their chaotropic character, classical inorganic POMs (such as the Lindqvist, Keggin or Wells–Dawson anions) can readily form inclusion (or partial-inclusion) complexes with suitable cyclodextrins (CDs). This is largely thanks to the complementarity of their molecular structures and is driven predominantly by favourable steric-fitting between the host and the guest oxocluster, and some hydrogen-bonding interactions.[21,86,184] Such inclusion complexes are stable in both solution and the solid-state and have recently been studied for their phase-transfer catalytic properties,[185] and as a novel tool for probing the self-assembly behaviours of small POMs by mass spectrometry.[186,187] That said, the formation of stable host–guest complexes between conventional POMs and cavitands (particularly curcubiturils and pillar-arenes, which do not share the excellent complementarity found in POM⊂CD systems) remains the exception rather than the rule, and in many cases, POM@cavitand complexes form crystalline networks in which the POM remains external to the macrocyclic cavity and often requires additional functionalisation of the macrocycle (*e.g.* appending cationic groups to electrostatically associate with the POM).[188–190] The development of hybrid POM@cavitand inclusion complexes therefore presents several potential advantages, allowing far greater synthetic control and access to a broad range of prospective new properties through the engineering of dynamic or stimuli-responsive host–guest interactions. This was exemplified by the pioneering 2012 study of Izzet, Ménand, Sollogoub, Proust and co-workers, who demonstrated the first example of hybrid POM@cavitand complexes between an organotin-functionalised Wells–Dawson and both α- and β-CDs.[191] Here, the iodoaryl moiety which has been anchored to the POM *via* the iodoaryl unit is found to be either partially (α-CD) or fully (β-CD) included within the host, forming a stable 1 : 1 complex which could be characterised in both the solution- and solid-state using a combination of ^{1}H NMR and single crystal X-ray diffraction studies. The binding constants were similar to that of iodobenzene with α-CD and β-CD, indicating the absence of specific interaction between the POM and the CD (Fig. 25).[192] Interestingly, in the presence of γ-CD the complexation of the hybrid turned out to be more complicated,[193] probably owing the possible binding of the γ-CD to the iodoaryl moiety and to the sidewall of the POM, as further observed with pristine Wells–Dawson POMs.[21] The authors also demonstrated a remarkable "self-healing" effect in the POM:CD complexes. When exposed to base, the organotin moiety is hydrolytically cleaved from the monolacunary POM (as is common to many hybrid POM species). This process is partially reversible on neutralisation of the solution, however after 4 cycles of hydrolysis and re-condensation of the organic group, only 20% of the original hybrid complex is found to remain, with most being lost as insoluble stannous salts and plenary (and thus unreactive) Wells–Dawson oxocluster, $[P_2W_{18}O_{62}]^{6-}$. Conversely, after four cycles of hydrolysis/neutralisation, POM@α–CD and POM@β–CD inclusion complexes are found to be more than 95% and 99% intact respectively, thanks to the protective influence of the cavitand, which prevents the organotin species from oligomerisation or disproportionation when exposed to base.

Further evidence for the potential to engineer unique supramolecular materials using hybrid POM design strategies was provided shortly thereafter by Wu and co-workers, who developed a switchable material based on the combination of azobenzene functionalised Anderson oxoclusters and a pyridinium-functionalised β-CD host (Fig. 26).[194] Exploiting the well-known photo-switching properties of the azobenzene–CD insertion complex,[195] alongside the electrostatic interaction of the cation-functionalised CD with the polyoxoanions, the authors successfully demonstrated the self-assembly of a new chiral, photo-switchable supramolecular network. In this case,

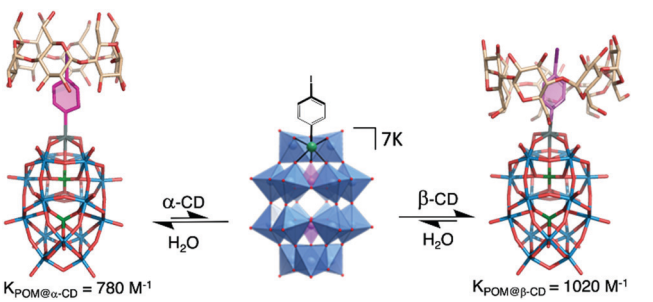

Fig. 25 Formation of the POM@α-CD (left) and POM@β-CD (right) inclusion complexes from an iodo-aryl functionalised Wells–Dawson hybrid (note: aryl group is highlighted pink in wireframe models for clarity). This figure has been adapted from ref. 191 with permission from John Wiley and Sons, copyright 2012.

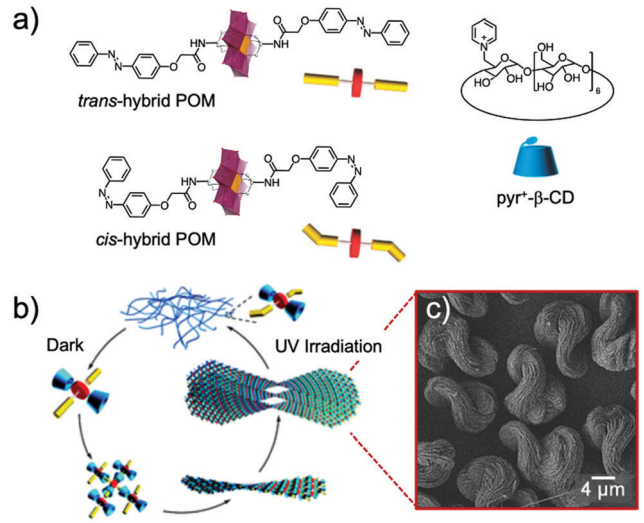

Fig. 26 (a) Molecular structures and simplified representations of the *trans*- and *cis*-isomers of an azobenzene functionalised Anderson-type hybrid-POM anion and a pyridinium-functionalised β-CD cation; (b) schematic showing the self-assembly of the *trans*-isomer of the hybrid-POM:β-CD complex into nanosized, chiral aggregates upon inclusion of the *trans*-azobenzene groups into the β-CD cavity and its subsequent disassembly into irregular nanofibres under UV-irradiation, driven by the photo-isomerisation of the azobenzene unit, and: (c) an SEM image of the right-handed chiral nanostructures formed by the extended hybrid-POM:CD inclusion complex. This figure has been adapted from ref. 194 with permission from the Royal Society of Chemistry, copyright 2013.

the hybrid POM in the *trans*-conformation forms a 1 : 2 inclusion complex with the CD host, allowing chiral-transfer from the intrinsically chiral β-CD molecules to the azobenzene units, which can then propagate throughout the whole material. This leads the *trans*-POM@CD complex to self-assemble into remarkable right-handed twisted lamellar structures as observed by SEM. When irradiated with UV-light, *cis*-isomerisation of the azobenzene units results in disassembly of the host–guest complex, resulting in a loss of chirality (as confirmed by circular dichroism spectroscopy (CDS)) and solubilisation of the merely electrostatically bound POM@CD complex which loses its unique morphology. The authors later built on this study by developing a new complex using a similar approach.[196] In this case, they designed a new single-sided, asymmetric Anderson hybrid in order to construct a three-component supramolecular material which included a cationic methylene blue (MB) dye alongside the azobenzene functionalised hybrid POM@α-CD inclusion complex. This allowed the authors to directly study chiral transfer from the CD host to the electrostatically bound dye molecules, using the hybrid POM as a bridging unit. By observing formation of an induced Cotton signal from the MB chromophores, CDS was used to confirm that formation of the POM inclusion complex is vital to transfer chirality from the hydrophobic cavity of the α-CD unit to the MB dye, which does not form an inclusion complex in the absence of the azobenzene-functionalised Anderson oxocluster.

The same group also recently reported a series of dynamic, photo-switchable materials based on the self-assembly of an organotin-functionalised Keggin POM containing a remote azobenzene moiety.[140] In aqueous solution, this hybrid spontaneously self-assembles into vesicles thanks to the amphiphilic nature of the hybrid oxocluster (see Section 3.2.3). When mixed with equimolar quantities of either α-CD or β-CD, an induced Cotton signal appears in the CDS corresponding to the azobenzene groups, indicative of chiral transfer from the internal cavity of the cavitand to the POM bound azobenzene moieties and dynamic light scattering measurements indicate rapid dissociation of the vesicles (hydrodynamic diameter of *ca.* 60 nm) to the monodispersed state which has an average hydrodynamic diameter of *ca.* 3.6 nm, closely matching the expected size of the POM@CD inclusion complex. Photo-switching of the azobenzene moieties with 365 nm light leads to the dissociation of the POM@CD inclusion complex, which reforms the self-assembled spherical particles, this phenomenon being entirely reversible. Finally, competitive binding studies with adamantane-1-carboxylic acid also allow control of the self-assembly behaviour of the hybrid POM, selectively binding with CD over the azobenzene–POM hybrid and thus favouring assembly of vesicles over the monodisperse POM@CD complex. In combination with the authors previous work, this study shows the impressive potential of this tailored building block approach in the design of novel supramolecular materials with new and remarkable features arising as a result of the precise control of the host–guest interaction between the POM and the cavitand host molecule.

The dynamic properties of host–guest systems also have significant implications for the design of new smart materials, and the direct integration of hybrid POM@CD inclusion complexes into polymers has also recently been explored. Song and co-workers demonstrated the preparation of new host–guest hydrogels, combining adamantane-functionalised Anderson-oxoclusters with an acrylamide functionalised β-CD monomer species.[197] Radical copolymerisation with additional acrylamide monomer forms a new supramolecular polymer, yielding a series of hydrogels with varying amounts of incorporated POM. Rheological analysis found that increasing concentrations of POM, which acts here as a supramolecular cross-linking species, leads to materials with higher elastic modulus due to an increased network density. Wu and co-workers have also recently utilised the combination of an anthracene-functionalised Anderson POM with γ-CD to facilitate the templated polymerisation of the hybrid POM units into linear chain polymers using the photo-dimerisation of the anthracene groups to form new C–C bonds between the oxoclusters (Fig. 27).[198] Here, the authors report two distinct new materials: a supramolecular polyrotaxane-type complex in which the anthracene units stack within the γ-CD cavity to form uniform and parallel linear strands of alternating POM and CD; and a covalent polymer in which the photo-dimerised anthracene reacts within the cavity of the γ-CD cavity to form highly linear polymer chains. Crucially, however, in the absence of the templating effect of the γ-CD unit, the hybrid POM complex forms globular assemblies, indicating the importance of the supramolecular templating effect provided by the host–guest interaction between the POM and the CD cavitand.

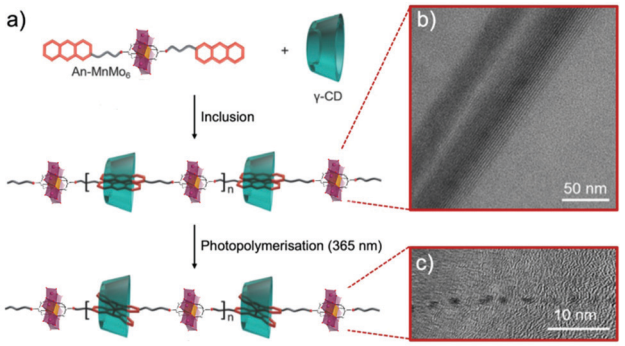

Fig. 27 (a) Schematic representations of the anthracene functionalised Anderson-type hybrid POM and γ-cyclodextrin, showing their self-assembly into a supramolecular polyrotaxane which can then be photo-polymerised into a covalent linear polymer chain; (b) TEM imaging of the supramolecular polyrotaxane, showing a bundle of highly linear adjacent polymer strands, and; (c) TEM imaging of an isolated single-chain of the covalent polymer (dark spots show individual POM anions arrayed along the polymer backbone). This figure has been adapted from ref. 198 with permission from the Royal Society of Chemistry, copyright 2019.

The effect of the host–guest interaction between hybrid POMs and suitable cavitands can also play a more subtle role in helping to moderate functionality. A clear example of this was reported recently by Kögerler and co-workers, who prepared a 1 : 2 POM:α-CD inclusion complex using a phenyl-arsonate functionalised $[M^{II}O_8Pd_{12}(C_6H_5AsO_3)_8]^{6-}$ (where M = Co, Ni, Zn) polyoxopalladate.[199] In this complex, the formation of the inclusion complex between the terminal phenyl-groups on the polyoxopalladate and the α-CD units was found to lead to a small but significant distortion to the cubic ligand-field of the centrally bound metal ion owing to the "chemical pressure" applied to the POM in the solid state through the formation of an inclusion complex. In the case of the Co analogue particularly, this structural distortion was significant enough to generate a slight single-ion magnetic anisotropy, which the authors studied *via* EPR, SQUID magnetometry and X-ray absorption techniques.

4.2 Hybrid POM complexes with carbon nanotubes

The rich, stable and highly tuneable multi-redox activity of POMs is one of the key properties driving interest in their use in the next-generation of energy and electronics technologies. As the primary limiting factors in their wider use relate mainly to their low surface area and lack of electrical conductivity in the solid state, a great deal of research effort has been invested in recent years into strategies to overcome these specific challenges.[18,200] Of particular interest has been the combination of POMs with various high surface area carbons, and especially low dimensionality nanostructures such as carbon nanotubes (CNTs), which have the potential for very high surface areas and electrical conductivity. Similar to the host–guest complexes discussed above, this field is still very much in its infancy though a number of different approaches have already emerged for the preparation of new POM@CNT composite materials. Promising results were reported very recently for example by Walsh, Khlobystov, Newton and co-workers, who demonstrated the direct encapsulation of $[P_2W_{18}O_{62}]^{6-}$ within single-walled carbon nanotubes (SWCNTs), which formed new electroactive composites with high POM loadings and notable chemical and electrochemical stability.[201] Far more commonly, POM@CNT composites have typically been formed by deposition of various POMs onto the exterior of the nanotube, either by aggregation/crystallisation of the oxocluster directly onto the CNT,[202,203] or by surface functionalisation of the carbon surface – either using direct chemical approaches or through combination with a modifier such as a cationic polymer – in order to facilitate stronger covalent or electrostatic interactions between the POM and the CNT.[168,204] Examples of the covalent coupling of hybrid POMs to CNTs *via* a peptide bond formation and their study as promising anode materials for Li-ion batteries were also reported.[205,206] Several challenges remain in each case however, the most notable of which being that direct modification of the sp^2 carbon framework can often have a negative effect on the optical and/or conductive properties of the CNT. Moreover, electrostatic association of the POM and CNT is highly susceptible to unwanted ion exchange reactions and can lead to issues centred around the long-term stability of the composite material.

The potential for carefully designed hybrid POMs to selectively and non-covalently interact with CNTs is therefore a promising route to develop stable, tuneable nanocomposites, which retain the attractive properties of both the POM and CNT components. This was first demonstrated by Song and co-workers in 2013, who used a non-covalent sidewall functionalisation approach in order to couple a pyrene-appended Keggin POM to SWCNTs by exploiting the strong π–π stacking interaction between the ligand and nanotube surface.[207] The new hybrid nanomaterial was characterised by high-resolution TEM (HR-TEM) imaging, which are decorated with discrete particles of *ca.* 1–1.5 nm diameter, corresponding well to the hybrid POM. Both Raman and fluorescence spectroscopy are also demonstrated to be useful tools for the characterisation of these supramolecular composites, particularly as association of the POM with the nanotube leads to a strong and characteristic quenching of the pyrene emission. The authors also studied this material as a novel Li-ion electrode material and found that it displays a high discharge capacity (580 mA h g^{-1} at a current density of 0.5 mA cm^{-2}), which is retained over at least 100 charge–discharge cycles with close to 100% coulombic efficiency. Notably, this is significantly better than the performance of the hybrid POM when used as an electrode material alone (*i.e.* in the absence of CNTs). This study was followed in 2015 by Song, Streb and co-workers, who prepared a similar composite material using a pyrene-functionalised Mn-Anderson POM hybrid combined with multi-walled carbon nanotubes.[208] In this case, the composite was employed as an anode material in a prototypical Li-ion cell, which displayed improved performance with a retained capacity of 665 mA h g^{-1} (at 0.5 mA cm^{-2}) after 100 cycles. More detailed electrochemical analysis *via* AC electrochemical impedance studies revealed that the supramolecular POM/CNT composite also showed

higher performance for both Li^+ ion transport and electrical conductivity than either the CNTs alone or a physical mixture of both POM and CNT components, helping to explain its superior electrochemical properties as a potential Li-ion anode material.

Proust, Guldi, Marti-Gastaldo and Coronado and co-workers also explored the use of π–π interactions to immobilise an organosilane derivative of Wells–Dawson POM onto SWCNTs in order to study the photophysical properties of POM/CNT composites (Fig. 28).[209] Whilst no obvious ground-state electronic communication between the POMs and CNTs was discernible, fluorescence spectra of the POM/CNT composites reveals both red-shifting and a strong quenching effect on the emission maxima associated with the nanotubes. This was rationalised as being due to an unusual photoinduced charge transfer interaction between the SWCNTs and the POM, as observed by transient absorption spectroscopy, resulting from the transient oxidation of the nanotube and concomitant reduction of the POM (unusual in this case because both SWCNTs and POMs are typically employed as electron acceptors). Given the stable and well-established multi-redox activity of many hybrid POM species, the authors note the potential of such composites in the design of new advanced photochemical dyads.

Aside from the electrochemical and photochemical energy applications described above, the potential for the design of hybrid POMs as a means to selectively disperse, solubilise and enrich CNTs has been studied recently by Prato, Bonchio and co-workers. The authors first explored the interaction of a bis-pyrene organosilane derivative of $[\gamma\text{-}SiW_{10}O_{36}]^{8-}$ with both C_{60} and C_{70} fullerenes, and with SWCNTs, in order to yield a range of new supramolecular nanostructures.[210] In the case of the fullerenes, both 0-D globular nano-aggregates and 2-D Langmuir films were prepared, with the hybrid POMs found to have a ten-times higher binding affinity for the larger fullerene due to the larger π-surface of the C_{70} guest. The hybrid POM was also combined with commercially available SWCNTs and analysis of the Raman spectra, and in particular the 'radial breathing mode' (RBM) of the nanotubes (which can be associated with SWCNTs of different diameters/chiralities), was used to observe a preferential interaction of the bis-pyrene POM hybrid with larger diameter nanotubes. Crucially, when the supramolecular composite was subjected to thorough washing with acid and base, the hybrid POM could be removed to regenerate the bare nanotube, indicating that this strategy may have some promise for CNT separation and processing.

More recently, the authors also explored the use of a pair of bis-tryptophan functionalised $[\gamma\text{-}SiW_{10}O_{36}]^{8-}$ enantiomers in comparison to the previously reported pyrene-functionalised analogue.[211] In this study, each of the three hybrid POM molecular 'tweezers' was combined with a commercially available mixture of SWCNTs and the interaction between each POM 'host' and the nanotube guests was characterised using a combination of UV-vis, fluorescence and Raman spectroscopies, alongside a computational analysis of the possible binding modes. As before, the normalised RBM intensities in the Raman spectra are highly diagnostic of the nature of the interaction of the POM with the CNT and find that the smaller, more polar tryptophan binding pocket favours enrichment of nanotubes with diameters below 1.1 nm, whilst the larger, more hydrophobic bis-pyrene binding pocket enriches nanotubes with diameters between 1.1–1.2 nm. As such, the results of this study are proposed to offer useful information with regards to engineering possible SWCNT/peptide interactions for use in drug delivery and future CNS-based therapies. Interestingly, a 2014 study by Song and co-workers can be related to this concept as it also explores the use of a bis-pyrene functionalised hybrid POM to facilitate the interaction of SWCNTs with human serum albumin protein.[212] In this work, the authors use high-resolution electron microscopy alongside XPS to demonstrate that the prior non-covalent functionalisation of the CNT with the hybrid POM greatly improves the nanotubes absorption capacity for human serum albumin as compared to either of the individual components. As such, this strategy may have interesting implications for the development of future biosensors or lab-on-a-chip type applications.

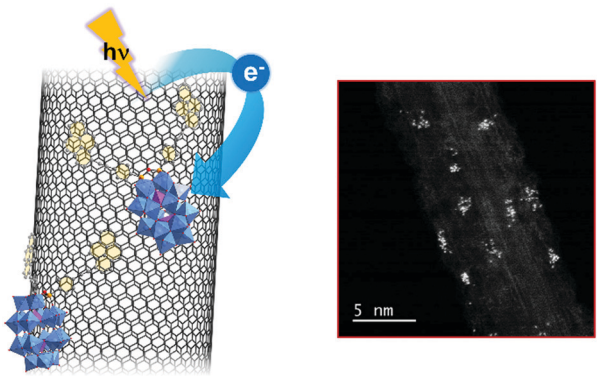

Fig. 28 (a) Non-covalent functionalisation of single-walled carbon nanotubes with a pyrene-functionalised Wells–Dawson oxocluster, highlighting the transient photo-driven charge transfer from the SWCNT to the appended POM complex, and: (b) HAADF-STEM imaging of the resultant nanocomposite (bright spots correspond to individual tungsten atoms in each POM). This figure has been adapted from ref. 209 with permission from the Royal Society of Chemistry, copyright 2014.

4.3 Hybrid POM complexes with biological structures

The interactions of POMs with biomolecules and their corresponding biological activity has been a target of study for many years.[213–216] Their high charge and strong hydrogen bonding character allows POMs to interact in a variety of interesting ways with biological substrates such as proteins, lipids and nucleic acids, whilst the extraordinary tuneability of POM structure and composition provides near limitless opportunities for researchers to tailor these properties.

Perhaps the most striking recent example of the application of POM–biomolecule interactions can be found in the award of the 2009 Nobel Prise in Chemistry to Ada Yonath, who was awarded a share of the prise for her seminal work in protein crystallography and uncovering the structure of the ribosome. In part, this work exploited the interaction of a simple $(NH_4)_6[P_2W_{18}O_{62}]$ Wells–Dawson oxocluster with specific sites in the ribosomal subunits of a model organism, *Thermus*

Thermophilus, to dramatically extend the resolution of the diffraction map from *ca.* 7–9 Å to 3 Å.[217] In recent years, the interaction of POMs with biological systems has expanded to encompass a range of different interests, including their exploration as protein crystallisation agents,[214,218] artificial enzyme mimics,[215] and metallodrugs.[216]

The potential for hybrid POMs in this area is also obvious. The ability to graft almost any organic functionality onto an inorganic POM with real synthetic control could, in some cases, represent a 'best-of-both-worlds' approach, where the functionality of the POM (be it as an imaging tool, a metallodrug, an enzyme mimic, *etc.*) could be selectively introduced to the intended substrate in a site-specific fashion by carefully controlling its specific binding interactions *via* the appended organic side-chains. In addition, the enhanced stability of covalently bound hybrid POMs could be a real advantage in elucidating mechanistic details of the mode of action of POMs in biological systems such as drug assays, where the relative ease with which the electrostatically-bound hybrids (where the organic functionality is appended to the POM as a charge balancing cation) can dissociate under biologically relevant conditions may make identifying the true active species all the more challenging.[219,220] As such, it is worth noting that while this section will attempt to serve as a brief overview of this growing field, it is difficult to fully encompass all research activities within the particular scope of this review and also that the exact nature of the non-covalent or supramolecular interactions which predominate in POM–biomolecule interactions is often, understandably, not as clear-cut as in many of the examples reported above.

As discussed above, one of the clearest success stories in this field in recent years is the application of POMs as crystallisation agents in protein crystallography. The interaction of POMs with proteins often serves two purposes: solving the "phase problem", and helping to stabilise the folded protein structure, aiding both crystallisation and improving the resolution of the crystal structure. In recent years, much of this work has been pioneered by Rompel and co-workers, who have studied the use of the tellurium-centred Anderson oxocluster $[TeMo_6O_{24}]^{6-}$ to resolve the previously unknown structures of a mushroom tyrosinase and aurone synthase.[221,222] Though most research in this area has focused exclusively on pristine POMs, the same group also recently explored the potential of a series of hybrid Anderson oxoclusters to be used as additives in the crystallisation of human and bovine serum albumin proteins (Fig. 29). In these studies, the authors prepared a series of Anderson oxoclusters with a range of both mono- and bis-substituted hydrophilic ligands (*e.g.* $-NH^{3+}$ or –OH terminated tris-bases),[223] and bis-substituted hydrophobic ligands (phenyl- or cinnamic acid-terminated groups),[224] and studied their stability under biologically relevant aqueous conditions in the presence of the relevant protein. In both cases, the oxoclusters showed excellent stability in a pH range of 4 to 9 and, critically, showed no hydrolytic reactivity towards the serum albumin proteins. The more hydrophilic species all showed clear interaction with the surface of BSA, leading to a charge inversion from positive to negative zeta potentials, indicating their broad

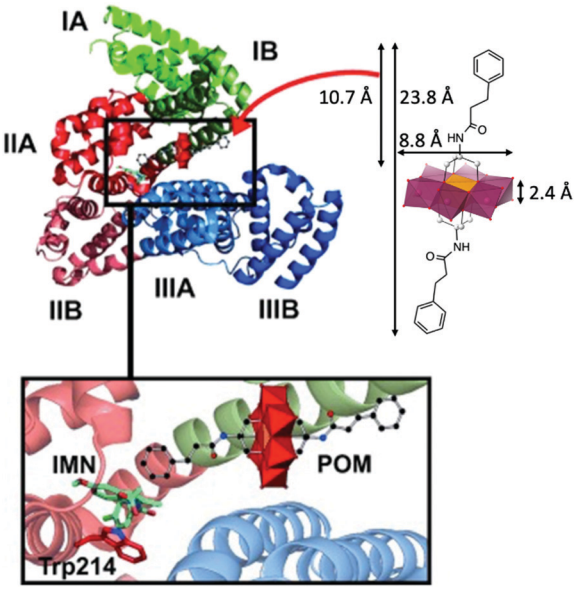

Fig. 29 Representation of the hypothetical binding site of a benzene-functionalised Anderson-type hybrid POM in Human Serum Albumin protein (shown as a ribbon structure with each subdomain depicted in a different colour). Shown inset is a closer view of the position of the hybrid POM within the HSA binding site alongside indomethacin (IMN) and tryptophan (Trp214) groups which are used to confirm binding of the POM through fluorescence studies. This figure has been adapted from ref. [224] with permission from John Wiley and Sons, copyright 2015.

suitability as additives. In the more hydrophobic hybrid POMs, fluorescence quenching measurements were employed to study the specific binding of the hybrid with HSA and from this the authors were able to propose a 1:1 interaction between the protein and the POM, identifying a specific binding interaction on a particular subdomain site in the protein structure. Though it is important to recognise that the use of hybrid POMs as macromolecular crystallisation agents is still at a very early stage, it is worth noting the authors' own perspective (expressed in a recent review)[225] that hybrid POMs may be particularly useful as additives in the notoriously challenging crystallisation of membrane proteins. This is because these proteins are typically highly hydrophobic, precluding the use of pristine POM additives, which bind to proteins mainly through polar interactions. As exemplified in Section 3.2, there are already numerous examples of surfactant-like hybrid POM amphiphiles, which may be interesting to explore for this application in the future.

Alongside these crystallisation studies, several other examples of interactivity between hybrid POMs and peptide or protein units have also been discussed recently in the literature. Recently, Bonchio and Carraro demonstrated the interaction of a bis-biotinylated $[\gamma\text{-}SiW_{10}O_{36}]^{8-}$ POM with the tetrameric avidin protein, exploiting the well-known host–guest chemistry of the biotin–avidin complex.[226] This study is interesting in that it clearly shows a dual-mode interaction between the hybrid-POM and the protein, where both weak and non-specific electrostatic association, and strong and highly site-specific host–guest binding can be determined by a combination of fluorimetry, CDS, UV-vis and surface-plasmon resonance studies.

In addition to these studies, the intra-molecular association of peptide chains when bound to POMs has also been explored. For instance, Cronin *et al.* demonstrated the use of a bis-functionalised Anderson oxocluster as an ''inorganic amino acid'' in the solid-supported preparation of a range of oligopeptide chains.[227] When used to prepare a symmetrical peptide sequence in which the POM is grafted to two identical 15-mer chains, an interesting structural feature was observed by CDS, whereby the 15-mer itself showed no obvious chirality however the new hybrid POM shows clear features characteristic of α-helix formation. Although the authors were unable to probe this feature further due to the limited solubility of the hybrid oligopeptide conjugate, it does suggest an interesting interplay between the POM and the appended biomolecules which leads to the formation of some secondary structure. A more recent study by Dumont, Lelli and Lacôte has explored the intra-molecular interactions between POMs and peptides in more detail.[228] In this work, the authors prepared a family of hybrid Wells Dawson oxoclusters to which a series of short polyglycine chains are appended and then used a combination of spectroscopic characterisation and molecular dynamics simulations to study the conformation of the peptide and its specific interaction with the surface of the POM. This found that the polyglycine chains fold towards the POM surface, forming ''zipper-like'' hydrogen bond networks where the specific structure is determined by the topology of the POM (the authors used different POM isomers), and that hydrogen-bonding interactions between the POM and the peptide chain serve to rigidify the normally conformationally flexible peptide, even when longer chain structures are used.

The interaction of hybrid POMs with oligonucleotides/DNA has also been explored recently by Hasenknopf, O'Sullivan and co-workers as a strategy for the electrochemical detection of polymerase chain reaction (PCR) products. The authors prepared organotin-functionalised Wells–Dawson and Keggin oxoclusters and conjugated them with a 5′-NH_2 terminated 21-mer oligonucleotide primer using an amide-coupling approach.[229] Though the small quantities of product are challenging for typical POM characterisation, the new conjugate was successfully analysed using a combination of electrospray ionisation mass spectrometry (ESI-MS) and vibrational spectroscopies. The resulting conjugates were then used in the PCR amplification of a sequence of *Francisella tularensis* and the resulting POM-bearing single-stranded DNA (ssDNA) was electrochemically characterised by hybridisation with a complimentary sequence appended to a gold electrode surface (Fig. 30). All hybrid POM/DNA conjugates were found to have detection limits in the sub-10 nM range, with the hybrid Wells–Dawson found to have the higher sensitivity thanks to its bulkier structure facilitating easier electron transfer. The authors then built on this study using a modified approach, coupling a 7-deaza-7-propargylamino purine base directly to the organotin-functionalised Keggin and Wells–Dawson POMs in order to facilitate direct incorporation of the redox tagged purine into the PCR product for improved electrochemical detection.[230] Most recently, the authors expanded the latter approach to explore the multiplexed detection of single nucleotide polymorphisms on a microfluidic electrode array.[231]

Hybrid POMs have also been explored in combination with a range of live cell types (*e.g.* viruses, bacteria and/or mammalian)

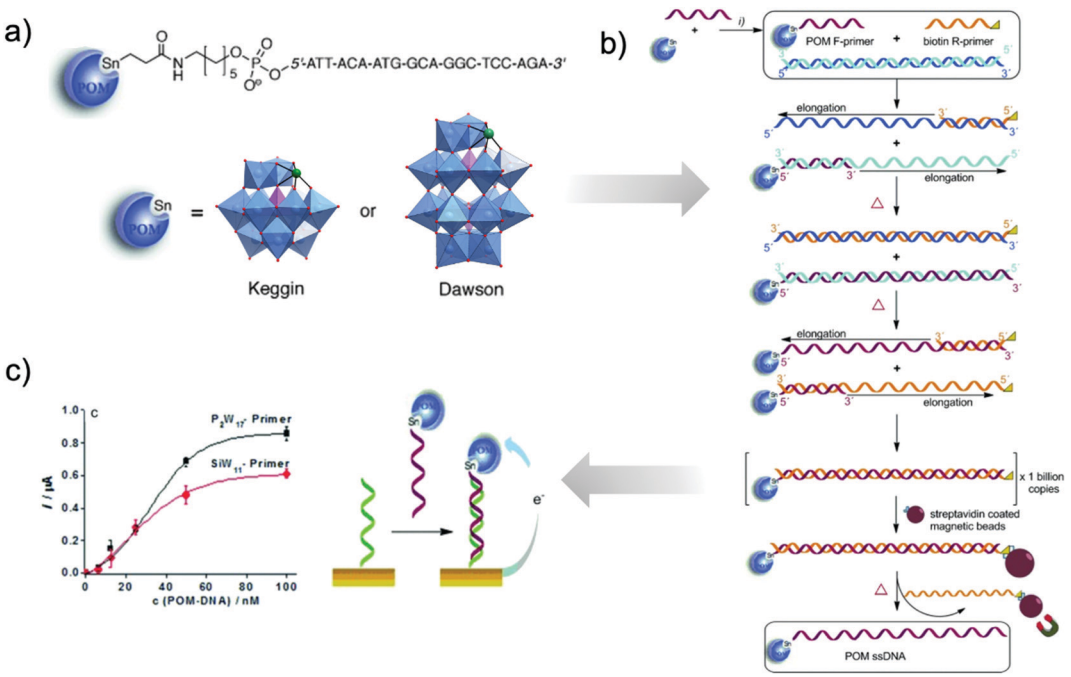

Fig. 30 Schematic of: (a) the bio-functionalisation of either Keggin- or Wells–Dawson-type POMs with an oligonucleotide for use as a forward-primer (F-primer) in PCR amplification (b) and the subsequent electrochemical detection of POM-labelled PCR products (c). This figure has been adapted from ref. 229 with permission from John Wiley and Sons, copyright 2015.

and are of obvious specific interest in the design and targeting of these species as novel metallodrugs in particular (*vide infra*). As might be expected, these interactions are often complex, difficult to characterise and can even be somewhat counterintuitive. As an example, Cronin *et al.* reported the preparation of an asymmetric Mn-Anderson hybrid POM self-assembled monolayer (SAM) functionalised with pyrene groups which was used for cell-adhesion studies with human fibroblast cells.[232] In this work, the hybrid POM SAM was found to be an effective adherent, however equivalent SAMs terminated in either pyrene groups or the amino-tris-base functionalised POM alone showed no cell adhesion properties, indicating the special utility of the hybrid POM nanostructure. POMs have also been shown to both disrupt,[233,234] and penetrate,[235,236] a variety of microbial and mammalian cell membranes, which allows their targeted use in a range of imaging, theranostic and metallodrug applications.[216] For instance, Patzke *et al.* have shown the covalent attachment of fluorescein to a Wells–Dawson oxocluster in order to study the cellular uptake and distribution of the hybrid POM in HeLa cells *via* confocal fluorescence microscopy.[237] The hybrid oxocluster was found to be stable at physiological pH, non-cytotoxic and had good cell uptake over 24 h, with the oxoclusters showing various dispersion modes throughout the cytoplasm.

Fabretti, Bonchio, Carraro and co-workers recently reported a similar study, preparing a family of fluorophore-functionalised $[\gamma\text{-}SiW_{10}O_{36}]^{8-}$ and $[A\text{-}\gamma\text{-}PW_9O_{34}]^{9-}$ hybrid oxoclusters to study their internalisation into model HEK cells.[238] Interestingly, the comparatively hydrophobic fluorophores (*i.e.* dansyl-, pyrene- and fluorescein-groups) make these hybrid POMs amphiphilic, and they self-assemble into spherical aggregates of *ca.* 80–200 nm in size when dispersed in the aqueous phase. This is highly significant because, as will be discussed in more detail below, the formation of vesicular/micellular structures appears to be particularly important in mediating interactions between the POM and the lipid bilayer of the cell membrane.[234,239] As such, the authors find that their hybrid POMs show good cell uptake and negligible cytotoxicity but in this case, that the localisation of the hybrid POM within the cells is dependent on both the nature of the oxocluster and fluorophore. For instance, dansyl- and pyrene-functionalised $\{SiW_{10}\}$ oxoclusters are mainly co-localised with the mitochondria, whereas the fluorescein–$\{SiW_{10}\}$ and $\{PW_9\}$ hybrids showed preferential targeting of the cell nuclei. This clearly indicates the multifaceted interplay between both the inorganic and organic components of the imaging agent with its cellular uptake behaviour, and highlights both the complexity of the challenge in elucidating clear design rules for bioactive hybrid POM species but also their immense potential for developing tuneable and highly specific biological interactions.

The final application for which POMs have been explored in a biological context is as novel metallodrugs and anti-microbial agents. The broader context of this field lies well outside the scope of this review, and readers are directed to several excellent recent summaries for a more detailed overview,[215,216,240] however it is fair to say that the vast majority of these approaches have relied on the use of the direct action of purely inorganic POMs (or their synergistic combination with more conventional antibiotics) to elicit a pharmacological effect. Broadly speaking, these approaches have found some initial successes although persistent issues with low activity (at least in comparison with other conventional medicines), poor stability under physiological conditions, and the long-term and significant toxicity of POMs have been identified as the most pressing problems. The use of hybrid POMs thus represents a unique opportunity to design more tailored systems with improved uptake/activity, stability and – most importantly – reduced cytotoxicity. This has been shown in recent studies where hybrid POMs are found to have superior properties in both antiviral applications, such as inhibition studies against HIV protease,[241] and in antibacterial studies against a broad range of Gram-positive and Gram-negative organisms.[242]

Pristine POMs have been known to have inhibitory activity against tumour cells since the 1960s,[243] however the use of hybrid POMs in this field has been an increasingly active area of research over the last decade in particular. For instance, a number of studies using a range of organoimido- and organobenzoyldiazenido-functionalised hexamolybdate Lindqvist-type POMs have shown significant inhibitory activity towards a range of human leucocythemia and breast cancer cell lines.[244–246] Dolbecq, Oldfield and co-workers also reported comparable trends in a series of bisphosphonate–polyoxomolybdate hybrids,[247,248] the most effective of which was complexed to the bisphosphonate-based drug zolendronate and showed promising activity against human sarcoma cells in a mouse xenograft, decreasing tumour volume by *ca.* 85% against the control whilst showing no adverse toxicity towards the mice. This trend follows that previously reported for an organotin-functionalised Keggin ion, $[GeW_9O_{34}\{Sn(OH)(n\text{-}Bu)\}_3]^{4-}$, which has substantial inhibitory *in vivo* activity against hepatocarcinoma mice models with markedly lower toxicity than the clinical chemotherapeutic, cyclophosphamide.[249]

The impressive pharmaceutical activity attainable by hybrid POMs was also observed recently in a tris-functionalised hexavanadate oxocluster grafted to amino acid esters, which was assayed against a range of human cancer cell lines and showed higher inhibitory activity than the clinically available chemotherapy drug 5-fluorouracil.[250] Hybrid Anderson oxoclusters have also shown promise as therapeutic agents, as recently demonstrated by Wang *et al.*, who found that a cholic-acid functionalised Mn-Anderson oxocluster showed promising inhibition against breast cancer cells *in vitro*, whilst being significantly less toxic to a non-cancerous control cell line.[251] It is important to note that in each of the cases highlighted above, a synergistic effect between both the POM and the organic group appears to be crucial, as the hybrid species are universally more active than either the parent oxocluster and/or the appended organic group (even if the exact mechanism still remains a mystery). That said, a recent report by Carraro, Ruzza and co-workers also highlights the difficulties of teasing out structure–activity relationships in biological systems and that much further work is required. In this study, a Mn-Anderson oxocluster was functionalised with a short-chain peptide sequence (demobensin-1, which is specific to receptors on cancer cells)

in order to study targeted therapy with the POM-based metallodrug.[252] In this case, however, the hybrid oxocluster is found to have similar activity towards HeLa cells as the parent tris-base Mn-Anderson, indicating a non-receptor mediated uptake mechanism. Interestingly, the authors note that this may be due to conformational effects caused by incorporation of the POM into the peptide sequence, as discussed in examples given above.[227,228]

The use of hybrid polyoxomolybdate metallodrugs also opens pathways to more complex or strategic molecular design strategies in order to enhance targeting and efficacy or add additional functionality. A notable example of this was reported by Chen, Hao and Wei, who demonstrated a novel *in situ* degradation strategy using a hexamolybdate oxocluster linked to a cleavable *N*-acylureido (acy) group by a 2-amino-3-methylbenzoxyl (AMB) linker.[253] The POM–AMB–acy hybrid was found to be metastable when tested in cell incubation medium, decomposing within 40 min to form MoO_4^{2-} as the primarily active species. Most remarkably, the hybrid POM was shown to have a strong inhibitory effect against malignant glioma cells (*ca.* 20× more effective than the clinically used antiglioma medication temozolomide) and was also found to be able to cross the blood–brain barrier *in vivo*. Another example by Yadollahi and co-workers exploit a hybrid $[GeW_9V_3O_{37}((CH_2O)_3N–Boc–Cys)]^{4-}$ oxocluster (Boc = *tert*-butyloxycarbonyl, Cys = cysteine) which is then post-synthetically coupled with thiolated mesoporous silica nanoparticles (*via* a disulphide bond) loaded with the anticancer drug doxorubicin, and the imaging agent fluorescein isothiocyanate (*via* deprotection of the Boc group).[254] The disulphide bond is cleavable within the unique environment of cancerous cells, causing decoupling of the hybrid POM from the nanoparticles, releasing both the fluorescent-tagged POM and the doxorubicin into the cellular environment. The nanocomposites were found to have superior activity against glioblastoma cells *in vitro* when compared to either the POM or chemotherapy drug alone.

In line with the broader themes of this review, the complex supramolecular assembly and non-covalent interactions between hybrid POM species and biological entities cannot be underestimated. This is most clearly demonstrated in an elegant study by Liu *et al.*, who developed an unusual long-chain alkoxysilane-modified Preyssler anion (Fig. 31), $[NaP_5W_{30}O_{110}\{Si(CH_2)_3NHCON(C_{16}H_{33})_2\}]^{14-}$, which spontaneously self-assembled into a liposome-like structure due to the amphiphilic character of the hybrid POM.[239] Whilst both the hybrid $\{P_5W_{30}\}$ oxocluster and the parent $\{P_5W_{30}\}$ Preyssler anion showed significantly higher antiproliferative properties against human colorectal cancer cells *vs.* 5-fluorouracil, the supramolecular assembly of the hybrid into vesicular structures was found to improve its inhibitory activity, particularly over shorter incubation times (*e.g.* <48 h). The authors used a biotinylated model membrane structure to elucidate the interaction between the both the hybrid POM liposomes and the parent inorganic POM with the cell membrane. This found that whilst both compounds rapidly associate with the lipid bilayer of the cell wall, the inorganic POM can easily dissociate back into the bulk whilst the hybrid oxocluster tends to strongly intercalate with the bilayer, forming a stable POM/lipid complex which facilitates its uptake into the cytoplasm. This model is therefore consistent with the greater activity of the hybrid complex, particularly over shorter incubation times.

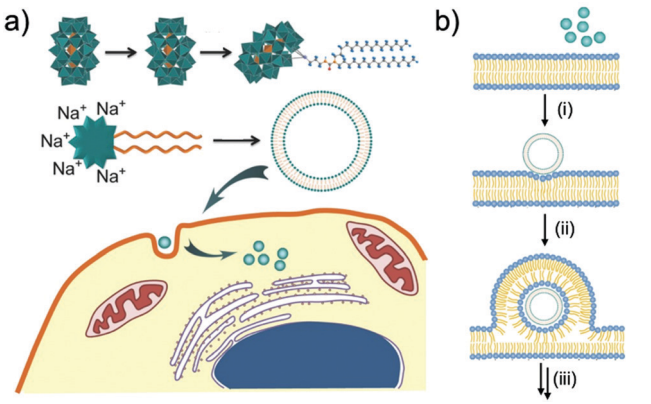

Fig. 31 (a) Schematic of the synthesis of a lipid-modified Preyssler-type hybrid POM and its self-assembly into vesicles which facilitate its membrane crossover and intracellular localisation within human colorectal tumour cells (*in vitro*), and; (b) proposed model of the interaction between hybrid POM vesicles and the phospholipid bilayer of the cell-membrane, showing: (i) binding of the POM-vesicle to the lipid membrane, (ii) trapping/intercalation of the vesicle within the membrane bilayer (preventing dissociation), and (iii) membrane crossover and uptake into cell interior. Colour code: $\{WO_6\}$ = teal polyhedra; $\{PO_4\}$ = orange polyhedra; Si = blue/grey; C = grey; N = orange; O = red; H = blue. This figure has been reproduced from ref. 239 with permission from John Wiley and Sons, copyright 2015.

In similarly elegant work, the authors built on this study to demonstrate how a tweezer-like organoplatinum-functionalised Keggin could be deployed as a potent pro-drug against human colorectal cancers when encapsulated into a block copolymer shell.[255] The resulting nanoparticles are able to intercalate with and penetrate the cell membrane as before, and the hybrid POM nanocomposite shows both superior anti-tumour activity and improved biocompatibility *vs.* cisplatin in mice models.

5 Perspectives

The organofunctionalisation of POMs offers a direct and highly controllable means modify both the electronic structure and physical character of the molecular species. Simultaneously, it entails the chemist to explore and subsequently tune the nature of the non-covalent interactions between neighbouring molecules and between these molecules and their environment. This highly specific supramolecular chemistry and its potential to extend the self-assembly of POMs into materials that bridge the molecular, nano, and macro length scales, will lead to new, as yet, unexplored potential applications in a range of technologies, spanning energy storage, data processing, site-specific catalysis, and biomolecular transformations.

To this end, the elaboration of hybrid POM nanoassemblies, whether as colloids or as nanomaterials, necessitates the implementation of additional characterisation techniques beyond those classically used to probe the characterisation

of POMs (*e.g.* multinuclear NMR or single crystal X-ray diffraction). To highlight just a few of these approaches, NMR diffusion experiments can give access to the self-diffusion coefficient (this technique being yet only adapted to discrete systems as colloids have T_2 relaxation times which are too short to probe adequately), dynamic light scattering can provide insights into the size and solution behaviours of POM-based nanoaggregates and X-ray scattering measurements allow solution phase structure determination of molecular assemblies or aggregates of sizes ranging from 1 to 100 nm, while also providing information on the molecular-level nanostructure. Microscopy techniques, especially TEM and cryo-TEM (despite the technical challenges posed by damage to samples by the high energy electron beam), have been widely and successfully employed owing to the very high electron density (and thus achievable imaging contrast) of most polyoxometalates. Cryo-TEM is particularly useful since it allows the direct observation of complex supramolecular nanostructures without being altered by the interaction with the substrate and/or the ultra-high vacuum required with classical electron microscopy techniques. That said, cryo-TEM is mostly limited to high freezing point solvents such as water or DMSO and it is still not widely employed in the POM community.

Though the application of advanced analytical techniques for the characterisation of POM-based assemblies and nanomaterials will surely continue to improve, it is also worth highlighting that theoretical studies also remain a considerable challenge owing to the time-consuming calculations required for such large systems containing a large number of heavy atoms.[256] As an example, density functional theory simulations are usually limited to systems containing just 4 discrete POM clusters. The combination of DFT with molecular dynamics simulation methods is, however, particularly well-suited for investigating aggregation processes at the molecular level. Promising first attempts, which outlined the importance of both solvation and the association of the POM with counter cations in the aggregation process have been recently reported,[90,257] though it must be noted that this approach is still limited to modest numbers of POM clusters. To address this, coarse-grained molecular dynamics simulations have proven effective as a method to considerably increase the size of simulated supramolecular assemblies. This approach has, for example, been investigated to study the formation of large Keplerate-type POM assemblies,[258,259] though further development is required in order to properly parametrise and account for the peculiar chaotropic character of POMs in particular.[176,178] As ever, the combination of experiment and theory is critical in order to provide the fundamental understanding of hybrid POM assembly in order to guide the further design of complex, multifunctional molecular architectures.

This review article outlines the enormous diversity in both the physical nature (*e.g.* molecular and supramolecular aggregates, colloidal micelles and vesicles, gels, liquid crystals and crystalline networks) and structure of hybrid POM-based self-assembled nanostructures. However, while materials using pristine (*i.e.* unmodified) POMs and transition metal substituted POMs are increasingly well-developed for application across a range of different fields (*e.g.* electrochemical storage,[200] dye-sensitised solar cells,[260] catalysis,[261] proton exchange membranes,[262] electrochromic devices,[164] to highlight but a few), the implementation of self-assembled hybrid POM nanostructures into tangible device configurations remains essentially unexplored, despite the indisputable advantages of these nanomaterials. This may, in part at least, be due to the typically more demanding synthesis of these materials in comparison to the often 'one-pot' nature of traditional POMs, but the potentially lower chemical and thermal robustness of these species must also be considered. Closer cooperation between experts in POM chemistry and materials scientists in particular, will be critical in closing this gap.

The advantages presented by the unique properties accessible through the continued design and development of hybrid POMs and their related nanostructures are, however, clear. Numerous examples of emerging areas of study have been presented above – ranging from the formation of dynamic nanocapsules, of interest for catalysis or energy storage, to the development of photoswitchable nanomaterials showing cooperative properties. Indeed, the continued development of nanostructured soft materials based on hybrid POMs, which combine long-range ordering with distinct, switchable functionalities would constitute a major advance and lead to a range of interesting potential applications as new nanoscale sensors or actuators. Furthermore, although POMs have very well-established (and highly tuneable) multi-redox activities – marking them as being of considerable interest as unique energy storage, electronic or catalytic species – POMs often exhibit low or negligible conductivity in the solid state.[263–265] Consequently, unless processed as thin films or embedded in a conductive matrix (*e.g.* conductive polymers or bulk or nanostructured carbons, *etc.*), full exploitation of the attractive redox chemistry of POM-based materials is highly challenging to achieve. The supramolecular-assembly of POM units *via* their hybridisation with a range of structure-directing and/or electronically active organic groups is therefore an especially interesting avenue for further study, and it will be particularly important to develop clear structure–property relationships and new design rules to govern the fabrication of new electronically active materials. Finally, there is unquestionably scope to develop the concept of tuneable POM-biomolecule interactions, perhaps in tandem with studies on the photo/electrochemical properties of the assembly. This challenging issue remains mostly unexplored, while the development of hybrid POMs with organic groups targeting site specific binding or molecular recognition for precise diagnosis and therapy would also constitute a major breakthrough in this field.

6 Conclusion

In summary, this review provides a comprehensive discussion of the supramolecular self-assembly of hybrid nanomaterials based on pre-defined organofunctionalised hybrid-polyoxometalate

synthons/building blocks. Hybrid-POMs offer almost unparalleled opportunities to seamlessly integrate both organic and inorganic functionalities into new, hierarchically structured assemblies, where the inherent redox, photochemical and catalytic reactivity of the metal oxide sub-unit can be combined with the highly tuneable structure-directing properties (either *via* covalent or non-covalent interactions) of the appended organic groups. As several excellent reviews have recently described the synthesis and functionalisation of hybrid POMs themselves, this review focuses exclusively on how the clearly defined structure, chemistry and directionality of these unique molecular building blocks allows for new semi-rational design approaches to be applied in the construction of larger molecular and supramolecular assemblies. Numerous synthetic strategies have emerged as the field has rapidly grown over the past decade or so, which we have broadly broken down into two distinct categories: (i) direct self-assembly, whereby metal-directed, amphiphilic, electrostatic or hydrogen-bonding interactions are used to generate new nanomaterials in both the solution and solid state, or; (ii) self-assembly mediated by a substrate, whereby non-covalent interactions between the hybrid POM synthon(s) and a range of possible host/guest species (ranging from other small molecules such as cavitands, through carbon nanomaterials and even large biomolecules) is used to generate new species or facilitate integration of the hybrid POM into larger biological systems such as microbes or mammalian cells. It is also important to note that while this field is still very much in its infancy, with rapid progress being made over only the last decade or so, several key examples of emerging or potential application areas have also been discussed, including in catalysis, energy storage, and biochemistry.

Author contributions

All authors contributed to data curation of the literature and writing the original draft. JMC, GG, GNN and GI conceptualised the review, performed reviewing and editing of the manuscript and contributed to visualisation of the figures. SA contributed additional visualisation of some 3D graphical assets.

Conflicts of interest

There are no conflicts to declare.

Acknowledgements

All authors thank the EPSRC International Network on Polyoxometalate Science for Advanced Functional Energy Materials (EP/S031170/1). GNN and JMC thank the Leverhulme Trust (RPG-2016-442) and the University of Nottingham Propulsion Futures Beacon of Excellence for support. E. H. thanks the Low Dimensional Materials and Interfaces Doctoral Training Programme at the University of Nottingham. S. A. thanks the EPSRC for funding through the Centre for Doctoral Training in Sustainable Chemistry (EP/L015633/1). KMH thanks the French National Research Agency (MESOMORPHICS project Grant ANR-20-CE06-0021) for PhD funding.

Notes and references

1 G. M. Whitesides, J. K. Kriebel and B. T. Mayers, *Self-Assembly and Nanostructured Materials*, Springer, Berlin, 2005.
2 N. Rahimi and R. Karimzadeh, *Appl. Catal., A*, 2011, **398**, 1–17.
3 E. Ruiz-Hitzky, P. Aranda, M. Darder and M. Ogawa, *Chem. Soc. Rev.*, 2011, **40**, 801–828.
4 E. Moulin, J. J. Cid and N. Giuseppone, *Adv. Mater.*, 2013, **25**, 477–487.
5 A. S. Tayi, A. K. Shveyd, A. C. H. Sue, J. M. Szarko, B. S. Rolczynski, D. Cao, T. J. Kennedy, A. A. Sarjeant, C. L. Stern, W. F. Paxton, W. Wu, S. K. Dey, A. C. Fahrenbach, J. R. Guest, H. Mohseni, L. X. Chen, K. L. Wang, J. F. Stoddart and S. I. Stupp, *Nature*, 2012, **488**, 485–489.
6 H. B. Yu, Y. Luo, K. Beverly, J. F. Stoddart, H. R. Tseng and J. R. Heath, *Angew. Chem., Int. Ed.*, 2003, **42**, 5706–5711.
7 J. R. Li, R. J. Kuppler and H. C. Zhou, *Chem. Soc. Rev.*, 2009, **38**, 1477–1504.
8 G. Ferey, C. Serre, T. Devic, G. Maurin, H. Jobic, P. L. Llewellyn, G. De Weireld, A. Vimont, M. Daturi and J. S. Chang, *Chem. Soc. Rev.*, 2011, **40**, 550–562.
9 S. Y. Reece, J. A. Hamel, K. Sung, T. D. Jarvi, A. J. Esswein, J. J. H. Pijpers and D. G. Nocera, *Science*, 2011, **334**, 645–648.
10 Y. L. Wu, K. E. Brown and M. R. Wasielewski, *J. Am. Chem. Soc.*, 2013, **135**, 13322–13325.
11 Y. Sun, C. Y. Chen and P. J. Stang, *Acc. Chem. Res.*, 2019, **52**, 802–817.
12 C. A. Hunter and H. L. Anderson, *Angew. Chem., Int. Ed.*, 2009, **48**, 7488–7499.
13 C. Rest, R. Kandanelli and G. Fernandez, *Chem. Soc. Rev.*, 2015, **44**, 2573.
14 C. J. Bruns, D. Fujita, M. Hoshino, S. Sato, J. F. Stoddart and M. Fujita, *J. Am. Chem. Soc.*, 2014, **136**, 12027–12034.
15 P. Luisi, *Found. Chem.*, 2002, **4**, 183–200.
16 H. N. Miras, J. Yan, D. L. Long and L. Cronin, *Chem. Soc. Rev.*, 2012, **41**, 7403–7430.
17 A. Misra, K. Kozma, C. Streb and M. Nyman, *Angew. Chem., Int. Ed.*, 2020, **59**, 596–612.
18 Y. F. Song and R. Tsunashima, *Chem. Soc. Rev.*, 2012, **41**, 7384–7402.
19 H. L. Li and L. X. Wu, *Polym. Int.*, 2020, **69**, 665–667.
20 K. I. Assaf and W. M. Nau, *Angew. Chem., Int. Ed.*, 2018, **57**, 13968–13981.
21 M. A. Moussawi, N. Leclerc-Laronze, S. Floquet, P. A. Abramov, M. N. Sokolov, S. Cordier, A. Ponchel, E. Monflier, H. Bricout, D. Landy, M. Haouas, J. Marrot and E. Cadot, *J. Am. Chem. Soc.*, 2017, **139**, 12793–12803.
22 P. C. Yin, D. Li and T. B. Liu, *Chem. Soc. Rev.*, 2012, **41**, 7368–7383.

23 M. Bonchio, Z. Syrgiannis, M. Burian, N. Marino, E. Pizzolato, K. Dirian, F. Rigodanza, G. A. Volpato, G. La Ganga, N. Demitri, S. Berardi, H. Amenitsch, D. M. Guldi, S. Caramori, C. A. Bignozzi, A. Sartorel and M. Prato, *Nat. Commun.*, 2019, **11**, 146–153.
24 G. H. Zhang, B. Y. Li, Y. Zhou, X. F. Chen, B. Li, Z. Y. Lu and L. X. Wu, *Nat. Commun.*, 2020, **11**, 425.
25 L. Yue, S. Wang, D. Zhou, H. Zhang, B. Li and L. X. Wu, *Nat. Commun.*, 2016, **7**, 10742.
26 T. Lunkenbein, M. Kamperman, Z. H. Li, C. Bojer, M. Drechsler, S. Forster, U. Wiesner, A. H. E. Muller and J. Breu, *J. Am. Chem. Soc.*, 2012, **134**, 12685–12692.
27 M. A. Alam, Y. S. Kim, S. Ogawa, A. Tsuda, N. Ishii and T. Aida, *Angew. Chem., Int. Ed.*, 2008, **47**, 2070–2073.
28 W. Li and L. X. Wu, *Polym. Int.*, 2014, **63**, 1750–1764.
29 J. M. Cameron, D. J. Wales and G. N. Newton, *Dalton Trans.*, 2018, **47**, 5120–5136.
30 G. Izzet, F. Volatron and A. Proust, *Chem. Rec.*, 2017, **17**, 250–266.
31 A. Proust, B. Matt, R. Villanneau, G. Guillemot, P. Gouzerh and G. Izzet, *Chem. Soc. Rev.*, 2012, **41**, 7605–7622.
32 M. P. Santoni, G. S. Hanan and B. Hasenknopf, *Coord. Chem. Rev.*, 2014, **281**, 64–85.
33 C. P. Pradeep, D.-L. Long, G. N. Newton, Y.-F. Song and L. Cronin, *Angew. Chem., Int. Ed.*, 2008, **47**(23), 4388–4391.
34 In this article, we define the POM functionalization as the covalent grating of one or several organic moieties onto the polyoxometalate framework.
35 A. J. Kibler and G. N. Newton, *Polyhedron*, 2018, **154**, 1–20.
36 J. X. Liu, X. B. Zhang, Y. L. Li, S. L. Huang and G. Y. Yang, *Coord. Chem. Rev.*, 2020, **414**, 213260.
37 L. Vila-Nadal and L. Cronin, *Nat. Rev. Mater.*, 2017, **2**, 17054.
38 A. V. Anyushin, A. Kondinski and T. N. Parac-Vogt, *Chem. Soc. Rev.*, 2020, **49**, 382–432.
39 A. Dolbecq, E. Dumas, C. R. Mayer and P. Mialane, *Chem. Rev.*, 2010, **110**, 6009–6048.
40 J. Spandl, C. Daniel, I. Brudgam and H. Hartl, *Angew. Chem., Int. Ed.*, 2003, **42**, 1163–1166.
41 S. Chakraborty, E. Schreiber, K. R. Sanchez-Lievanos, M. Tariq, W. W. Brennessel, K. E. Knowles and E. M. Matson, *Chem. Sci.*, 2021, **12**, 12744–12753.
42 B. E. Petel, R. L. Meyer, M. L. Maiola, W. W. Brennessel, A. M. Muller and E. M. Matson, *J. Am. Chem. Soc.*, 2020, **142**, 1049–1056.
43 G. S. Kim, K. S. Hagen and C. L. Hill, *Inorg. Chem.*, 1992, **31**, 5316–5324.
44 S. Fujimoto, J. M. Cameron, R. J. Wei, K. Kastner, D. Robinson, V. Sans, G. N. Newton and H. Oshio, *Inorg. Chem.*, 2017, **56**, 12169–12177.
45 J. M. Cameron, S. Fujimoto, K. Kastner, R.-J. Wei, D. Robinson, V. Sans, G. N. Newton and H. H. Oshio, *Chem. – Eur. J.*, 2016, **23**(1), 47–50.
46 J. M. Cameron, S. Fujimoto, R.-J. Wei, G. N. Newton and H. Oshio, *Dalton Trans.*, 2018, **47**(31), 10590–10594.
47 B. Matt, S. Renaudineau, L. M. Chamoreau, C. Afonso, G. Izzet and A. Proust, *J. Org. Chem.*, 2011, **76**, 3107–3112.
48 K. Nomiya, Y. Togashi, Y. Kasahara, S. Aoki, H. Seki, M. Noguchi and S. Yoshida, *Inorg. Chem.*, 2011, **50**, 9606–9619.
49 C. N. Kato, Y. Kasahara, K. Hayashi, A. Yamaguchi, T. Hasegawa and K. Nomiya, *Eur. J. Inorg. Chem.*, 2006, 4834–4842.
50 S. Aoki, T. Kurashina, Y. Kasahara, T. Nishijima and K. Nomiya, *Dalton Trans.*, 2011, **40**, 1243–1253.
51 C. R. Mayer, I. Fournier and R. Thouvenot, *Chem. – Eur. J.*, 2000, **6**, 105–110.
52 F. B. Xin and M. T. Pope, *Inorg. Chem.*, 1996, **35**, 5693–5695.
53 F. B. Xin, M. T. Pope, G. J. Long and U. Russo, *Inorg. Chem.*, 1996, **35**, 1207–1213.
54 F. B. Xin and M. T. Pope, *Organometallics*, 1994, **13**, 4881–4886.
55 R. Cao, K. P. O'Halloran, D. A. Hillesheim, S. Lense, K. I. Hardcastle and C. L. Hill, *CrystEngComm*, 2011, **13**, 738–740.
56 R. Chakrabarty, P. S. Mukherjee and P. J. Stang, *Chem. Rev.*, 2011, **111**, 6810–6918.
57 T. Yamada, K. Otsubo, R. Makiura and H. Kitagawa, *Chem. Soc. Rev.*, 2013, **42**, 6655–6669.
58 A. Schmidt, A. Casini and F. E. Kuhn, *Coord. Chem. Rev.*, 2014, **275**, 19–36.
59 R. Ricco, C. Pfeiffer, K. Sumida, C. J. Sumby, P. Falcaro, S. Furukawa, N. R. Champness and C. J. Doonan, *CrystEngComm*, 2016, **18**, 6532–6542.
60 See special issue of The 7th International Conference on Metal-Organic Frameworks & Open Framework Compounds (MOF2020), *Chem. Soc. Rev.*, 2020.
61 X. Z. Yan, S. J. Li, J. B. Pollock, T. R. Cook, J. Z. Chen, Y. Y. Zhang, X. F. Ji, Y. H. Yu, F. H. Huang and P. J. Stang, *Proc. Natl. Acad. Sci. U. S. A.*, 2013, **110**, 15585–15590.
62 S. Datta, M. L. Saha and P. J. Stang, *Acc. Chem. Res.*, 2018, **51**, 2047–2063.
63 B. Nohra, H. El Moll, L. M. R. Albelo, P. Mialane, J. Marrot, C. Mellot-Draznieks, M. O'Keeffe, R. N. Biboum, J. Lemaire, B. Keita, L. Nadjo and A. Dolbecq, *J. Am. Chem. Soc.*, 2011, **133**, 13363–13374.
64 L. M. Rodriguez-Albelo, A. R. Ruiz-Salvador, A. Sampieri, D. W. Lewis, A. Gomez, B. Nohra, P. Mialane, J. Marrot, F. Secheresse, C. Mellot-Draznieks, R. N. Biboum, B. Keita, L. Nadjo and A. Dolbecq, *J. Am. Chem. Soc.*, 2009, **131**, 16078–16087.
65 S. Uchida and N. Mizuno, *Coord. Chem. Rev.*, 2007, **251**, 2537–2546.
66 S. Favette, B. Hasenknopf, J. Vaissermann, P. Gouzerh and C. Roux, *Chem. Commun.*, 2003, 2664–2665.
67 J. W. Han, K. I. Hardcastle and C. L. Hill, *Eur. J. Inorg. Chem.*, 2006, 2598–2603.
68 J. W. Han and C. L. Hill, *J. Am. Chem. Soc.*, 2007, **129**, 15094–15095.
69 A. Abhervé, M. Palacios-Corella, J. M. Clemente-Juan, R. Marx, P. Neugebauer, J. van Slageren, M. Clemente-

León and E. Coronado, *J. Mater. Chem. C*, 2015, **3**, 7936–7945.
70 J. Yan, H. Huang, Z. Miao, Q. Zhang and Y. Yan, *Macromolecules*, 2019, **52**, 9545–9554.
71 L. Liu, L. Hu, Q. Liu, Z.-L. Du, F.-B. Li, G.-H. Li, X.-J. Zhu, W.-Y. Wong, L. Wang and H. Li, *Dalton Trans.*, 2015, **44**, 306–315.
72 L. Liu, L. Hu, Q. Liu, S.-Z. Liu, F.-B. Li, L. Li, L. Peng, D.-H. Yao, W.-Y. Wong and Z.-L. Du, *J. Organomet. Chem.*, 2015, **792**, 102–108.
73 X.-X. Li, Y.-X. Wang, R.-H. Wang, C.-Y. Cui, C.-B. Tian and G.-Y. Yang, *Angew. Chem., Int. Ed.*, 2016, **55**, 6462–6466.
74 F.-J. Yazigi, C. Wilson, D.-L. Long and R. S. Forgan, *Cryst. Growth Des.*, 2017, **17**, 4739–4748.
75 M.-C. Zhu, Y.-Y. Huang, J.-P. Ma, S.-M. Hu, Y. Wang, J. Guo, Y.-X. Zhao and L.-S. Wang, *Cryst. Growth Des.*, 2019, **19**, 925–931.
76 Z. Chen, H. An, H. Zhang and Y. Hu, *CrystEngComm*, 2013, **15**, 4711–4720.
77 J. Als-Nielsen and D. McMorrow, *Elements of modern x-ray physics*, Wiley, New York, 2001.
78 J. Maes, N. Castro, K. De Nolf, W. Walravens, B. Abecassis and Z. Hens, *Chem. Mater.*, 2018, **30**, 3952–3962.
79 J. Kang, B. Xu, Z. Peng, X. Zhu, Y. Wei and D. R. Powell, *Angew. Chem., Int. Ed.*, 2005, **44**, 6902–6905.
80 M.-P. Santoni, A. K. Pal, G. S. Hanan, M.-C. Tang, K. Venne, A. Furtos, P. Ménard-Tremblay, C. Malveau and B. Hasenknopf, *Chem. Commun.*, 2012, **48**, 200–202.
81 M. Piot, S. Hupin, H. Lavanan, C. Afonso, L. Bouteiller, A. Proust and G. Izzet, *Inorg. Chem.*, 2017, **56**, 8490–8496.
82 G. Izzet, A. Macdonell, C. Rinfray, M. Piot, S. Renaudineau, E. Derat, B. Abécassis, C. Afonso and A. Proust, *Chem. – Eur. J.*, 2015, **21**, 19010–19015.
83 A. Guinier and G. Fournet, *Small Angle Scaterring of X-Rays*., Wiley, New York, 1955.
84 M. Li, W. Y. Wang and P. C. Yin, *Chem. – Eur. J.*, 2018, **24**, 6639–6644.
85 M. Nyman, *Coord. Chem. Rev.*, 2017, **352**, 461–472.
86 Y. L. Wu, R. F. Shi, Y. L. Wu, J. M. Holcroft, Z. C. Liu, M. Frasconi, M. R. Wasielewski, H. Li and J. F. Stoddart, *J. Am. Chem. Soc.*, 2015, **137**, 4111–4118.
87 G. Izzet, B. Abécassis, D. Brouri, M. Piot, B. Matt, S. A. Serapian, C. Bo and A. Proust, *J. Am. Chem. Soc.*, 2016, **138**, 5093–5099.
88 M. Piot, B. Abécassis, D. Brouri, C. Troufflard, A. Proust and G. Izzet, *Proc. Natl. Acad. Sci. U. S. A.*, 2018, **115**, 8895–8900.
89 R. Salles, B. Abecassis, E. Derat, D. Brouri, A. Bernard, Q. C. Zhang, A. Proust, C. Desmarets and G. Izzet, *Inorg. Chem.*, 2020, **59**, 2458–2463.
90 M. S. Centellas, M. Piot, R. Salles, A. Proust, L. Tortech, D. Brouri, S. Hupin, B. Abecassis, D. Landy, C. Bo and G. Izzet, *Chem. Sci.*, 2020, **11**, 11072–11080.
91 X.-X. Li, X. Ma, W.-X. Zheng, Y.-J. Qi, S.-T. Zheng and G.-Y. Yang, *Inorg. Chem.*, 2016, **55**, 8257–8259.
92 Y. Zhu, P. C. Yin, F. P. Xiao, D. Li, E. Bitterlich, Z. C. Xiao, J. Zhang, J. Hao, T. B. Liu, Y. Wang and Y. G. Wei, *J. Am. Chem. Soc.*, 2013, **135**, 17155–17160.
93 T. Ito, H. Yashiro and T. Yamase, *Langmuir*, 2006, **22**, 2806–2810.
94 L. de Viguerie, A. Mouret, H. P. Brau, V. Nardello-Rataj, A. Proust and P. Bauduin, *CrystEngComm*, 2012, **14**, 8446–8453.
95 H. L. Li, H. Sun, W. Qi, M. Xu and L. X. Wu, *Angew. Chem., Int. Ed.*, 2007, **46**, 1300–1303.
96 B. Li, W. Li, H. L. Li and L. X. Wu, *Acc. Chem. Res.*, 2017, **50**, 1391–1399.
97 L. Leclercq, A. Mouret, A. Proust, V. Schmitt, P. Bauduin, J. M. Aubry and V. Nardello-Rataj, *Chem. – Eur. J.*, 2012, **18**, 14352–14358.
98 B. Naskar, O. Diat, V. Nardello-Rataj and P. Bauduin, *J. Phys. Chem. C*, 2015, **119**, 20985–20992.
99 S. Polarz, S. Landsmann and A. Klaiber, *Angew. Chem., Int. Ed.*, 2014, **53**, 946–954.
100 J. N. Israelachvili, *Intermolecular and Surface Forces*, Academic Press, 3rd edn, 2011.
101 D. Li, P. C. Yin and T. B. Liu, *Dalton Trans.*, 2012, **41**, 2853–2861.
102 J. Zhang, Y. F. Song, L. Cronin and T. B. Liu, *J. Am. Chem. Soc.*, 2008, **130**, 14408–14409.
103 P. C. Yin, P. F. Wu, Z. C. Xiao, D. Li, E. Bitterlich, J. Zhang, P. Cheng, D. V. Vezenov, T. B. Liu and Y. G. Wei, *Angew. Chem., Int. Ed.*, 2011, **50**, 2521–2525.
104 M. H. Rosnes, C. Musumeci, C. P. Pradeep, J. S. Mathieson, D. L. Long, Y. F. Song, B. Pignataro, R. Cogdell and L. Cronin, *J. Am. Chem. Soc.*, 2010, **132**, 15490–15492.
105 C. P. Pradeep, M. F. Misdrahi, F. Y. Li, J. Zhang, L. Xu, D. L. Long, T. B. Liu and L. Cronin, *Angew. Chem., Int. Ed.*, 2009, **48**, 8309–8313.
106 J. Zhang, Y. F. Song, L. Cronin and T. B. Liu, *Chem. – Eur. J.*, 2010, **16**, 11320–11324.
107 J. Zhang, T. B. Liu, S. S. Mal and U. Kortz, *Eur. J. Inorg. Chem.*, 2010, 3195–3200.
108 M. F. Misdrahi, M. H. Wang, C. P. Pradeep, F. Y. Li, C. Lydon, L. Xu, L. Cronin and T. B. Liu, *Langmuir*, 2011, **27**, 9193–9202.
109 A. Chaumont and G. Wipff, *Eur. J. Inorg. Chem.*, 2013, 1835–1853.
110 J. M. Pigga, M. L. Kistler, C. Y. Shew, M. R. Antonio and T. B. Liu, *Angew. Chem., Int. Ed.*, 2009, **48**, 6538–6542.
111 T. B. Liu, *Langmuir*, 2010, **26**, 9202–9213.
112 Y. F. Wang and I. A. Weinstock, *Dalton Trans.*, 2010, **39**, 6143–6152.
113 Y. K. Han, Y. Xiao, Z. J. Zhang, B. Liu, P. Zheng, S. J. He and W. Wang, *Macromolecules*, 2009, **42**, 6543–6548.
114 Y. Xiao, Y. K. Han, N. Xia, M. B. Hu, P. Zheng and W. Wang, *Chem. – Eur. J.*, 2012, **18**, 11325–11333.
115 D. Li, J. Song, P. C. Yin, S. Simotwo, A. J. Bassler, Y. Y. Aung, J. E. Roberts, K. I. Hardcastle, C. L. Hill and T. B. Liu, *J. Am. Chem. Soc.*, 2011, **133**, 14010–14016.
116 S. Landsmann, M. Luka and S. Polarz, *Nat. Commun.*, 2012, **3**, 1299.
117 R. C. Chambers, E. J. O. Atkinson, D. McAdams, E. J. Hayden and D. J. A. Brown, *Chem. Commun.*, 2003, 2456–2457.

118 J. J. Giner-Casares, G. Brezesinski, H. Mohwald, S. Landsmann and S. Polarz, *J. Phys. Chem. Lett.*, 2012, **3**, 322–326.
119 S. Landsmann, C. Lizandara-Pueyo and S. Polarz, *J. Am. Chem. Soc.*, 2010, **132**, 5315–5321.
120 A. Klaiber, S. Landsmann, T. Loffler and S. Polarz, *New J. Chem.*, 2016, **40**, 919–922.
121 A. Klaiber, C. Lanz, S. Landsmann, J. Gehring, M. Drechsler and S. Polarz, *Langmuir*, 2016, **32**, 10920–10927.
122 V. Jallet, G. Guillemot, J. Lai, P. Bauduin, V. Nardello-Rataj and A. Proust, *Chem. Commun.*, 2014, **50**, 6610–6612.
123 V. Jallet, *Conception de Polyoxométallates Amphiphiles Pour La Catalyse d'oxydation En Microémulsion*, Université Pierre et Marie Curie, 2014, vol. **6**.
124 I. Kozhevnikov, *Catalysis by Polyoxometalates*, Chichester, England, 2002.
125 S. S. Wang and G. Y. Yang, *Chem. Rev.*, 2015, **115**, 4893–4962.
126 C. Venturello, E. Alneri and M. Ricci, *J. Org. Chem.*, 1983, **48**, 3831–3833.
127 K. Sato, M. Aoki, M. Ogawa, T. Hashimoto and R. Noyori, *J. Org. Chem.*, 1996, **61**, 8310–8311.
128 C. Venturello, R. Daloisio, J. C. J. Bart and M. Ricci, *J. Mol. Catal.*, 1985, **32**, 107–110.
129 R. Neumann and A. M. Khenkin, *J. Org. Chem.*, 1994, **59**, 7577–7579.
130 R. Ishimoto, K. Kamata and N. Mizuno, *Angew. Chem., Int. Ed.*, 2012, **51**, 4662–4665.
131 Y. Ishii, K. Yamawaki, T. Ura, H. Yamada, T. Yoshida and M. Ogawa, *J. Org. Chem.*, 1988, **53**, 3587–3593.
132 R. Yahya, M. Craven, E. F. Kozhevnikova, A. Steiner, P. Samunual, I. V. Kozhevnikov and D. E. Bergbreiter, *Catal. Sci. Technol.*, 2015, **5**, 818–821.
133 J. M. Bregeault, M. Vennat, L. Salles, J. Y. Piquemal, Y. Mahha, E. Briot, P. C. Bakala, A. Atlamsani and R. Thouvenot, *J. Mol. Catal. A: Chem.*, 2006, **250**, 177–189.
134 G. Maayan, R. Popovitz-Biro and R. Neumann, *J. Am. Chem. Soc.*, 2006, **128**, 4968–4969.
135 A. Mouret, L. Leclercq, A. Muhlbauer and V. Nardello-Rataj, *Green Chem.*, 2014, **16**, 269–278.
136 P. C. Yin, J. Wang, Z. C. Xiao, P. F. Wu, Y. G. Wei and T. B. Liu, *Chem. – Eur. J.*, 2012, **18**, 9174–9178.
137 P. C. Yin, A. Bayaguud, P. Cheng, F. Haso, L. Hu, J. Wang, D. Vezenov, R. E. Winans, J. Hao, T. Li, Y. G. Wei and T. B. Liu, *Chem. – Eur. J.*, 2014, **20**, 9589–9595.
138 K. Chen, A. Bayaguud, H. Li, Y. Chu, H. C. Zhang, H. L. Jia, B. F. Zhang, Z. C. Xiao, P. F. Wu, T. B. Liu and Y. G. Wei, *Nano Res.*, 2018, **11**, 1313–1321.
139 Y. Yan, H. B. Wang, B. Li, G. F. Hou, Z. D. Yin, L. X. Wu and V. W. W. Yam, *Angew. Chem., Int. Ed.*, 2010, **49**, 9233–9236.
140 H. B. Li, F. R. Jiang, G. H. Zhang, B. Li and L. X. Wu, *Dalton Trans.*, 2019, **48**, 5168–5175.
141 Y. Chu, A. Saad, P. C. Yin, J. Y. Z. Wu, O. Oms, A. Dolbecq, P. Mialane and T. B. Liu, *Chem. – Eur. J.*, 2016, **22**, 11756–11762.
142 K. Kastner, A. J. Kibler, E. Karjalainen, J. A. Fernandes, V. Sans and G. N. Newton, *J. Mater. Chem. A*, 2017, **5**, 11577–11581.
143 S. Amin, J. M. Cameron, J. A. Watts, D. A. Walsh, V. Sans and G. N. Newton, *Mol. Syst. Des. Eng.*, 2019, **4**, 995–999.
144 E. Hampson, J. M. Cameron, S. Amin, J. Kyo, J. A. Watts, H. Oshio and G. N. Newton, *Angew. Chem., Int. Ed.*, 2019, **58**, 18281–18285.
145 E. Hampson, J. M. Cameron, J. A. Watts and G. N. Newton, *Chem. Commun.*, 2020, **56**, 8237–8240.
146 C. L. Peake, A. J. Kibler, G. N. Newton and D. A. Walsh, *ACS Appl. Energy Mater.*, 2021, **4**(9), 8765–8773.
147 A. Klaiber and S. Polarz, *ACS Nano*, 2016, **10**, 10041–10048.
148 A. Klaiber, T. Kollek, S. Cardinal, N. Hug, M. Drechsler and S. Polarz, *Adv. Mater. Interfaces*, 2018, **5**, 1701430.
149 X. Y. Chen, H. Li, P. C. Yin and T. B. Liu, *Chem. Commun.*, 2015, **51**, 6104–6107.
150 J. Lesage de La Haye, J. M. Guigner, E. Marceau, L. Ruhlmann, B. Hasenknopf, E. Lacote and J. Rieger, *Chem. – Eur. J.*, 2015, **21**, 2948–2953.
151 P. Judeinstein, *Chem. Mater.*, 1992, **4**, 4–7.
152 A. R. Moore, H. Kwen, A. M. Beatty and E. A. Maatta, *Chem. Commun.*, 2000, 1793–1794.
153 C. R. Mayer, R. Thouvenot and T. Lalot, *Chem. Mater.*, 2000, **12**, 257–260.
154 C. R. Mayer, R. Thouvenot and T. Lalot, *Macromolecules*, 2000, **33**, 4433–4437.
155 C. R. Mayer, V. Cabuil, T. Lalot and R. Thouvenot, *Angew. Chem., Int. Ed.*, 1999, **38**, 3672–3675.
156 B. Keita and L. Nadjo, *Mater. Chem. Phys.*, 1989, **22**, 77–103.
157 K. Nomiya, H. Murasaki and M. Miwa, *Polyhedron*, 1986, **5**, 1031–1033.
158 W. Qi and L. X. Wu, *Polym. Int.*, 2009, **58**, 1217–1225.
159 Y. F. Wang and I. A. Weinstock, *Chem. Soc. Rev.*, 2012, **41**, 7479–7496.
160 C. R. Mayer, S. Neveu and V. Cabuil, *Angew. Chem., Int. Ed.*, 2002, **41**, 501–503.
161 S. Sutter, B. Trepka, S. Siroky, K. Hagedorn, S. Theiss, P. Baum and S. Polarz, *ACS Appl. Mater. Interfaces*, 2019, **11**, 15936–15944.
162 C. Martin, K. Kastner, J. M. Cameron, E. Hampson, J. A. Fernandes, E. K. Gibson, D. A. Walsh, V. Sans and G. N. Newton, *Angew. Chem., Int. Ed.*, 2020, **59**, 14331–14335.
163 A. Gillet, S. Cher, M. Tasse, T. Blon, S. Alves, G. Izzet, B. Chaudret, A. Proust, P. Demont, F. Volatron and S. Tricard, *Nanoscale Horiz.*, 2021, **6**, 271–276.
164 S. M. Wang, J. Hwang and E. Kim, *J. Mater. Chem. C*, 2019, **7**, 7828–7850.
165 B. Fleury, M. Billon, F. Duclairoir, L. Dubois, A. Fanton and G. Bidan, *Thin Solid Films*, 2011, **519**, 3732–3738.
166 D. Fattakhova-Rohlfing, J. Rathousky, Y. Rohlfing, O. Bartels and M. Wark, *Langmuir*, 2005, **21**, 11320–11329.
167 D. Velessiotis, A. M. Douvas, P. Dimitrakis, P. Argitis and N. Glezos, *Microelectron. Eng.*, 2012, **97**, 150–153.
168 F. M. Toma, A. Sartorel, M. Iurlo, M. Carraro, P. Parisse, C. Maccato, S. Rapino, B. R. Gonzalez, H. Amenitsch, T. Da

Ros, L. Casalis, A. Goldoni, M. Marcaccio, G. Scorrano, G. Scoles, F. Paolucci, M. Prato and M. Bonchio, *Nat. Commun.*, 2010, **2**, 826–831.
169 Y. Martinetto, B. Pegot, C. Roch-Marchal, B. Cottyn-Boitte and S. Floquet, *Eur. J. Inorg. Chem.*, 2020, 228–247.
170 C. G. Lin, W. Chen, S. Omwoma and Y. F. Song, *J. Mater. Chem. C*, 2015, **3**, 15–18.
171 X. L. Zhu, C. Hessin, A. Salame, L. Sosa-Vargas, D. Kreher, C. Adachi, A. Proust, P. Mialane, J. Marrot, A. Bouchet, M. Sliwa, S. Mery, B. Heinrich, F. Mathevet and G. Izzet, *Angew. Chem., Int. Ed.*, 2021, **60**, 8419–8424.
172 V. Kulikov, N. A. B. Johnson, A. J. Surman, M. Hutin, S. M. Kelly, M. Hezwani, D. L. Long, G. Meyer and L. Cronin, *Angew. Chem., Int. Ed.*, 2017, **56**, 1141–1145.
173 S. J. Li, Y. F. Zhou, N. N. Ma, J. Zhang, Z. P. Zheng, C. Streb and X. N. Chen, *Angew. Chem., Int. Ed.*, 2020, **59**, 8537–8540.
174 J. Tang, X. Y. Li, H. Wu, L. J. Ren, Y. Q. Zhang, H. X. Yao, M. B. Hu and W. Wang, *Langmuir*, 2016, **32**, 460–467.
175 L. J. Ren, H. K. Liu, H. Wu, M. B. Hu and W. Wang, *Adv. Mater.*, 2020, **32**, 1805863.
176 C. Ma, H. Wu, Z. H. Huang, R. H. Guo, M. B. Hu, C. Kubel, L. T. Yan and W. Wang, *Angew. Chem., Int. Ed.*, 2015, **54**, 15699–15704.
177 H. Liu, J. C. Luo, W. P. Shan, D. Guo, J. Wang, C. H. Hsu, M. J. Huang, W. Zhang, B. Lotz, W. B. Zhang, T. B. Liu, K. Yue and S. Z. D. Cheng, *ACS Nano*, 2016, **10**, 6585–6596.
178 X. S. Hou, G. L. Zhu, L. J. Ren, Z. H. Huang, R. B. Zhang, G. Ungar, L. T. Yan and W. Wang, *J. Am. Chem. Soc.*, 2018, **140**, 1805–1811.
179 H. K. Liu, L. J. Ren, H. Wu, Y. L. Ma, S. Richter, M. Godehardt, C. Kubel and W. Wang, *J. Am. Chem. Soc.*, 2019, **141**, 831–839.
180 Y. Yu and J. Rebek, *Acc. Chem. Res.*, 2018, **51**, 3031–3040.
181 J. Murray, K. Kim, T. Ogoshi, W. Yao and B. C. Gibb, *Chem. Soc. Rev.*, 2017, **46**, 2479–2496.
182 N. L. Strutt, H. C. Zhang, S. T. Schneebeli and J. F. Stoddart, *Acc. Chem. Res.*, 2014, **47**, 2631–2642.
183 J. A. Foster and J. W. Steed, *Angew. Chem., Int. Ed.*, 2010, **49**, 6718–6724.
184 M. A. Moussawi, M. Haouas, S. Floquet, W. E. Shepard, P. A. Abramov, M. N. Sokolov, V. P. Fedin, S. Cordier, A. Ponchel, E. Monflier, J. Marrot and E. Cadot, *J. Am. Chem. Soc.*, 2017, **139**, 14376–14379.
185 L. B. Ni, H. Li, H. J. Xu, C. Shen, R. Z. Liu, J. Xie, F. M. Zhang, C. Chen, H. X. Zhao, T. F. Zuo and G. W. Diao, *ACS Appl. Mater. Interfaces*, 2019, **11**, 38708–38718.
186 C. Falaise, M. A. Moussawi, S. Floquet, P. A. Abramov, M. N. Sokolov, M. Haouas and E. Cadot, *J. Am. Chem. Soc.*, 2018, **140**, 11198–11201.
187 P. Su, A. J. Smith, J. Warneke and J. Laskin, *J. Am. Soc. Mass Spectrom.*, 2019, **30**, 1934–1945.
188 X. Fang, P. Kogerler, L. Isaacs, S. Uchida and N. Mizuno, *J. Am. Chem. Soc.*, 2009, **131**, 432–433.
189 J. Tian, Z. Y. Xu, D. W. Zhang, H. Wang, S. H. Xie, D. W. Xu, Y. H. Ren, H. Wang, Y. Liu and Z. T. Li, *Nat. Commun.*, 2016, **7**, 11580.
190 F. Zhou, L. L. Zeng, W. Guo, Y. Z. Yan, F. Wu and M. Pan, *Int. J. Energy Res.*, 2019, **43**, 7095–7106.
191 G. Izzet, M. Ménand, B. Matt, S. Renaudineau, L. M. Chamoreau, M. Sollogoub and A. Proust, *Angew. Chem., Int. Ed.*, 2012, **51**, 487–490.
192 Q. X. Guo, S. H. Luo and Y. C. Liu, *J. Inclusion Phenom.*, 1998, **30**, 173–182.
193 Unpublished results.
194 L. Yue, H. Ai, Y. Yang, W. J. Lu and L. X. Wu, *Chem. Commun.*, 2013, **49**, 9770–9772.
195 A. Harada, *Acc. Chem. Res.*, 2001, **34**, 456–464.
196 B. Zhang, L. Yue, Y. Wang, Y. Yang and L. X. Wu, *Chem. Commun.*, 2014, **50**, 10823–10826.
197 C. G. Lin, G. D. Fura, Y. Long, W. M. Xuan and Y. F. Song, *Inorg. Chem. Front.*, 2017, **4**, 789–794.
198 W. M. Guan, G. X. Wang, J. B. Ding, B. Li and L. X. Wu, *Chem. Commun.*, 2019, **55**, 10788–10791.
199 M. Stuckart, N. V. Izarova, J. van Leusen, A. Smekhova, C. Schmitz-Antoniak, H. Bamberger, J. van Slageren, B. Santiago-Schubel and P. Kogerler, *Chem. – Eur. J.*, 2018, **24**, 17767–17778.
200 Y. C. Ji, L. J. Huang, J. Hu, C. Streb and Y. F. Song, *Energy Environ. Sci.*, 2015, **8**, 776–789.
201 J. W. Jordan, G. A. Lowe, R. L. McSweeney, C. T. Stoppiello, R. W. Lodge, S. T. Skowron, J. Biskupek, G. A. Rance, U. Kaiser, D. A. Walsh, G. N. Newton and A. N. Khlobystov, *Adv. Mater.*, 2019, **31**, 1904182.
202 N. Kawasaki, H. Wang, R. Nakanishi, S. Hamanaka, R. Kitaura, H. Shinohara, T. Yokoyama, H. Yoshikawa and K. Awaga, *Angew. Chem., Int. Ed.*, 2011, **50**, 3471–3474.
203 J. Hu, Y. C. Ji, W. Chen, C. Streb and Y. F. Song, *Energy Environ. Sci.*, 2016, **9**, 1095–1101.
204 M. Genovese and K. Lian, *ACS Appl. Mater. Interfaces*, 2016, **8**, 19100–19109.
205 W. Chen, L. J. Huang, J. Hu, T. F. Li, F. F. Jia and Y. F. Song, *Phys. Chem. Chem. Phys.*, 2014, **16**, 19668–19673.
206 Y. C. Ji, J. Hu, L. J. Huang, W. Chen, C. Streb and Y. F. Song, *Chem. – Eur. J.*, 2015, **21**, 6469–6474.
207 D. Ma, L. Y. Liang, W. Chen, H. M. Liu and Y. F. Song, *Adv. Funct. Mater.*, 2013, **23**, 6100–6105.
208 L. J. Huang, J. Hu, Y. C. Ji, C. Streb and Y. F. Song, *Chem. – Eur. J.*, 2015, **21**, 18799–18804.
209 C. Bosch-Navarro, B. Matt, G. Izzet, C. Romero-Nieto, K. Dirian, A. Raya, S. I. Molina, A. Proust, D. M. Guldi, C. Marti-Gastaldo and E. Coronado, *Chem. Sci.*, 2014, **5**, 4346–4354.
210 G. Modugno, Z. Syrgiannis, A. Bonasera, M. Carraro, G. Giancane, L. Valli, M. Bonchio and M. Prato, *Chem. Commun.*, 2014, **50**, 4881–4883.
211 Z. Syrgiannis, G. Trautwein, M. Calvaresi, G. Modugno, F. Zerbetto, M. Carraro, M. Prato and M. Bonchio, *Eur. J. Inorg. Chem.*, 2019, 374–379.
212 Y. C. Ji, T. F. Li and Y. F. Song, *Ind. Eng. Chem. Res.*, 2014, **53**, 11566–11570.
213 P. F. Gao, Y. Q. Wu and L. X. Wu, *Soft Matter*, 2016, **12**, 8464–8479.

214 A. Bijelic and A. Rompel, *Chemtexts*, 2018, **4**, 10.
215 L. S. Van Rompuy and T. N. Parac-Vogt, *Curr. Opin. Biotechnol*, 2019, **58**, 92–99.
216 A. Bijelic, M. Aureliano and A. Rompel, *Angew. Chem., Int. Ed.*, 2019, **58**, 2980–2999.
217 F. Schluenzen, A. Tocilj, R. Zarivach, J. Harms, M. Gluehmann, D. Janell, A. Bashan, H. Bartels, I. Agmon, F. Franceschi and A. Yonath, *Cell*, 2000, **102**, 615–623.
218 A. Bijelic and A. Rompel, *Coord. Chem. Rev.*, 2015, **299**, 22–38.
219 H. Liu, Y. L. Zou, L. Zhang, J. X. Liu, C. Y. Song, D. F. Chai, G. G. Gao and Y. F. Qiu, *J. Coord. Chem.*, 2014, **67**, 2257–2270.
220 J. Q. Sha, X. Li, Y. H. Zhou, P. F. Yan, G. M. Li and C. Wang, *Solid State Sci.*, 2011, **13**, 1972–1977.
221 C. Molitor, A. Bijelic and A. Rompel, *Chem. Commun.*, 2016, **52**, 12286–12289.
222 S. G. Mauracher, C. Molitor, R. Al-Oweini, U. Kortz and A. Rompel, *acta Crystallogr., Sect. D: Biol. Crystallogr.*, 2014, **70**, 2301–2315.
223 A. Blazevic, E. Al-Sayed, A. Roller, G. Giester and A. Rompel, *Chem. – Eur. J.*, 2015, **21**, 4762–4771.
224 E. Al-Sayed, A. Blazevic, A. Roller and A. Rompel, *Chem. – Eur. J.*, 2015, **21**, 17800–17807.
225 A. Blazevic and A. Rompel, *Coord. Chem. Rev.*, 2016, **307**, 42–64.
226 V. A. Zamolo, G. Modugno, E. Lubian, A. Cazzolaro, F. Mancin, L. Giotta, D. Mastrogiacomo, L. Valli, A. Saccani, S. Krol, M. Bonchio and M. Carraro, *Front. Chem.*, 2018, **6**, 278.
227 C. Yvon, A. J. Surman, M. Hutin, J. Alex, B. O. Smith, D. L. Long and L. Cronin, *Angew. Chem., Int. Ed.*, 2014, **53**, 3336–3341.
228 D. Vilona, D. Lachkar, E. Dumont, M. Lelli and E. Lacôte, *Chem. – Eur. J.*, 2017, **23**, 13323–13327.
229 A. M. Debela, M. Ortiz, V. Beni, S. Thorimbert, D. Lesage, R. B. Cole, C. K. O'Sullivan and B. Hasenknopf, *Chem. – Eur. J.*, 2015, **21**, 17721–17727.
230 M. Ortiz, A. M. Debela, M. Svobodova, S. Thorimbert, D. Lesage, R. B. Cole, B. Hasenknopf and C. K. O'Sullivan, *Chem. – Eur. J.*, 2017, **23**, 10597–10603.
231 N. Chahin, L. A. Uribe, A. M. Debela, S. Thorimbert, B. Hasenknopf, M. Ortiz, I. Katakis and C. K. O'Sullivan, *Biosens. Bioelectron.*, 2018, **117**, 201–206.
232 Y. F. Song, N. McMillan, D. L. Long, S. Kane, J. Malm, M. O. Riehle, C. P. Pradeep, N. Gadegaard and L. Cronin, *J. Am. Chem. Soc.*, 2009, **131**, 1340–1341.
233 B. X. Jing, M. Hutin, E. Connor, L. Cronin and Y. X. Zhu, *Chem. Sci.*, 2013, **4**, 3818–3826.
234 A. Sakamoto, K. Unoura and H. Nabika, *J. Phys. Chem. C*, 2018, **122**, 1404–1411.
235 Z. M. Zhang, X. P. Duan, S. Yao, Z. S. Wang, Z. K. Lin, Y. G. Li, L. S. Long, E. B. Wang and W. B. Lin, *Chem. Sci.*, 2016, **7**, 4220–4229.
236 L. Ni, P. Greenspan, R. Gutman, C. Kelloes, M. A. Farmer and F. D. Boudinot, *Antiviral Res.*, 1996, **32**, 141–148.
237 G. Geisberger, E. B. Gyenge, D. Hinger, P. Bosiger, C. Maake and G. R. Patzke, *Dalton Trans.*, 2013, **42**, 9914–9920.
238 G. Modugno, E. Fabbretti, A. Dalle Vedove, T. Da Ros, C. Maccato, H. S. Hosseini, M. Bonchio and M. Carraro, *Eur. J. Inorg. Chem.*, 2018, 4955–4961.
239 L. Fu, H. Q. Gao, M. Yan, S. Z. Li, X. Y. Li, Z. F. Dai and S. Q. Liu, *Small*, 2015, **11**, 2938–2945.
240 A. Bijelic, M. Aureliano and A. Rompel, *Chem. Commun.*, 2018, **54**, 1153–1169.
241 A. Flutsch, T. Schroeder, M. G. Grutter and G. R. Patzke, *Bioorg. Med. Chem. Lett.*, 2011, **21**, 1162–1166.
242 P. Yang, Z. G. Lin, G. Alfaro-Espinoza, M. S. Ullrich, C. I. Rat, C. Silvestru and U. Kortz, *Inorg. Chem.*, 2016, **55**, 251–258.
243 H. N. Mukherjee, *J. Indian Med. Assoc.*, 1965, **44**, 477–479.
244 L. S. Wang, P. C. Yin, J. Zhang, F. P. Xiao, Z. K. Fang, W. W. Fu, Y. G. Wei and S. J. Xue, *Eur. J. Inorg. Chem.*, 2017, 5475–5484.
245 H. Yu, S. L. Le, X. H. Zeng, J. Y. Zhang and J. L. Xie, *Inorg. Chem. Commun.*, 2014, **39**, 135–139.
246 S. She, S. T. Bian, J. Hao, J. W. Zhang, J. Zhang and Y. G. Wei, *Chem. – Eur. J.*, 2014, **20**, 16987–16994.
247 A. Boulmier, X. X. Feng, O. Oms, P. Mialane, E. Riviere, C. J. Shin, J. Q. Yao, T. Kubo, T. Furuta, E. Oldfield and A. Dolbecq, *Inorg. Chem.*, 2017, **56**, 7558–7565.
248 J. D. Compain, P. Mialane, J. Marrot, F. Secheresse, W. Zhu, E. Oldfield and A. Dolbecq, *Chem. – Eur. J.*, 2010, **16**, 13741–13748.
249 Z. X. Dong, R. K. Tan, J. Cao, Y. Yang, C. F. Kong, J. Du, S. Zhu, Y. Zhang, J. Lu, B. Q. Huang and S. X. Liu, *Eur. J. Med. Chem.*, 2011, **46**, 2477–2484.
250 X. K. Hu, H. Wang, B. Huang, N. Li, K. H. Hu, B. L. Wu, Z. C. Xiao, Y. H. Wei and P. F. Wu, *J. Inorg. Biochem.*, 2019, **193**, 130–132.
251 H. K. Yang, Y. X. Cheng, M. M. Su, Y. Xiao, M. B. Hu, W. Wang and Q. Wang, *Bioorg. Med. Chem. Lett.*, 2013, **23**, 1462–1466.
252 D. Ventura, A. Calderan, C. Honisch, S. Krol, S. Serrati, M. Bonchio, M. Carraro and P. Ruzza, *Peptide Sci.*, 2018, **110**, e24047.
253 S. She, S. T. Bian, R. C. Huo, K. Chen, Z. H. Huang, J. W. Zhang, J. Hao and Y. G. Wei, *Sci. Rep.*, 2016, **6**, 33529.
254 D. Karimian, B. Yadollahi and V. Mirkhani, *Microporous Mesoporous Mater.*, 2017, **247**, 23–30.
255 T. Sun, W. Cui, M. Yan, G. Qin, W. Guo, H. Gu, S. Liu and Q. Wu, *Adv. Mater.*, 2016, **28**(34), 7397–7404.
256 G. Toupalas, J. Karlsson, F. A. Black, A. Masip-Sanchez, X. Lopez, Y. Ben M'Barek, S. Blanchard, A. Proust, S. Alves, P. Chabera, I. P. Clark, T. Pullerits, J. M. Poblet, E. A. Gibson and G. Izzet, *Angew. Chem., Int. Ed.*, 2021, **60**, 6518–6525.
257 E. Nikoloudakis, K. Karikis, M. Laurans, C. Kokotidou, A. Sole-Daura, J. J. Carbo, A. Charisiadis, G. Charalambidis, G. Izzet, A. Mitraki, A. M. Douvas, J. M. Poblet, A. Proust and A. G. Coutsolelos, *Dalton Trans.*, 2018, **47**, 6304–6313.

258 R. Carr, I. A. Weinstock, A. Sivaprasadarao, A. Muller and A. Aksimentiev, *Nano Lett.*, 2008, **8**, 3916–3921.
259 Z. N. Liu, T. B. Liu and M. Tsige, *Sci. Rep.*, 2016, **6**, 26595.
260 L. Chen, W. L. Chen, X. L. Wang, Y. G. Li, Z. M. Su and E. B. Wang, *Chem. Soc. Rev.*, 2019, **48**, 260–284.
261 C. T. Buru and O. K. Farha, *ACS Appl. Mater. Interfaces*, 2020, **12**, 5345–5360.
262 L. Zhai and H. L. Li, *Molecules*, 2019, **24**, 3425.
263 M. J. Turo, L. F. Chen, C. E. Moore and A. M. Schimpf, *J. Am. Chem. Soc.*, 2019, **141**, 4553–4557.
264 R. Tsunashima, Y. Iwamoto, Y. Baba, C. Kato, K. Ichihashi, S. Nishihara, K. Inoue, K. Ishiguro, Y. F. Song and T. Akutagawa, *Angew. Chem., Int. Ed.*, 2014, **53**, 11228–11231.
265 R. Tsunashima, I. Nakamura, R. Oue, S. Koga, H. Oki, S. Noro, T. Nakamura and T. Akutagawa, *Dalton Trans.*, 2017, **46**, 12619–12624.

